Distinct effects of the two major types of UV-induced DNA lesions on DNA damage responses

Kai-Feng Hung

A dissertation
submitted in partial fulfillment of the
requirements for the degree of

Doctor of Philosophy

University of Washington

2015

Reading Committee:

Paul Nghiem, Chair
Masaoki Kawasumi
Richard B. Presland
Julia M. Sidorova

Program Authorized to Offer Degree:

Oral Biology

University of Washington

Abstract

Distinct effects of the two major types of UV-induced DNA lesions on DNA damage responses

Kai-Feng Hung

Chair of the Supervisory Committee:
Professor Paul Nghiem
Departments of Medicine/Dermatology and Oral Health Sciences (adjunct)

The most prevalent human carcinogen is sunlight-associated UV, a physiologic dose of which generates thousands of DNA lesions per cell, mostly of two types: cyclobutane pyrimidine dimers (CPDs) and 6-4 photoproducts (6-4PPs). To cope with these lesions that are DNA-distorting and mutagenic, cells trigger ATR-mediated checkpoint signaling to regulate diverse processes including cell cycle arrest, DNA replication, DNA repair, and apoptosis. These ATR-mediated processes determine the mutagenic outcomes of UV-damaged cells. Thus, elucidating the fundamental mechanism by which cells sense UV lesions and activate DNA damage response pathways would be important for our understanding and control of UV carcinogenesis. Although it is known that UV generates distinct types of lesions and triggers DNA damage responses, it remains unclear whether and how these two structurally distinct types of UV lesions are different in their abilities to activate ATR. We hypothesized that there are striking differences in the mechanisms and impact of these two lesion types on DNA replication and DNA damage responses. To determine the individual contributions of CPD and 6-4PP to ATR activation (Aim 1), we generated cells with a single type of lesion (using photolyases that selectively repair either CPD or 6-4PP) and evaluated lesion-specific ATR activation by multiparameter flow cytometry. Strikingly, we found that the ATR-Chk1 pathway is potently activated by 6-4PP, but not by CPD lesions. To investigate the mechanism by which only 6-4PP activates ATR (Aim 2), we examined the effect of each lesion type on replication progression. Using microfluidic-assisted replication track analysis (maRTA), we found that 6-4PPs, but not

CPDs, markedly impede DNA replication across the genome. Moreover, we demonstrated that only 6-4PPs preferentially become surrounded by single-stranded DNA in S phase, indicating selective and prolonged replication blockage at 6-4PPs. Taken together, 6-4PPs, although 8-fold fewer in number than CPDs, are critical for replication blockage and activation of the UV-induced ATR-Chk1 pathway. This study identifying the respective roles of CPD and 6-4PP lesions that occur at dipyrimidine sites provides a molecular basis for their remarkably distinct effects on DNA damage responses and insight into the mechanisms of UV carcinogenesis.

Acknowledgments

I am very grateful to my mentor Dr. Paul Nghiem for his support and mentorship throughout the period of my study. Paul has guided me on how to propose a scientific viewpoint, develop critical/logical thinking, “idiotize” a highly complex concept, and deliver an engaging and clear presentation. Paul successfully collaborates with people, effectively organizes a team, and kindly takes care of patients, all of which teach me how to become a better leader, mentor and doctor.

I am also grateful to Dr. Masaoki Kawasumi for his tireless teaching. Masaoki taught me how to conduct an experiment and make every experiment informative. Masaoki is always well prepared for every task, carefully handles every step, and comprehensively records every detail. Masaoki showed me how important these behaviors are to a researcher and scientist. Masaoki always pushes me to improve myself and to a higher level.

I am very thankful to my Doctoral Supervisory Committee: Dr. Julia Sidorova has shared with us her powerful and optimized assay as well as many invaluable suggestions for our study. Drs. Bradley Preston and Richard Presland provided us critical advice and direction. Dr. Ssu-Kuang Chen has been supportive, always giving me enormous encouragement.

Finally, I want to thank my colleagues in our lab for being so kind and helpful to me. They made our lab a wonderful place for me to work for years.

Dedication

To my family

For your constant love and support

Table of Contents

List of Figures

Chapter 1. Ultraviolet-induced DNA damage and responses

1.1 Ultraviolet (UV) irradiation induces DNA damage

Solar UV irradiation

Ultraviolet (UV) irradiation is the most prevalent carcinogen in humans, leading to diverse skin malignancies that outnumber all other cancers combined (1-3). The UV spectrum has been classified into UVA (320-400 nm), UVB (280-320 nm), and UVC (< 280 nm) (**Figure 1.1**). UVC and the majority of the UVB fraction of sunlight are absorbed by the stratospheric ozone layer in the Earth's atmosphere. Thus, the solar UV spectrum that reaches the surface of the earth includes mostly UVA and a small fraction of UVB, which comprise 95% and 5%, respectively, of terrestrial sunlight. The genotoxic effects of sunlight are likely attributed to the fraction of UVB rather than UVA (4-6), because UVB is more absorbed by DNA than UVA. However, UVA induces oxidative DNA damage and also plays a role in the pathogenesis of certain cutaneous malignancies including melanoma (7).

CPD and 6-4PP are the two major types of UV-induced DNA lesions

UV often damages DNA through dimerization at dipyrimidine sites (two pyrimidine bases juxtaposed in tandem in the nucleotide sequence) (**Figure 1.2**). The two major types of UV-induced DNA lesions are cyclobutane pyrimidine dimer (CPD) and pyrimidine (6-4) pyrimidone photoproduct (6-4PP) (8). Formation of these lesions is UV wavelength-dependent: longer wavelengths generate smaller number of lesions (9). Although UVB and UVC efficiently generate both types of lesions, UVA generates only small quantities of CPD lesions and is nearly incapable of inducing 6-4PP lesions (10, 11). Compared to CPD, 6-4PP lesions are 8-fold less frequently generated by the physiologically relevant spectrum UVB or 4-fold less frequently

generated by high-energy UVC (8). Upon further irradiation with wavelengths longer than 290 nm, 6-4PP lesions can be converted via the photoisomerization reaction into Dewar valence isomers (12, 13). Structurally, CPD lesions arise from the formation of a four-membered ring involving C_5 and C_6 of two adjacent pyrimidine bases, whereas 6-4PP lesions are formed by a covalent bond between C_6 of one pyrimidine and C_4 of the adjacent pyrimidine (**Figure 1.3**). Due to the distinct pattern of dimerization, CPD and 6-4PP differentially distort the DNA helix: 6-4PP is more DNA-distorting (44º bending of DNA helix) than CPD (9º helix bending) (14, 15) (**Figure 1.4**).

CPD and 6-4PP exhibit distinct biological effects

CPD and 6-4PP lesions are simultaneously and instantaneously generated upon UV irradiation. Interestingly, these two major types of UV lesion exhibit distinct biological effects in several regards. Although both types of UV lesion block replicative polymerases and hence require specialized polymerases to bypass, the bypass process is less efficient and more error-prone for 6-4PP than CPD (16, 17). Moreover, while both types of UV lesions are associated with UV-induced apoptosis, 6-4PP lesions are more apoptotic than CPD on a per-lesion basis (18). To date, whether CPD and 6-4PP have differential contributions to UV-associated DNA damage response has not been investigated. A study to determine the respective effects of CPD and 6-4PP on DNA damage response pathways would provide insight into the fundamental mechanism by which cells sense UV lesions and in turn determine the balance of cellular outcomes, such as DNA repair, mutation incorporation, and cell death.

1.2 Repair of UV-induced DNA lesions: nucleotide excision repair (NER) and photorepair

NER is the primary DNA repair mechanism of UV lesions in humans

Nucleotide excision repair (NER) is an important mechanism for repair of a variety of bulky DNA lesions generated by environmental carcinogens including UV (19-21). In humans, UV-induced DNA lesions are primarily removed by NER. NER is composed of two subpathways: global genome NER (GG-NER) and transcription-coupled NER (TC-NER), which repair DNA lesions on nontranscribed and transcribed portions of the genome, respectively. Both GG-NER and TC-NER are multistep processes involving a recognition step that leads to partial unwinding of DNA surrounding the lesion, an excision step in which a lesion-containing oligonucleotide is removed, and gap-filling and ligation steps (**Figure 1.5**). While sharing many common factors, these two subpathways differ in their initial damage recognition steps. Specifically, GG-NER recognizes the DNA lesion through the XPC-RAD23B and UV-DDB/XPE protein complexes, whereas TC-NER is initiated by CSA and CSB upon blockage of RNA polymerase. Following the initial lesion recognition, the two subpathways are common in subsequent steps: The XPB and XPD helicases unwind the DNA duplex around the lesion, followed by the binding of RPA and XPA that facilitates the recruitment of other NER components. Next, the XPF and XPG endonucleases create dual incisions a few nucleotides away from the lesion to excise the lesion-containing oligonucleotide (~30 nt in length). The resulting single-stranded DNA (ssDNA) gap is then filled, using the undamaged strand as a template, by DNA polymerases δ, ε, and κ in mammalian cells (22-24). Notably, although NER repairs both CPD and 6-4PP lesions, the kinetics of GG-NER for CPD and 6-4PP are not identical. Indeed, although the underlying mechanism is unclear, the repair of 6-4PP by GG-NER is much faster than that of CPD lesions (2 hr half-life for 6-4PP versus 33 hr for CPD) (25). It is plausible that the greater speed of repair of 6-4PP lesions is due to its more pronounced distortion of the DNA helix, and hence more rapid recognition by the XPC protein (21).

Genetic disorders caused by defective NER

The clinical relevance of NER components is highlighted by DNA repair disorders in humans: xeroderma pigmentosum (XP), Cockayne syndrome (CS), and trichothiodystrophy (TTD) (26). XP is an autosomal recessive disorder characterized by hypersensitivity to UV-induced DNA lesions and high frequency of skin carcinogenesis. Patients with XP are classified into eight genetic complementation groups (XP-A to XP-G and XP-Variant (XP-V)), based on defects in eight different genes that encode proteins involved in NER. Notably, XP-V is not defective in NER but is abnormal in the ability to continue replication following UV-induced DNA damage. In contrast to XP, neither Cockayne syndrome nor trichothiodystrophy patients are predisposed to skin cancer development, perhaps in part because they typically do not survive long enough to be at risk for skin cancer development (27). CS is related to mutations in CSA and CSB genes, leading to a defective TC-NER subpathway, neurological/developmental abnormalities, and a severely reduced lifespan. Patients with TTD (caused by mutations in XPB, XPD, and TTD genes) are characterized by short, brittle hair and developmental defects.

Photorepair – a UV lesion-specific repair system

Many organisms are equipped with another repair system – photorepair – to eliminate UV-induced DNA lesions (28, 29). In contrast to the complexity of the NER pathway, photorepair is mediated by a single enzyme, a “photolyase”, which directly converts UV lesions back to the original structure, in the process using visible light as an energy source (**Figure 1.6**). Notably, photolyases exhibit substrate specificities to either CPD lesions (CPD-photolyase) or 6-4PP lesions (6-4PP-photolyase), and so far, no photolyase has been shown to repair both types of lesion. Photolyases are employed in bacteria, lower eukaryotes, plants, and some animals including marsupials. However, this repair system is absent in human and other placental mammals (e.g., mice), implying that photolyase genes have been lost during evolution. Although

it is unclear why photolyases would have been lost evolutionarily, NER could be more advantageous than photolyases in lesion repair because NER-mediated repair does not require the energy of light and hence is not limited to times when daylight is available.

1.3 DNA damage checkpoints

DNA damage checkpoints are mechanisms by which cells sense and cope with various types of DNA damage, coordinating cellular processes such as cell cycle arrest, DNA repair, and apoptosis (30). Ataxia telangiectasia mutated (ATM) and ataxia telangiectasia and Rad3-related (ATR) are key regulators that are activated by DNA damage and initiate signal transduction pathways for the DNA damage checkpoints. Both ATM and ATR are phosphoinositide 3-kinase (PI3K)-related protein kinases (PIKKs), exhibiting a similar overall structural organization (31) and a preference for phosphorylating Ser or Thr residues followed by Gln (the minimum ATM/R phosphorylation motif SQ or TQ) (32). These two kinases are activated by different types of DNA damage: ATM is activated primarily by DNA double-strand breaks, whereas ATR is activated by stalled DNA replication (33). Given the fact that ATR plays a critical role in coping with aberrant DNA replication blockage that may otherwise lead to genomic instability, elucidating the mechanism of ATR activation is of considerable importance in cancer prevention and therapy.

ATR activation

The initial step of ATR activation is the formation of single-stranded DNA (ssDNA) following DNA damage such as UV irradiation (30) (**Figure 1.7**). Specifically, UV irradiation induces DNA lesions that block replicative polymerases but not MCM (minichromosome maintenance) helicases. Uncoupling of DNA unwinding (by MCM helicases) from DNA synthesis (by replicative polymerase) generates long stretches of ssDNA that are then bound by replication protein A (RPA), an ssDNA-binding protein. This RPA-coated ssDNA recruits ATR kinase through its functional partner, ATR-interacting protein (ATRIP), thereby enabling the ATR-ATRIP complex to localize to the sites of DNA damage. The localization of ATR-ATRIP to the DNA damage sites, however, is not sufficient to fully activate the ATR kinase. Instead, it

requires the recruitment of additional mediator proteins, including Rad17-RFC complex, the Rad9-Rad1-Hus1 (9-1-1) complex, and TopBP1. Rad17-RFC complex facilitates the binding of 9-1-1 to DNA (34), leading to the recruitment of TopBP1 in proximity to the ATR-ATRIP complex at a stalled replication fork (35-38). TopBP1 then stimulates the kinase activity of ATR for full activation (39-41) and facilitates ATR to interact with its substrates (42).

Essential functions of ATR

Once the ATR activation complex has been assembled in response to replication stalling, ATR phosphorylates its downstream targets, including Chk1 and p53 that are transiently localized to sites of DNA damage on chromatin (30, 43, 44). Phosphorylated Chk1 is then released from chromatin and diffuses globally throughout the nucleus to transmit checkpoint signaling (45-47). Notably, ATR phosphorylates Chk1 at Ser345 (48, 49), which is required for robust activation of the Chk1 kinase (50). A key target of the Chk1 kinase is CDC25, a phosphatase that promotes cell cycle transition into mitotic (M) phase by dephosphorylating cyclin-dependent kinases (51). Phosphorylation of CDC25 inhibits its phosphatase activity, leading to G_2 arrest (52-54). Therefore, the ATR-Chk1 pathway is critical for preventing mitotic entry following DNA damage (48, 55). ATR is also required to inhibit new origin firing (56), thereby ensuring a sufficient quantity of available RPA to bind ssDNA (57) and stabilizing stalled replication forks (58). Inhibition of ATR in cells with DNA damage results in premature chromatin condensation, a hallmark of premature entry into mitosis before completion of DNA replication (59). Thus, the ATR pathway plays an important role in ensuring DNA replication after genotoxic stress (33).

ATR inhibition suppresses UV carcinogenesis

Although ATR has been thought to play a role in the maintenance of genomic integrity, surprisingly, several lines of evidence suggest that ATR inhibition could suppress UV

carcinogenesis. Indeed, previous studies showed that oral intake or topical application of caffeine (a nonspecific ATR inhibitor) reduces the incidence of UV-induced skin cancer development in mice (60, 61). In addition, with chronic UV treatment, transgenic mice expressing a kinase-inactive form of ATR in skin had 69% fewer tumors, compared to littermate controls with normal ATR function (62). In parallel, multiple human epidemiological studies have revealed that coffee or tea intake decreases the risk of UV-associated nonmelanoma skin cancers (63-67). Most importantly, consumption of caffeinated coffee (but not decaffeinated coffee) is associated with a dose-dependent decrease in the risk of developing nonmelanoma skin cancers (65, 67). The cancer-preventive effect of caffeinated beverage intake is likely due to ATR inhibition. Mechanistically, caffeine or ATR inhibition can augment UV-induced apoptosis (68-70), eliminating DNA-damaged cells and reducing the likelihood of these cells to develop into cancer. A better understanding of the mechanism by which UV activates ATR thus has implications for the prevention of UV-induced skin cancers.

1.4 Mechanisms to cope with unrepaired DNA damage: translesion synthesis (TLS) and repriming

DNA replication carried out by replicative polymerases (polymerase ε and δ) in a highly accurate manner is of upmost importance to cells. However, these high-fidelity polymerases are intolerant to any alteration of nucleotides in the template DNA. The presence of an altered base, if not repaired, causes stalling of replication forks, increasing the possibility of fork collapse and cell death. To cope with these DNA lesions, cells mainly rely on two mechanisms – translesion synthesis and repriming – to ensure the completion of replication (**Figure 1.8**). For translesion synthesis, the replicative polymerases are replaced by specialized polymerases to continue DNA synthesis past the damaged nucleotides. For repriming, DNA synthesis restarts downstream of the DNA lesions, leaving an ssDNA gap that is then filled subsequently through a separate process. These two mechanisms may promote cell survival by facilitating completion of DNA replication; however, mutations may be incorporated because low-fidelity polymerases are involved in these processes.

Translesion synthesis (TLS)

Translesion synthesis (TLS) is an evolutionarily conserved process that allows replication across DNA lesions using specialized polymerases. In eukaryotes, DNA polymerases (Pol) specialized in TLS are Pol η, Pol κ, Pol ι, and Rev1 in the Y-family, and Pol ζ in the B-family of the DNA polymerases (71). Replicative and TLS polymerases possess the same basic structure consisting of “fingers”, “thumb”, and “palm” domains. However, “fingers” and “thumb” domains of TLS polymerases are small, thereby creating additional flexibility to accommodate a distorted DNA template (72-74) (**Figure 1.9**). Because of this property, it is generally supposed that TLS polymerases could replicate across lesions by relaxing the

Watson-Crick base pairing between an incoming dNTP and the distorted DNA template. In addition, unlike replicative polymerases, TLS polymerases lack 3'-to-5' exonuclease proofreading activity (75, 76). These features of TLS polymerases may decrease the fidelity of DNA replication and, hence, TLS is often considered to be error-prone. Indeed, compared to replicative polymerases with error rates of 10^{-6} to 10^{-8} (77), TLS polymerases insert approximately one incorrect nucleotide for every 10 to 10^3 bases replicated (75, 77, 78). Notably, TLS polymerases have different substrate specificities and, in some circumstances, could be relatively error-free, depending on the DNA lesion and the TLS polymerases used. For example, Pol η reliably and accurately incorporates two adenines opposite a thymine-thymine CPD (TT-CPD) (79). Underscoring the significance of pol η, mutations in the *POLH* gene encoding Pol η in humans result in the variant form of xeroderma pigmentosum (XP-V) (80, 81). Importantly, although XP-V patients have normal DNA repair capacity, defective Pol η results in predisposition to UV-associated skin cancers (26, 82).

How does TLS work?

TLS requires stepwise polymerase switches between replicative (high-fidelity) and TLS (low-fidelity) polymerases (75, 83, 84) (**Figure 1.10**). Specifically, stalled replicative polymerases are exchanged with TLS polymerases to insert a nucleotide opposite a DNA-distorting lesion in an error-prone manner and extend from the mismatched base pair (85). After TLS polymerases synthesize a short stretch of nucleotides beyond the lesion (typically 5 to 60 nt; 20 nt on average) (86), a further polymerase switch occurs to reinstate the replicative DNA polymerases and resume accurate DNA synthesis. These stepwise polymerase switches ensure that low-fidelity TLS polymerases are employed only for a short stretch of nucleotides beyond the DNA-distorting lesion, minimizing the likelihood of mutation incorporation.

How is TLS regulated?

The regulation of TLS is coordinated by PCNA (proliferating cell nuclear antigen), a homotrimeric protein complex that encircles double-stranded DNA and functions as a DNA sliding clamp to strengthen the interaction between DNA template and polymerase and promote the processivity of replicative DNA polymerases. In response to DNA damage, PCNA is mono-ubiquitinated by Rad6-Rad18 to facilitate the recruitment of TLS polymerases that contain evolutionarily conserved ubiquitin-binding domains (UBM and UBZ) (87, 88). Interestingly, several studies suggest that ATR may also be involved in the recruitment of certain TLS polymerases to sites of DNA damage. It has been shown that ATR-mediated phosphorylation of polymerase η facilitates its intracellular translocation to stalled replication fork (89), which is seen as formation of foci in the nucleus, and is necessary for efficient bypass of UV lesions (90). In addition, Mec1 (homolog of mammalian ATR) kinase activity promotes the recruitment of the polymerase ζ-Rev1 complex to DNA double-strand breaks (91). Although a regulator role of ATR in TLS has been suggested, whether ATR promotes bypass of a specific type of UV lesion awaits further investigation.

Repriming

In addition to TLS that enables DNA synthesis opposite UV lesions, stalled DNA replication can be resolved by repriming. In the repriming model, a new primer is synthesized downstream of a replication-blocking lesion, leaving a small ssDNA gap, to resume DNA replication (**Figure 1.8**). This model is supported by previous findings: discontinuous elongation of replication forks (92) and accumulation of ssDNA gaps along UV-damaged replicated duplexes (93).

Repriming requires a primase activity to synthesize a new primer downstream of a DNA lesion. It has been shown that the DNA polymerase α-primase complex initiates DNA synthesis

of the leading strand at each origin and synthesis of each Okazaki fragment in the lagging strand by synthesizing a short RNA primer (8–12 ribonucleotides) extended by the addition of ~20 deoxyribonucleotides (94); however, it remained elusive whether the DNA polymerase α-primase complex is responsible for repriming following UV irradiation. Recently, PrimPol was identified as an enzyme that has primase and TLS polymerase activities and promotes repriming following UV (95, 96). The primase activity of PrimPol preferentially uses deoxyribonucleotides, unlike conventional RNA primases that use ribonucleotides, and thus PrimPol is well suited for repriming as it minimizes the need for RNA processing (97).

Repriming and TLS are not mutually exclusive, and these two processes likely cooperate to complete DNA replication in the presence of DNA lesions (92, 98). Upon replication blockage, DNA replication can efficiently resume downstream of a DNA lesion via repriming. This leaves a small ssDNA gap, but the gap could be filled by TLS after completion of bulk replication. Indeed, it has been shown that TLS operates effectively after chromosomal replication, outside S phase (99).

1.5 UV mutagenesis and carcinogenesis

UV signature mutation and carcinogenesis

UV-induced DNA lesions are normally removed by nucleotide excision repair, preventing mutation incorporation. Unrepaired DNA lesions lead to genetic mutations through deamination or error-prone translesion synthesis (**Figure 1.11**). Unrepaired cytosine-containing CPDs contribute to characteristic "UV signature mutation": cytosine (C) to thymine (T) (or CC to TT) transition at dipyrimidine sites. UV signature mutations in the *p53* gene are found in over 50% of the most common types of skin cancer (basal cell carcinoma (BCC) and squamous cell carcinoma (SCC)) (100, 101) as well as in actinic keratosis, a precursor for SCC (102). These "UV signature" mutations occur most frequently at nine mutation hotspots in important functional regions of the *p53* gene (100).

Mutations in the *p53* tumor suppressor gene play a critical role in UV carcinogenesis. Sunlight mutates *p53* early; Normal sun-exposed skin carries clonal patches of *p53*-mutated keratinocytes, 60–3,000 cells in size (103). These clones are present at frequencies exceeding 40 cells per cm^2 (as much as 4% of the epidermis). Mutations in genes responsible for carcinogenesis (e.g., *p53*) confer mutator phenotype including resistance to apoptosis. Once a *p53* mutation arises, subsequent UV exposures eliminate UV-damaged normal cells but spare apoptosis-resistant p53 mutants (104, 105), and thus, sunlight is a key driver of clonal expansion of p53 mutants. Although clonal expansion of mutant cells increases opportunities to receive additional mutations for tumor development, UV carcinogenesis is a long process requiring many hours of UV irradiation. The cumulative dose of sunlight required to cause BCC or SCC in adults is fairly large, approximately 10,000 and 70,000 hours of exposure, respectively (106). Compared with the general population, xeroderma pigmentosum patients (deficient in repair of UV-induced DNA lesions) under the age of 20 years have a 10,000-fold

increase in the frequency of UV-associated skin cancers, highlighting the importance of DNA repair in cancer prevention (26).

Mutagenicity of CPD

CPD is considered to be the major mutagenic lesion because CPD is the most abundant type of UV-induced DNA lesions and is slowly repaired by NER. Bypass of CPD is preferentially mediated by Pol η in a relatively accurate manner (107, 108). In the absence of Pol η (as in XP-V patients), mutation frequency is significantly increased, suggesting that Pol η plays a pivotal role in minimizing mutagenesis (107, 108). Although TLS by Pol η is relatively error-free, Pol η could be involved in UV mutagenesis (**Figure 1.11**). Spontaneous deamination of cytosine (C) or 5-methylcytosine (mC) base within a CPD lesion converts these bases to a uracil (U) or thymine (T), respectively (109-112). Error-free TLS of a deaminated CPD by Pol η correctly inserts an adenine (A) opposite the U or T base (113, 114). At the next round of replication, replicative polymerase correctly inserts a thymine opposite an adenine, finally leading to the C-to-T UV signature mutation. Notably, CPD can be bypassed by error-prone TLS: Pol ι frequently misinserts a nucleotide opposite a CPD lesion (115, 116). Also, Pol κ and Pol ζ can facilitate mutagenic bypass of CPD by extending from the mismatched base pair (108, 117).

Mutagenicity of 6-4PP

Due to the fact that 6-4PP lesions are less frequently generated and are more rapidly repaired, the contribution of 6-4PP lesions to UV mutagenesis has been thought to be less significant than CPD lesions. However, if not repaired, bypass of 6-4PP lesions is highly mutagenic (16), because there is no TLS polymerase capable of 6-4PP bypass in an error-free manner. TLS of 6-4PP is more complicated and inefficient than that of CPD. The TLS of 6-4PP requires two polymerases that sequentially act as an inserter and as an extender (117). Pol η,

Pol ι, and unexpectedly Pol δ often misinsert a nucleotide opposite a 6-4PP lesion (the insertion step) but cannot extend from the inserted nucleotide (115, 118, 119). The extension step essentially requires pol ζ (117, 120). Therefore, 6-4PP bypass is slow and mutagenic (16).

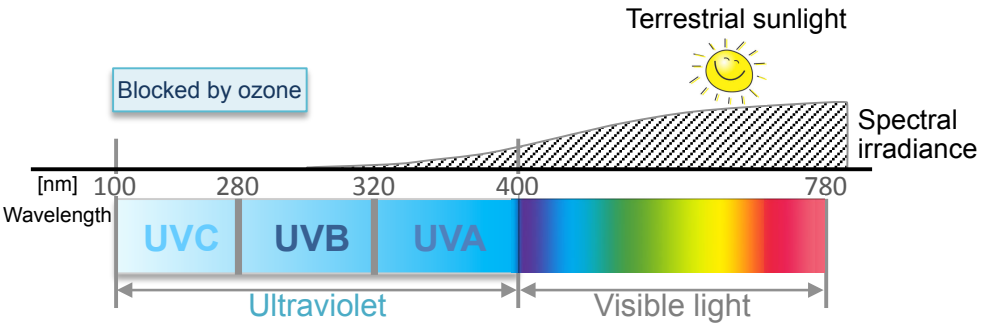

Figure 1.1 The subdivisions of the solar UV spectrum.

Shorter UV wavelengths are blocked by stratospheric ozone. Terrestrial sunlight contains UVA and UVB components at wavelengths of ~300 nm and longer.

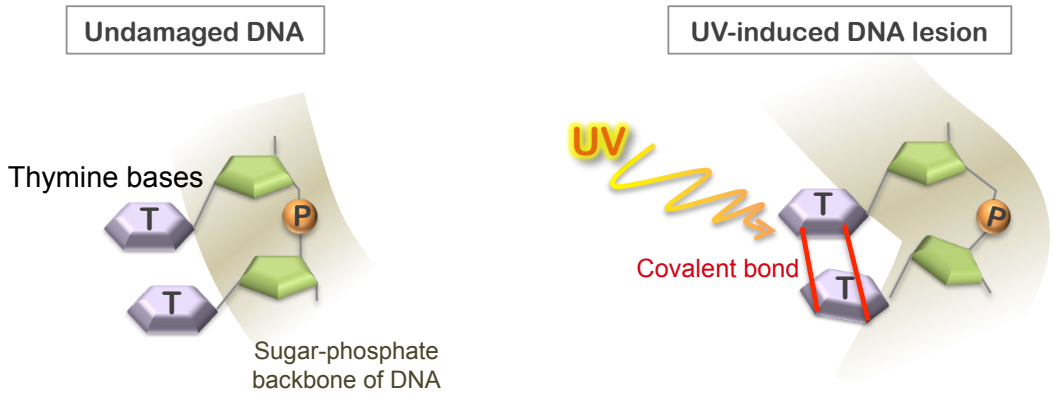

Figure 1.2 UV generates DNA lesions at dipyrimidine sites.

UV lesions (pyrimidine dimers) are formed through a photochemical reaction at dipyrimidine sites, where two pyrimidine bases (two thymines are shown as an example) are juxtaposed in tandem in the nucleotide sequence of DNA, following direct UV energy absorption by DNA bases.

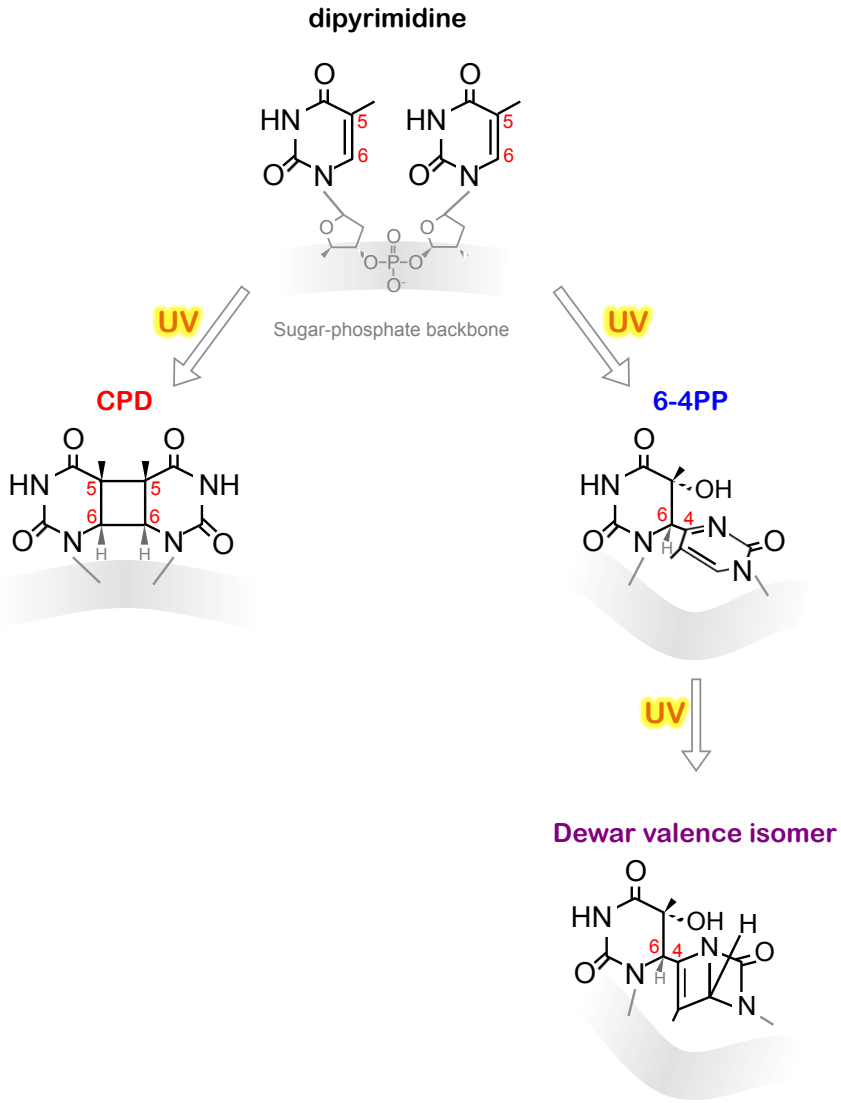

Figure 1.3 UV generates distinct pyrimidine photoproducts.

Cyclobutane pyrimidine dimer (CPD) corresponds to the formation of a four-membered ring involving C5 and C6 of adjacent pyrimidine bases. Pyrimidine (6-4) pyrimidone photoproduct (6-4PP) is formed by a noncyclic bond between C6 and C4 of adjacent pyrimidine bases. Upon exposure to long-wavelength UV irradiation, 6-4PP is further converted to Dewar valence isomer.

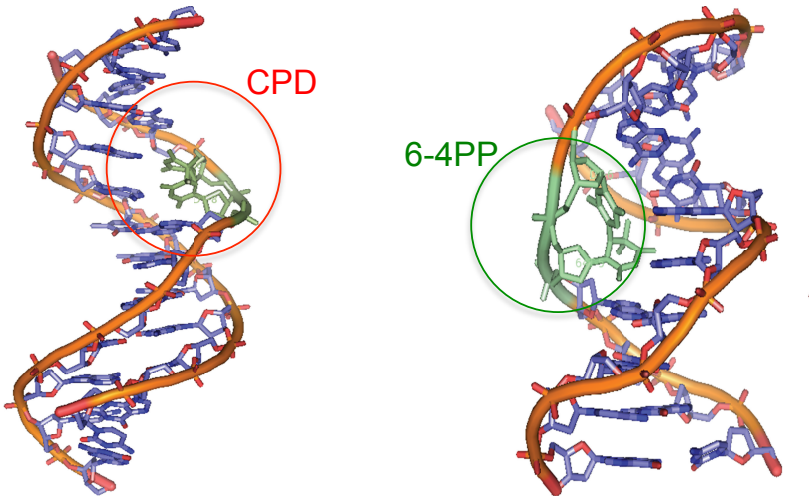

Figure 1.4 UV-induced DNA lesions distort DNA helix.

A 6-4PP lesion (right) distorts the DNA helix severely, whereas a CPD lesion (left) distorts DNA more mildly. Adapted with permission from Rastogi RP, et al. J Nucleic Acids (2010) 2010:592980.

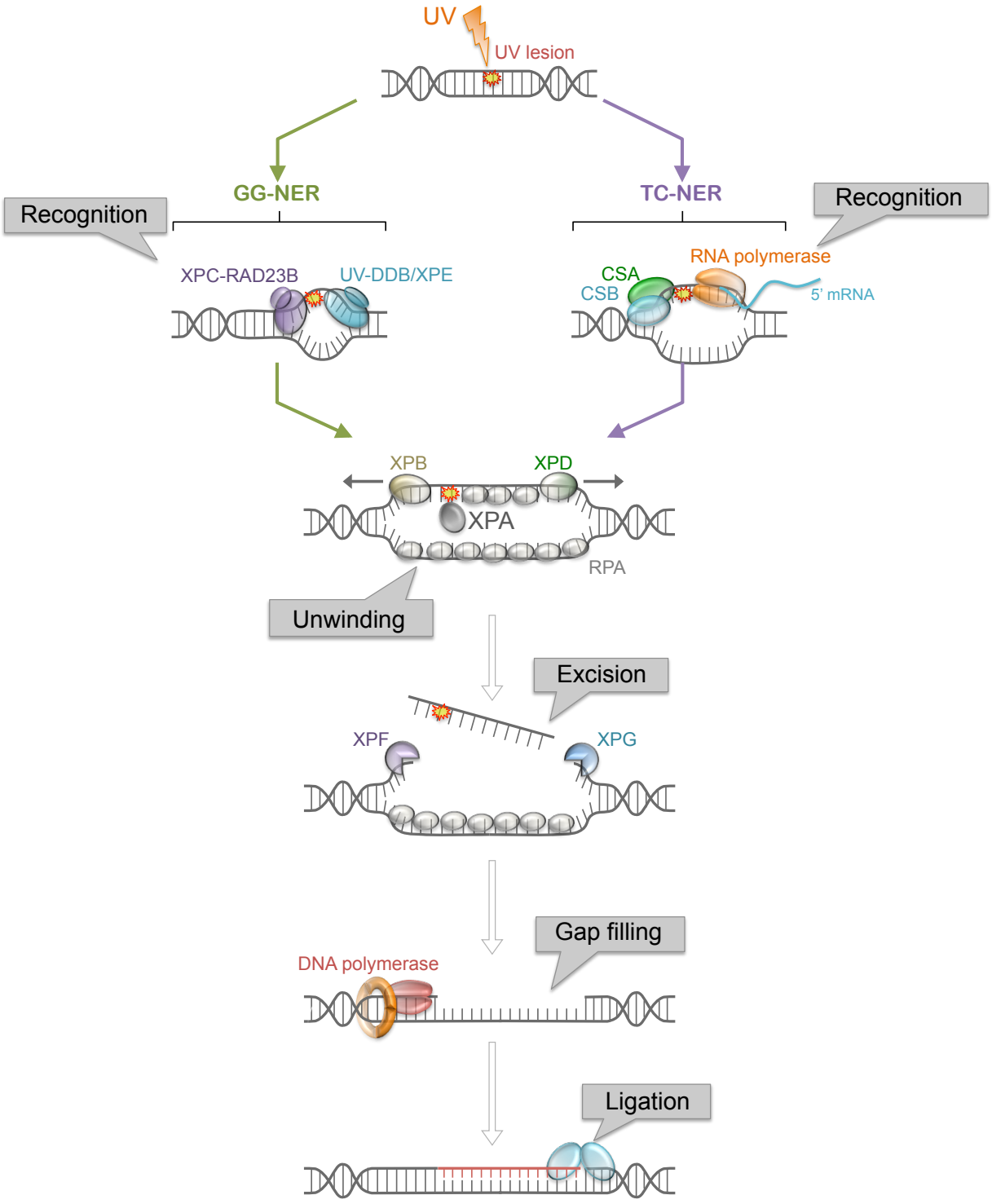

Figure 1.5 Nucleotide excision repair (NER).

In the global genome NER (GG-NER; top left) subpathway, the damage sensor complex XPC-RAD23B, with the help of UV-DDB/XPE, recognizes the UV lesions. In the transcription-coupled

NER (TC-NER; top right) subpathway, UV lesions are sensed during transcript elongation by the stalling of RNA polymerase, leading to the binding of CSA and CSB that initiate the repair process. After lesion recognition, the DNA duplex surrounding the lesion is unwound by XPB and XPD helicases. Unwound strands are stabilized by replication protein A (RPA), and XPA binds to altered nucleotides on ssDNA. XPA then recruits XPF and XPG to make dual incisions 5' and 3' to the lesion. The lesion-containing oligonucleotide (22-30 nt) is excised, resulting in an ssDNA gap that is subsequently filled by DNA polymerases. The NER is completed after ligation of the nick following gap filling. Modified from Marteijn JA, et al. Nat Rev Mol Cell Biol (2014) 15:465.

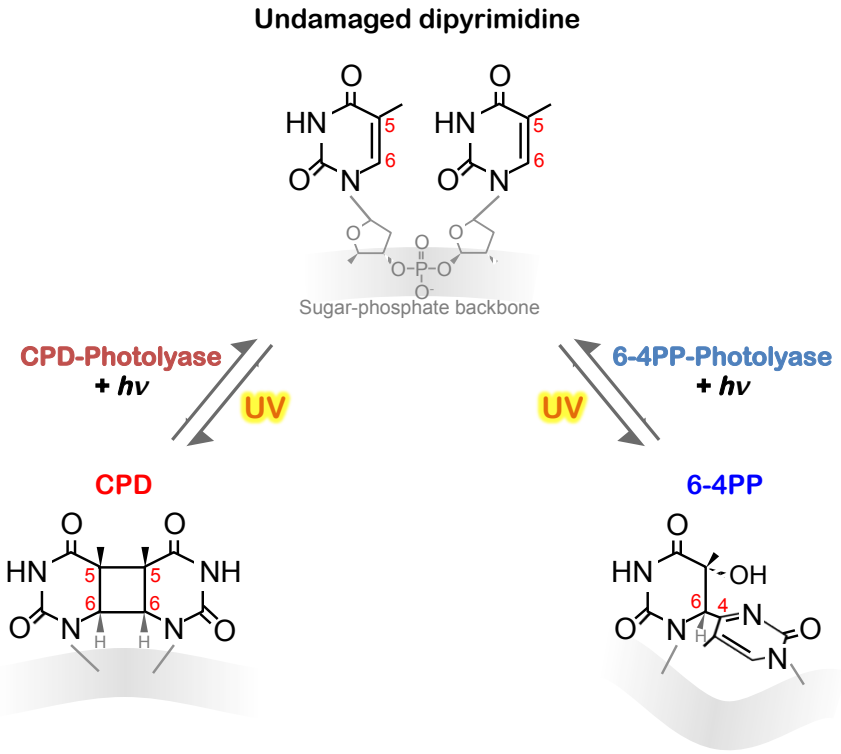

Figure 1.6 Light-dependent, lesion-specific photorepair.

Photorepair mediated by photolyases directly converts CPD or 6-4PP to its original undamaged structure using the energy of visible light (*hν*). This photorepair does not involve damage excision or DNA synthesis.

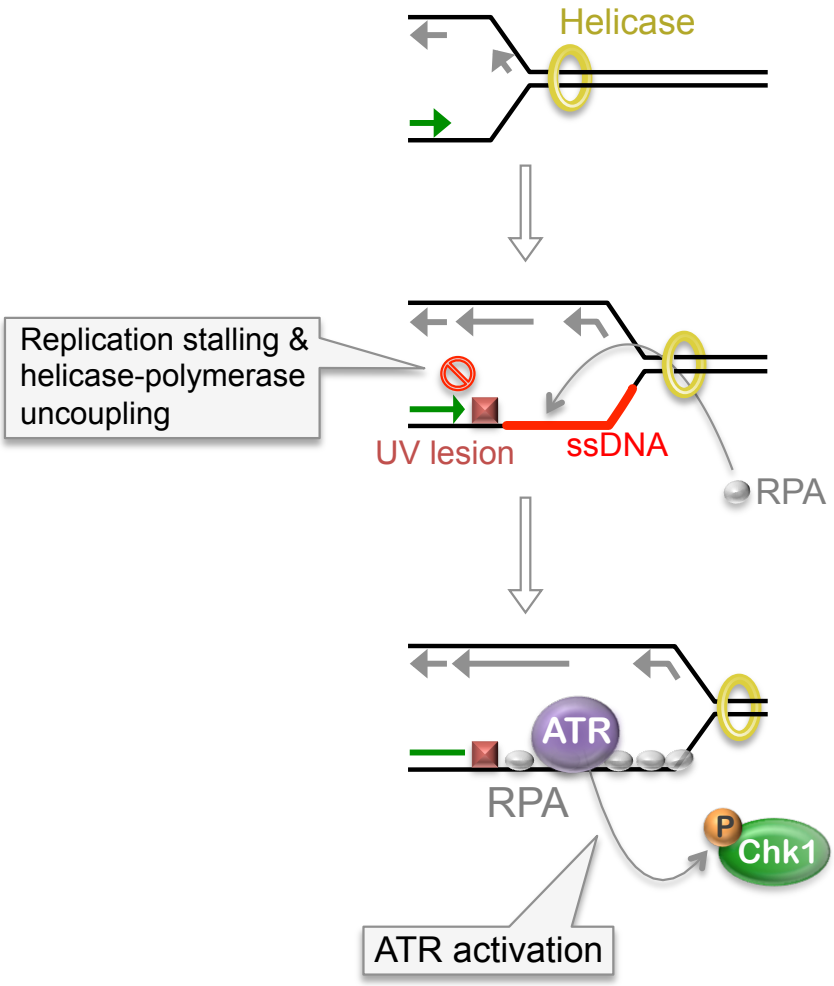

Figure 1.7 Model of ATR activation.

UV lesions block replicative polymerase, while replicative helicase continues unwinding the DNA duplex. Uncoupling of helicase and DNA polymerase generates long stretches of single-stranded DNA (ssDNA) that recruits ATR and promotes the assembly of relevant complex proteins (not shown). Activated ATR phosphorylates Chk1 and other substrates.

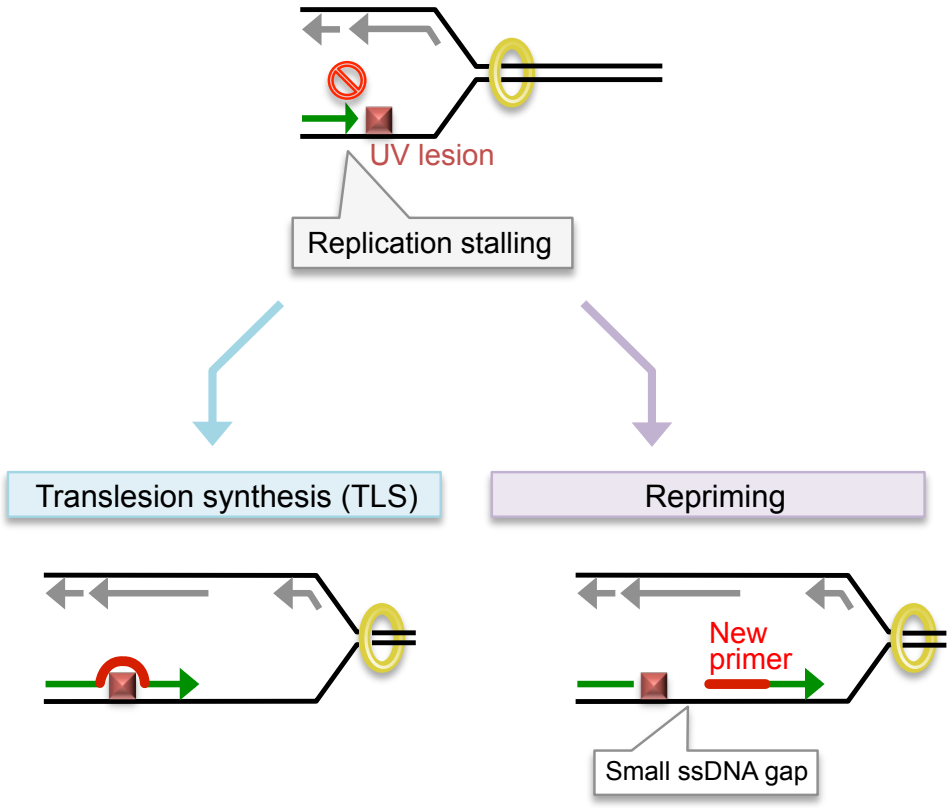

Figure 1.8 Model of DNA damage tolerance by two distinct mechanisms.
Following replication blockage at a UV lesion (depicted on the leading strand), DNA replication can continue by translesion synthesis (TLS) that inserts nucleotides opposite a lesion (left). Alternatively, a new primer can be synthesized downstream of a lesion, leaving a small ssDNA gap, to resume DNA replication (right).

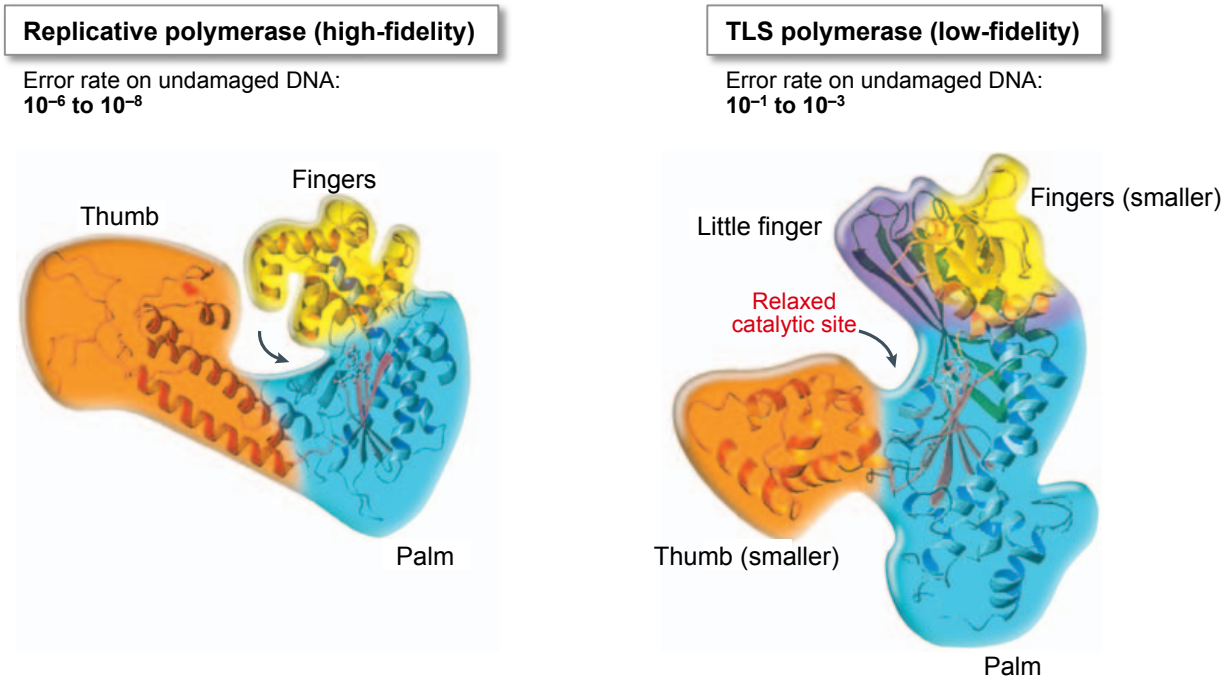

Figure 1.9 Structures of a high-fidelity replicative DNA polymerase and a low-fidelity TLS polymerase.

Compared to replicative polymerase (left), TLS polymerase (right) has unusually small "fingers" domain and "thumb" domain, resulting in a relaxed catalytic site (right black arrow). This highly accessible site accommodates mismatched base pairs as well as various DNA lesions. Adapted with permission from Friedberg EC. Nat Rev Mol Cell Biol (2005) 6:943. Error rates are taken from Kunkel TA. J Biol Chem (2004) 279:16895.

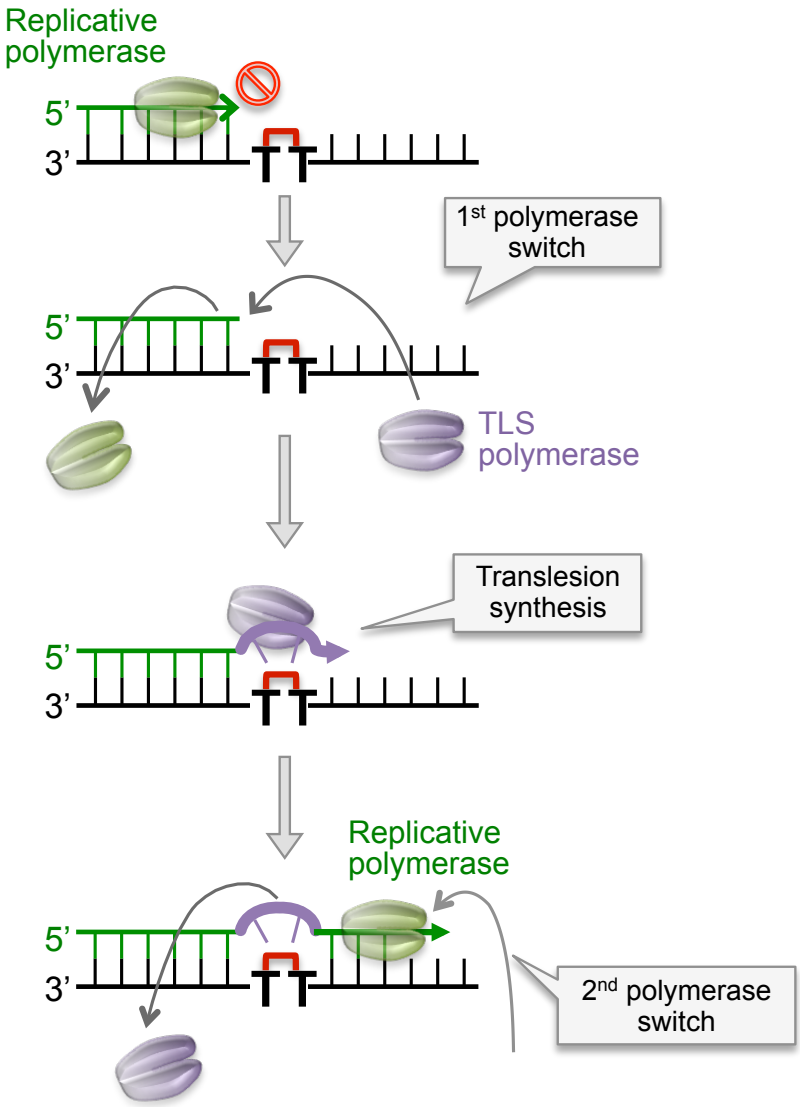

Figure 1.10 Stepwise polymerase switches during translesion synthesis (TLS).
When a replicative DNA polymerase (green) stalls at a UV lesion (red bracket), DNA polymerase is switched to TLS polymerase (purple). The TLS polymerase then inserts nucleotides opposite the DNA-distorting UV lesion but is error-prone. After passing the lesion, the second polymerase switch restores the replicative polymerase to the DNA template, and the high-fidelity DNA synthesis resumes.

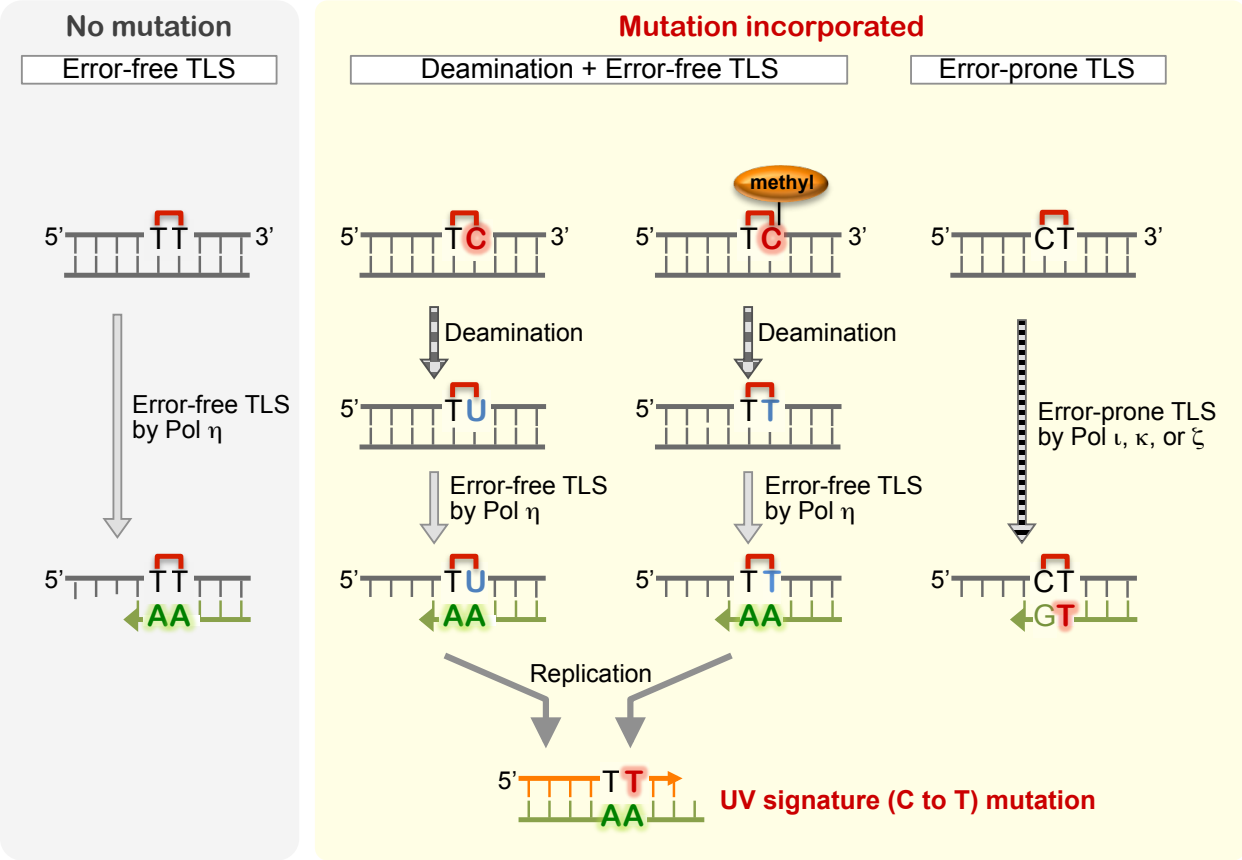

Figure 1.11 Multiple mechanisms by which CPD is bypassed with or without mutation incorporation.

(**Left**: Error-free TLS) CPD (red bracket) can be bypassed by Pol η which is relatively error-free. (**Middle**: Deamination + Error-free TLS) Cytosine or 5-methylcytosine within a CPD lesion is prone to spontaneous deamination, resulting in uracil or thymine, respectively. Bypass of deaminated CPD by "error-free" Pol η leads to "mutation" incorporation.

(**Right**: Error-prone TLS) CPD bypass by other TLS polymerases (such as Pol ι, κ, or ζ) could be error-prone.

Chapter 2. How might cells sense UV-DNA lesions for DNA damage response activation?

2.1 Single-stranded DNA is essential for ATR activation

The mechanism of ATR activation has been extensively studied due to its critical role as a master regulator of cellular responses to DNA damage. Activation of ATR is triggered by single-stranded DNA (ssDNA), which is generated by uncoupling of helicases from DNA polymerases that are blocked at replication-stalling lesions. The critical role of ssDNA in ATR activation has been demonstrated in studies using purified human proteins (121), human cell-free extracts (122), and *Xenopus* egg extracts (123). Specifically, the size of ssDNA gap (flanked by double-stranded DNA) determines the level of ATR activation (123), and approximately 70 nt of ssDNA segment is required for the recruitment of ATR-ATRIP complex to ssDNA (121) and for ATR-mediated Chk1 phosphorylation (122). Thus, the ability of DNA lesion to block replication and subsequently generate ssDNA gap may determine the level of ATR activation. Thus far, it remains unclear whether the two major types of UV lesion (CPD and 6-4PP) are different in their abilities to induce ssDNA and activate the ATR pathway.

2.2 Efficiencies of translesion synthesis across CPD and 6-4PP are different

Replication stalling could be overcome by translesion synthesis (TLS), a process that employs specialized polymerases for nucleotide insertion opposite DNA lesions. Therefore, the efficiencies of TLS across distinct UV lesions may determine the ability of each lesion type to induce ssDNA formation and ATR activation. TLS efficiency across specific types of lesion has been investigated in cells using double-stranded plasmids with a single ssDNA gap opposite to either a CPD or 6-4PP lesion (16). In this system, filling of 6-4PP-containing ssDNA gaps is less efficient than that of CPD-containing gaps. This difference in TLS across CPD and 6-4PP is likely due to differential processivity of TLS polymerases for distinct lesion types. Indeed, it has been shown that polymerase η is sufficient for replication across CPD (124), whereas replication across 6-4PP requires a more complex mechanism often involving polymerases η and ζ (85). In this two-polymerase mechanism, polymerase η first inserts a nucleotide opposite the 3'-base of a 6-4PP, which is then extended by polymerase ζ to complete TLS across 6-4PP. Because polymerase η (the inserter polymerase) is particularly inefficient in nucleotide insertion opposite 6-4PP (85), the completion of TLS across 6-4PP may be delayed. As a consequence, ssDNA generated at 6-4PP lesions may persist, whereas ssDNA generated at CPD lesions could be short-lived. Although these previous studies indicate that TLS across 6-4PP lesions on plasmids or oligonucleotides is delayed (16, 85), it remains elusive whether or not DNA replication across the genome in the presence of 6-4PP is delayed.

Replication stalling can also be resolved by repriming, which is *de novo* primer synthesis downstream of a lesion to resume DNA replication. Efficient repriming may minimize the uncoupling of helicases and DNA polymerases, thereby reducing ssDNA formation and ATR activation. However, no prior study has determined whether repriming downstream of a CPD or 6-4PP lesion could occur with the same efficiency.

2.3 Outstanding question in the field of UV-induced DNA damage responses

The outstanding question, which is the main focus of the present study, is how cells sense UV-induced DNA lesions and activate DNA damage response pathways that control the balance of cellular outcomes between cell cycle checkpoint, lesion repair, mutation incorporation, and cell death. Two structurally distinct types of UV-induced DNA lesions (CPD and 6-4PP) may have different abilities to block DNA replication and activate the DNA damage response pathway. However, no prior studies have demonstrated the individual effect of each lesion type on the DNA damage signaling including the ATR-Chk1 pathway. Carrying out such studies has been difficult because thousands of CPD and 6-4PP lesions are instantaneously generated in cells, and because the ATR-Chk1 pathway is typically activated within minutes following UV irradiation. Cells with a specific type of UV lesion could be generated by using photolyases, which specifically eliminate either CPD or 6-4PP, in combination with NER deficiency that well preserves both types of lesion long after UV exposure (**Figure 2.1**). Dissection of the respective roles of CPD and 6-4PP in DNA damage responses will provide mechanistic insight into how cells sense UV lesions for diverse cellular outcomes.

2.4 Hypothesis and specific aims

Hypothesis

We hypothesize that two structurally distinct types of UV-induced DNA lesions (CPD and 6-4PP) have different abilities to block DNA replication and activate the ATR-Chk1 pathway.

Specific aims

In Aim 1, we will determine the individual contributions of two major types of UV lesions (CPD and 6-4PP) to activation of the ATR-Chk1 pathway.

In Aim 2, we will determine the mechanism by which one or more type(s) of UV-induced DNA lesions (CPD and 6-4PP) activate the ATR-Chk1 pathway.

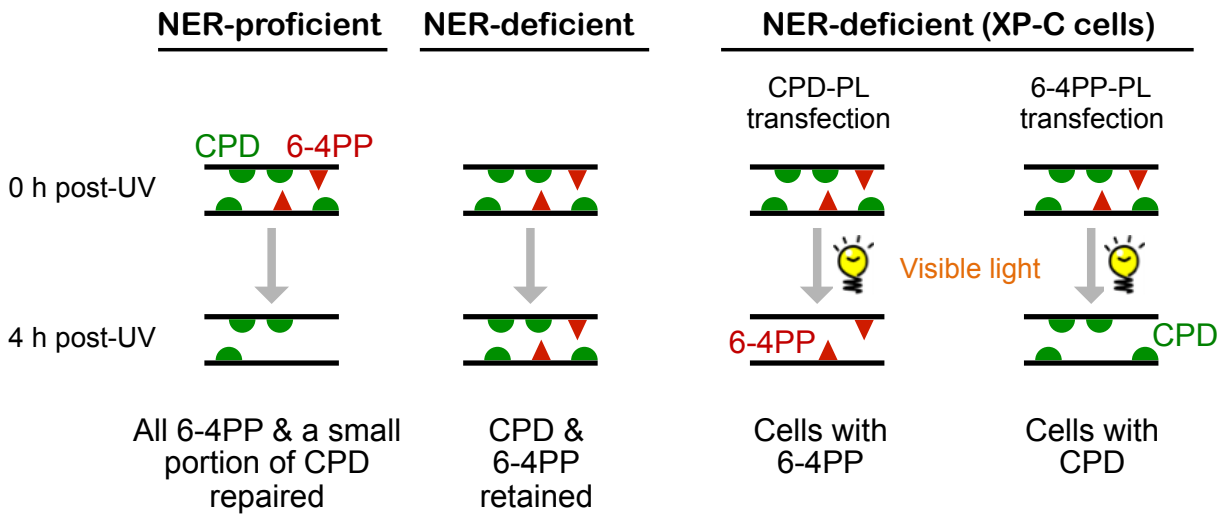

Figure 2.1 Generation of cells with a single type of UV lesion by combining NER deficiency and photolyases.

NER-proficient cells efficiently repair 6-4PP (2 h half-life for 6-4PP versus 33 h for CPD). NER-deficient cells (e.g., XP-C cells) are unable to repair both types of lesion. CPD-photolyase (CPD-PL) and 6-4PP-photolyase (6-4PP-PL) with visible light illumination specifically repair CPD or 6-4PP, respectively. By combining NER-deficient cells and transfection of lesion-specific photolyases, cells with a single type of UV lesion can be generated.

Chapter 3. UV-induced replication blockage and ATR activation are mediated by 6-4 photoproducts

Kai-Feng Hung,[1,2] Julia M. Sidorova,[3] Paul Nghiem,[1,4,*] and Masaoki Kawasumi[1,*]

[1]Division of Dermatology, Department of Medicine, University of Washington, Seattle, WA 98109, USA
[2]Department of Oral Health Sciences, University of Washington, Seattle, WA 98195, USA
[3]Department of Pathology, University of Washington, Seattle, WA 98195, USA
[4]Clinical Research Division, Fred Hutchinson Cancer Research Center, Seattle, WA 98109, USA

*Correspondence should be addressed to M.K. (kawasumi@uw.edu) or P.N. (pnghiem@uw.edu).

Contact Information
Masaoki Kawasumi, MD, PhD
Division of Dermatology, Department of Medicine, University of Washington
850 Republican Street, Brotman 242, Seattle, WA 98109, USA
Phone: 206-221-4594; Fax: 206-221-4364; E-mail: kawasumi@uw.edu

Paul Nghiem, MD, PhD
Division of Dermatology, Department of Medicine, University of Washington
850 Republican Street, Brotman 242, Seattle, WA 98109, USA
Phone: 206-221-2632; Fax: 206-221-4364; E-mail: pnghiem@uw.edu

3.1 Summary

The most prevalent human carcinogen is sunlight-associated UV, a physiologic dose of which generates thousands of DNA lesions per cell, mostly of two types: cyclobutane pyrimidine dimers (CPDs) and 6-4 photoproducts (6-4PPs). It has been difficult to determine the respective contributions of these two lesion types to the signaling events that regulate cell cycle progression, DNA replication, and cell death. Here we coupled multiparameter flow cytometry with lesion-specific photolyases that eliminate either CPDs or 6-4PPs and determined their roles in DNA damage responses. Strikingly, only 6-4PP lesions activated the ATR-Chk1 DNA damage pathway. Mechanistically, 6-4PPs, but not CPDs, impeded DNA replication across the genome as revealed by microfluidic-assisted replication track analysis. Furthermore, single-stranded DNA accumulated preferentially at 6-4PPs during DNA replication, indicating selective and prolonged replication blockage at 6-4PPs. These findings suggest that 6-4PPs, although 8-fold fewer in number than CPDs, are the major trigger for UV-induced DNA damage responses.

3.2 Introduction

Ultraviolet (UV) irradiation is the most prevalent carcinogen in humans, leading to diverse skin malignancies that outnumber all other cancers combined (2). UV often damages DNA by forming dimers at dipyrimidine sites, and approximately 100,000–200,000 DNA lesions are generated per diploid cell in human skin by a moderate dose of UV (1 hr of sunlight; equivalent to ~30 mJ/cm^2 UVB (280-320 nm)) (30, 125). UV-induced DNA lesions are critical in the pathogenesis of UV-induced skin cancer (126), and these DNA lesions are typically removed through the nucleotide excision repair (NER) pathway (127). NER is defective in xeroderma pigmentosum (XP), a genetic disorder characterized by UV hypersensitivity and predisposition to UV-induced skin cancer (26). UV generates two major types of DNA lesions: cyclobutane pyrimidine dimer (CPD) and pyrimidine (6-4) pyrimidone photoproduct (6-4PP). These two lesions are structurally distinct: 6-4PP is more DNA-distorting (44º bend of DNA helix) than CPD (9º helix bend) (15). Compared to CPDs, 6-4PPs are 8-fold less frequently generated by the cancer-relevant UVB spectrum (8) and are much more efficiently repaired by NER (2 hr half-life for 6-4PP versus 33 hr for CPD) (25).

In response to UV damage, cells activate DNA damage response pathways that elicit cell cycle checkpoints and DNA repair processes to maintain genomic integrity (30). During S phase, UV-damaged DNA causes replication fork stalling (128) that triggers activation of the ATR (ataxia telangiectasia and Rad3-related) kinase (129). Specifically, UV irradiation causes helicase-polymerase uncoupling: the replicative DNA polymerase stalls at a DNA lesion while the MCM (minichromosome maintenance) replicative helicase continues unwinding the DNA duplex (129). This uncoupling leads to generation of long stretches of single-stranded DNA (ssDNA) (93) that are then bound by replication protein A (RPA) (130). The RPA-coated ssDNA recruits ATR kinase through its functional partner, ATR-interacting protein (ATRIP), to sites of DNA damage (121, 131). Remarkably, more than 10 mediator proteins are recruited to the site

of DNA damage for full activation of the ATR pathway (132). Once the ATR activation complex has assembled in response to DNA damage, ATR activates downstream effectors by phosphorylating numerous targets including Chk1 and p53 (30, 43). ATR-mediated phosphorylation of the Chk1 kinase at Ser345 is critical for Chk1 activation (50) and preventing mitotic entry (48, 55). ATR is also required to inhibit new origin firing (56), thereby ensuring a sufficient quantity of available RPA to bind ssDNA and stabilizing stalled replication forks (57). Inhibition of ATR in cells with DNA damage results in premature chromatin condensation, a hallmark of premature entry into mitosis before completion of DNA replication (59). Thus, the ATR pathway plays an important role in ensuring DNA replication after genotoxic stress.

Although ATR promotes survival of cells after UV irradiation (68), such cells may be at high risk for incorporating DNA mutations. Thus, targeting ATR may be beneficial to prevent UV carcinogenesis. Remarkably, our prior study showed that skin-targeted genetic inhibition of ATR indeed suppresses UV-induced skin cancer development (62). These results suggest that UV-damaged cells, which have mutagenic lesions and thus have the potential to develop into cancer, may preferentially require ATR for survival. Compared to CPD, 6-4PP is more mutagenic (16, 133) and is more potent in inducing apoptosis on a per-lesion basis (18), implying that these two lesions are fundamentally different in triggering DNA damage responses. However, it remains unclear whether CPD and 6-4PP have distinct effects on activation of the ATR-Chk1 pathway that is a central regulator of cellular responses to UV irradiation. Understanding the precise signal for triggering the DNA damage response from each lesion type that has distinct mutagenic properties may provide the molecular basis for novel approaches to prevent UV carcinogenesis.

In the present study, we investigated the respective roles of CPD and 6-4PP in ATR activation by generating cells with only one major type of UV lesion. We employed CPD- and 6-4PP-specific photolyases, the enzymes that can specifically repair either type of lesion using the energy of visible light to convert a pyrimidine dimer in DNA back to its original structure (18, 29).

Surprisingly, we found that 6-4PP potently activates the ATR-Chk1 pathway, whereas cells with CPD lesions alone showed no evidence of ATR pathway activation. We also determined that only 6-4PP markedly blocks replication progression, a plausible mechanism for robust ATR activation mediated by this UV lesion type. Taken together, these findings provide mechanistic insight into how two structurally distinct UV lesions have remarkably different effects on cellular DNA damage responses.

3.3 Results

UV activates the ATR-Chk1 pathway exclusively in S phase

Phosphorylation of Chk1 at Ser345 by the ATR kinase is the hallmark indicator of ATR activation following UV irradiation (48, 49). To characterize the effect of UV lesions on the ATR pathway, we investigated the cell cycle-specific induction of Chk1 phosphorylation in cells that could or could not efficiently remove UV-induced DNA lesions by nucleotide excision repair (NER). Flow cytometry was used because of its capability to simultaneously assess multiple parameters including cell cycle status on a per-cell basis. In cells that are proficient in NER (HCT116: human colon carcinoma cell line with wild-type p53) (134, 135), UV-induced phosphorylation of Chk1 was detected exclusively in S phase, as assessed by multiparameter flow cytometry (**Figure 3.1A**). Similarly, NER-deficient cells (XP-C: immortalized fibroblasts derived from xeroderma pigmentosum complementation group C patient with no expression of XPC protein) (136) also exhibited strong correlation of Chk1 phosphorylation with S phase (**Figure 3.1B**). Thus, the specificity of Chk1 phosphorylation for S phase is not affected by the ability of cells to repair UV-induced DNA damage.

The S phase-specific induction of Chk1 phosphorylation was also examined through labeling replicating cells by incorporation of EdU, a thymidine analog. Indeed, Chk1 was phosphorylated exclusively in cells that were synthesizing DNA (EdU-incorporating), but not in non-S phase (EdU-negative) cells after UV irradiation (**Figure 3.1C**). Phosphorylation of Chk1 following UV was further examined by precisely discriminating cell cycle status based on a combination of EdU incorporation and DNA content (**Figure 3.1D**). Among five subpopulations based on cell cycle status (G_1, early S, S, early G_2, and G_2/M), UV-induced Chk1 phosphorylation was restricted to early S phase and S phase (**Figure 3.1E**). Importantly, phosphorylated Chk1 was entirely absent in G_1 phase (**Figure 3.1E**).

To determine the kinetics of Chk1 phosphorylation after UV irradiation, NER-proficient (HCT116) and NER-deficient (XP-C) cells were UV-irradiated and harvested at different time points up to 10 hr post-UV. Phosphorylation of Chk1 was rapidly induced by UV (within 30 min) in S phase in both cell types (**Figure 3.S1**). After peak induction, UV-induced phosphorylation of Chk1 declined in HCT116 cells (**Figure 3.S1A**) but was sustained in XP-C cells (**Figure 3.S1B**). Taken together, phosphorylation of Chk1 is induced rapidly and exclusively in S phase in both NER-proficient and NER-deficient cells. However, persistence of phosphorylated Chk1 following UV may be associated with the continued presence of UV lesions in cells.

Development of a flow cytometry assay that allows detection of both phosphoproteins and UV lesions

To dissect the role of each type of UV lesion in phosphorylation-mediated ATR signaling, an assay that allows detection of both phosphoproteins and UV-induced DNA lesions is needed. For UV lesion detection, antibodies that specifically recognize CPD or 6-4PP have been widely used. Anti-CPD (clone TDM-2) and anti-6-4PP (clone 64M-2) antibodies were established using UV-irradiated, heat-denatured single-stranded DNA (ssDNA) as the immunogen (137). This approach ultimately led to distinct mouse monoclonal antibodies that specifically recognize a single lesion type. Because these epitopes (CPD and 6-4PP) are likely obscured in double-stranded DNA (dsDNA), detection of UV lesions by these antibodies may require DNA denaturation. Hydrochloric acid (HCl) has been previously used to denature DNA prior to detection of UV lesions by flow cytometry (135), and we also observed that HCl allowed detection of the UV lesion signal (**Figure 3.S2A**). However, this strong acid treatment eliminated our ability to detect phosphorylated Chk1 (**Figure 3.S2B**). Because DNase I is an endonuclease that introduces random single-stranded nicks and can facilitate formation of ssDNA (138), we tested whether DNase I could be used to expose UV lesions to antibodies without destroying phosphoproteins. Indeed, DNase treatment enabled UV lesions to be efficiently detected

(**Figure 3.S2A**) while also preserving the ability to detect Chk1 phosphorylation (**Figure 3.S2B**). Therefore, this DNase-based flow cytometry assay represents a useful tool to investigate interactions between UV lesions and phosphorylation-associated signaling pathways.

Identification of cells expressing photolyase by flow cytometry

To determine the individual effect of CPD and 6-4PP lesions on ATR activation, it was necessary to generate cells that had a single type of UV lesion. Because NER has higher efficiency for 6-4PP than CPD, 6-4PP lesions are far more transient than CPD lesions in repair-competent cells (25). Thus, to retain both types of UV lesions for investigation, an NER-deficient XP-C cell line (GM15983) (136) was selected for this study. We also made use of lesion-specific photolyases, which are not present in humans, to selectively repair a single type of lesion (either CPD or 6-4PP) using the energy of visible light (18, 29). To identify the subpopulation of cells that express photolyase after transfection to human cell lines, CPD-photolyase (CPD-PL) or 6-4PP-photolyase (6-4PP-PL) cDNA was subcloned into a polyhistidine (His)-tagged mammalian expression vector.

In XP-C cells transfected with control vector (empty vector without photolyase), both CPD and 6-4PP persisted 2 hr after UV irradiation in the presence or absence of visible light (**Figure 3.2A, first row**). This validates the NER deficiency of this cell type and ensures that illuminating cells with visible light does not affect the levels of CPD and 6-4PP. After transfection of the relevant photolyase vector, cells expressing His-tagged CPD-PL or 6-4PP-PL (**Figure 3.2A, left**) were identified by flow cytometry for subsequent analysis. As expected, repair of each lesion type was restricted to cells that expressed the corresponding photolyase and were also exposed to visible light (**Figure 3.2A, second and third rows**). This light-dependent, lesion-specific repair (photorepair) occurred with the same efficiency regardless of cell cycle phase (DNA content) (**Figure 3.2A**). Notably, the difference in 6-4PP signals between sham and

UV was smaller than that of CPD, likely because 6-4PP lesions are known to be generated less frequently than CPD by the same dose of UV irradiation (8-fold less by UVB (8)).

To determine the duration of visible light illumination required for sufficient photorepair, the kinetics of photorepair were investigated. Sufficient photorepair of CPD or 6-4PP lesions generated by 30 mJ/cm^2 UVB irradiation required 1–2 hr exposure of visible light (**Figure 3.2B**). By combining flow cytometry with lesion-specific photolyase transfection in NER-deficient cells as well as sufficient visible light illumination, we were able to select cells carrying only a single major type of UV lesion (CPD or 6-4PP).

6-4PP, but not CPD, potently activates the ATR-Chk1 pathway

Although photolyases can selectively eliminate either CPD or 6-4PP, the specific role of each lesion type in DNA damage responses still cannot be determined if these responses had already been induced before lesion-specific photorepair was complete. To circumvent this problem, we designed a system in which CPD or 6-4PP lesions were eliminated in cells that had not yet entered S phase. After lesion-specific photorepair is complete in non-S phase cells, if these cells subsequently enter S phase, the effect of a single major type of UV lesion on ATR-Chk1 activation can be determined. Specifically, photolyase-transfected cells were labeled with EdU prior to UV irradiation to mark cells that were irradiated in S phase (**Figure 3.3A**). Immediately following UV irradiation, cells were illuminated with visible light for 2 hr to sufficiently photorepair the desired type(s) of lesion. Cells were then incubated in the dark for 7 hr to allow cell cycle progression and subsequently labeled with BrdU to identify cells that were in S phase at the time of harvest. In this experimental setting, EdU(–)BrdU(+) cells should represent the desired population: cells that were UV-irradiated outside S phase, underwent photorepair, and subsequently entered S phase with only the desired type(s) of UV lesion present.

To experimentally determine whether the EdU(–)BrdU(+) population was composed of cells that newly entered S phase after UV, cells were stained with propidium iodide (PI) to assess their cell cycle profile. The cell cycle status of non-replicating cells (EdU(–)BrdU(–)) showed DNA content equivalent to G_1 phase (**Figure 3.3B, blue line**), suggesting that this double negative population was likely in G_1 at the time of irradiation and remained in G_1 phase at harvest. In contrast, the EdU(–)BrdU(+) population had a cell cycle profile that was right-shifted toward higher DNA content (**Figure 3.3B, red line**) compared to that of EdU(–)BrdU(–), indicating that, as expected, this population was composed of cells that had newly entered S phase after UV.

The respective effects of CPD and 6-4PP on ATR-Chk1 activation could then be determined in cells that newly entered S phase with the desired lesion type (**Figure 3.3C**). In UV-irradiated cells that carried both CPD and 6-4PP (control), phosphorylation of Chk1 was robustly induced upon S phase entry (**Figure 3.3C, black bar**). In cells in which CPD was repaired but 6-4PP remained (CPD-PL), phosphorylation of Chk1 was induced to a level similar to UV-irradiated cells that still had both CPD and 6-4PP (**Figure 3.3C, gray bar**). In contrast, in cells that had newly entered S phase with only CPD remaining (6-4PP-PL), phosphorylation of Chk1 was not induced and stayed at the basal level equivalent to sham-irradiated control cells (**Figure 3.3C, hatched bar**). In cells that had neither CPD nor 6-4PP (CPD-PL + 6-4PP-PL), phosphorylation of Chk1 remained at a level equivalent to sham-irradiated control cells (**Figure 3.3C, white bar**). These results demonstrate that 6-4PP, but not CPD, has a potent ability to induce phosphorylation of Chk1. The same results were obtained from a separate XP-C cell line (GM16093) that is derived from a different XP-C patient (139) (**Figure 3.S3**), suggesting that the predominance of 6-4PP in inducing phosphorylation of Chk1 was not limited to a particular cell line. This striking difference in the abilities of CPD and 6-4PP to induce phosphorylation of Chk1 suggests that 6-4PP is the lesion responsible for UV-induced ATR activation, and that CPD does not have a role in activating the ATR-Chk1 pathway in S phase.

6-4PP lesions, but not CPD, delay DNA replication progression

Because 6-4PP is the main lesion type for activating the ATR-Chk1 pathway (**Figure 3.3C**), we hypothesized that 6-4PP may selectively block DNA replication progression. To assess replication progression in cells with a specific type of lesion, photolyase-transfected cells were pulse-labeled with two thymidine analogs (IdU and EdU) separately for 1 hr each and analyzed with microfluidic-assisted replication track analysis (maRTA) (140) (**Figure 3.4A**). Specifically, as an internal control for unperturbed DNA replication, cells were first labeled with IdU prior to UV (or sham) irradiation. Immediately following UV (or sham) irradiation, photolyase-transfected cells were illuminated with visible light for photorepair and were subsequently labeled with EdU to assess replication progression across a single major type of UV lesion. After harvest, cells expressing His-tagged photolyase were collected by flow sorting for subsequent analysis. DNA was then extracted from these sorted cells for quantitative analysis of replication progression in the presence of a specific type of lesion using maRTA. In this technique, pulse-labeled DNA is aligned on a glass slide using laminar flow through microchannels and is subsequently visualized by immunostaining for IdU and EdU. The length of each labeled DNA segment (replication track) was measured at the single molecule level for analysis. Because the same period of time (1 hr) was used for both labels, shorter track lengths of the 2nd label (after UV) compared to the 1st label (prior to UV) reflect delayed replication progression following UV.

Immuno-slot blot analysis using extracted DNA showed that each lesion type was repaired consistent with the expression of the relevant photolyase, validating lesion-specific photorepair in cells collected by flow sorting (**Figure 3.4B**). To assess replication progression in the presence of a specific type of lesion, replication track lengths of the 1st (pre-UV) and 2nd (post-UV and photorepair) labels were compared (**Figure 3.4C**). The lengths of replication tracks were not altered after sham irradiation and exposure to visible light, indicating that these

treatments had no effect on replication (**Figure 3.4C, upper panel**). In UV-irradiated cells with both CPD and 6-4PP remaining, track lengths of post-UV replication (2nd label, red) were shorter than those of pre-UV replication (1st label, green), indicating that replication is slowed by UV lesions (**Figure 3.4C, control vector, UVB**). Similarly, in UV-irradiated cells that had only 6-4PP remaining, track lengths were shorter in post-UV replication than in pre-UV replication, indicating that 6-4PP lesions potently slow replication progression (**Figure 3.4C, CPD-PL, UVB**). In contrast, in UV-irradiated cells that had only CPD remaining, track lengths of pre-UV and post-UV replication were essentially identical (**Figure 3.4C, 6-4PP-PL, UVB**). This indicates that CPD has no effect on replication progression, and that 6-4PP is critical for slowing replication. Consistently, in cells that had neither CPD nor 6-4PP, no difference of track lengths was observed between pre-UV and post-UV replication (**Figure 3.4C, CPD-PL + 6-4PP-PL, UVB**). Taken together, a combination of photolyase, flow sorting, and maRTA enabled the analysis of replication progression in cells with a single major type of lesion. Strikingly, we found that 6-4PP, but not CPD, is the critical type of lesion that effectively slows replication progression.

6-4PP lesions preferentially become surrounded by ssDNA during post-UV replication

Upon DNA replication blockage, ssDNA is typically generated adjacent to replication-blocking lesions after replicative helicases are uncoupled from stalled DNA polymerases (93, 129). If the antibodies used for detection of either CPD or 6-4PP are specific to lesions on ssDNA, replication-blocking lesions would thus be preferentially detected. Lesions that are unable to block DNA replication as well as those that have not encountered replication forks would reside in dsDNA, and UV lesions on dsDNA would therefore not be efficiently detected by such antibodies. To validate the specificity of the available antibodies (anti-CPD (TDM-2) and anti-6-4PP (64M-2)) (137) for their respective epitopes on ssDNA (but not on dsDNA), we compared lesion detection using DNA that was heat-denatured or left unheated. Genomic DNA

samples were prepared in two ways regarding the order of DNA extraction and UV irradiation: (i) genomic DNA was extracted from sham- or UV-irradiated cells ("in cells" irradiation), or (ii) genomic DNA was extracted from unirradiated cells and was then sham- or UV-irradiated outside of cells ("*in vitro*" irradiation). These two types of DNA samples were then left unheated or heated at 100ºC for denaturation. Immuno-slot blot analysis using an anti-ssDNA antibody showed strong signals in heat-denatured DNA receiving sham or UV irradiation (**Figure 3.5A, left**). This finding indicates that 10 min of 100ºC heat treatment is sufficient to generate ssDNA for antibody recognition. In these heat-denatured samples, CPD and 6-4PP were detected in UV-irradiated DNAs using the relevant antibody (**Figure 3.5A, middle and right**). In contrast, ssDNA was not detected in unheated samples, indicating that DNA remained double-stranded (**Figure 3.5A, left**). In these unheated samples that persisted as dsDNA, essentially no signals of CPD or 6-4PP were detected using lesion-specific antibodies even when DNAs were UV-irradiated (**Figure 3.5A, middle and right**). These results demonstrate that lesion-specific antibodies preferentially recognize CPD or 6-4PP lesions that are on ssDNA, but not on dsDNA.

Because ssDNA is generated adjacent to UV lesions that block DNA replication, the presence of ssDNA-surrounded lesions may reflect the level of replication blockage at each major type of UV lesion (133). Using the validated lesion-specific antibodies under non-denaturing conditions, we detected replication-blocking lesions that are left on ssDNA (**Figure 3.5B**). As a positive control, we treated fixed cells with DNase to detect UV lesions regardless of whether or not lesions were surrounded by ssDNA. In cells treated with DNase, CPD and 6-4PP were detected immediately after irradiation (**Figure 3.5B, blue population, UVB 0 hr**) and remained at a high level 10 hr post-irradiation (**Figure 3.5B, blue population, UVB 10 hr**) due to the deficiency of NER in XP-C cells. In contrast, in UV-irradiated cells without subsequent DNase treatment, both types of lesion were minimally detected immediately after UV irradiation (**Figure 3.5B, red population, UVB 0 hr**), as opposed to DNase-treated cells (**Figure 3.5B, blue population, UVB 0 hr**). This indicates that UV lesions were not surrounded by ssDNA

immediately after irradiation and therefore not accessible to the antibodies, likely because replication across UV lesions had not yet occurred. However, CPD and 6-4PP were partially detected only in S phase 10 hr after UV irradiation in cells without DNase treatment (**Figure 3.5B, red population, UVB 10 hr**). Because lesion detection under non-denaturing conditions was limited to S phase, it is likely that this signal resulted from replication blockage that generated ssDNA at these lesions.

To characterize the kinetics of replication blockage at CPD and 6-4PP, signals from ssDNA-surrounded CPD and 6-4PP were evaluated in cells harvested at different time points after UV irradiation. Signal intensities of CPD and 6-4PP were normalized relative to baseline ('zero'; sham irradiation at 0 hr) and '1.0' (UVB 30 mJ/cm^2 at 0 hr with DNase treatment). In S phase, the signal of ssDNA-surrounded CPD increased slightly after UV but remained at a low level for the duration of the experiment (**Figure 3.5C, left, DNase(–)**). Our finding that CPD lesions only very minimally became surrounded by ssDNA suggests that CPD lesions do not prolong replication blockage. In contrast, the 6-4PP signal markedly and continuously increased (**Figure 3.5C, right, DNase(–)**), indicating that 6-4PP preferentially became surrounded by ssDNA. This striking time-dependent increase in the signal of ssDNA-surrounded 6-4PP suggests that DNA synthesis across 6-4PP is impeded and that replication blockage at 6-4PP is prolonged.

3.4 Discussion

UV irradiation provokes diverse cellular responses to cope with DNA damage, most prominently via the ATR-Chk1 pathway (30). However, no prior studies have revealed the molecular mechanism by which one or more type(s) of UV-induced DNA lesion (CPD or 6-4PP) activates this pathway. Carrying out such a study has proven elusive because thousands of both types of lesion are instantaneously generated in UV-irradiated cells, and activation of the ATR-Chk1 pathway is rapidly initiated after UV (within 3 minutes) in S phase cells. Although photolyases are capable of selectively removing a specific type of UV-induced DNA lesion, photolyase-mediated repair requires more than an hour of visible light illumination for near-complete repair. We overcame these issues by combining photolyases, NER-deficient cells, cell cycle tracking, and multiparameter flow cytometry optimized to detect UV lesions, thymidine analogs, and phosphoproteins. This approach revealed the surprising finding that 6-4PPs, although fewer in number than CPDs, are the critical lesion type for activating the ATR-Chk1 pathway during S phase. In support of the specificity of this effect, we found that only 6-4PPs impede DNA replication and prolong replication blockage.

The finding that 6-4PPs mediate ATR-Chk1 activation is supported by independent experiments that compare cells that differ in UV lesion repair (NER proficient versus deficient). Specifically, as shown in **Figure 3.S1A** and in previous studies (68, 141), UV-induced Chk1 phosphorylation begins to decrease by 1–2 hr after irradiation in NER-proficient cells, coinciding with rapid repair of 6-4PP lesions (25, 134). In contrast, in NER-deficient cells in which neither CPDs nor 6-4PPs are repaired, phosphorylation of Chk1 after UV was sustained for at least 10 hr (**Figure 3.S1B**). Due to the fact that 6-4PP lesions have a half-life of 2 hr (versus 33 hr for CPD) in NER-proficient cells (25), the presence of unrepaired 6-4PP lesions is the major difference between NER-proficient and NER-deficient cells during this time frame. Thus, the striking difference in the kinetics of UV-induced Chk1 phosphorylation between these two cell

types supports the notion that 6-4PP is the pivotal lesion type required for the ATR-Chk1 pathway activation.

Our finding that replication tracks were unaffected by CPDs yet were strikingly shortened by 6-4PPs suggests that only the latter perturb replication fork progression following UV. This raises the question of how DNA replication proceeds essentially unimpeded in the presence of CPD, whereas 6-4PP lesions are strongly inhibitory to replication progression. Prior studies suggest that there are two major mechanisms by which DNA replication can continue following replicative polymerase blockage: direct bypass across a lesion via translesion synthesis (TLS) (16, 75), or replication restart downstream of a lesion via repriming (92). Therefore, a plausible explanation for our findings is that TLS and/or replication restart is very efficient at CPD lesions but is delayed at 6-4PP lesions. Thus far, it remains unclear whether and how cells preferentially employ TLS or replication restart for a specific type of lesion. Replication restart occurs downstream of a lesion, leaving an ssDNA gap that could span 400 nucleotides (93). Of note, these ssDNA gaps are too short to be reliably detected in the maRTA assay we used (detection limit is 3 μm, equivalent to 12 kb). However, ssDNA gaps of this size are more than sufficient to be identified by lesion-specific antibodies that can recognize either CPD or 6-4PP contained within only 8 bases of ssDNA (137). After verifying the ssDNA-specificity of these antibodies, we found that CPD lesions developed a stable, low-level ‘signal’ of ssDNA surrounding them exclusively in S phase. In contrast, the signal of 6-4PP lesions surrounded by ssDNA continuously increased over several hours to nearly 10-fold above the level detected shortly after UV (**Figure 3.5C**). A plausible model is that DNA replication promptly resumes downstream of a CPD lesion through repriming, initially generating an ssDNA gap (transiently detectable by the antibody) that is soon filled by TLS. In this model, an ssDNA gap at a CPD lesion is transient, and new short-lived gaps are created as DNA replication progresses without significant slowing. In contrast, 6-4PP lesions persistently block DNA replication, perhaps because TLS and/or replication restart is persistently impeded at 6-4PP lesions. This prolonged

replication blockage corresponds to the ability of 6-4PP to activate the ATR-Chk1 pathway, presumably by recruiting RPA to regions of persistent ssDNA surrounding 6-4PP lesions.

Although this study allowed the determination of the relative effects of these UV lesions on DNA damage responses, this experimental setting has certain limitations. The use of NER-deficient cell lines was crucial to retain and identify the respective role of each UV-induced lesion because 6-4PP lesions in particular are normally rapidly removed by NER. Among the different types of NER deficiency, xeroderma pigmentosum complementation groups A and C (XP-A and XP-C) are deficient in repair of both CPD and 6-4PP lesions, whereas XP complementation groups D and E are only partially defective in repair of 6-4PP, meaning that the latter two types are not suitable for such studies (136, 142, 143). Because XP-A cells (but not XP-C cells) are compromised in their ability to activate ATR in response to UV (141), only XP-C cells are suitable for studying the effects of UV-induced DNA lesions on the ATR-Chk1 pathway. Notably, because ATR activation is limited to S phase, cells must be dividing frequently in order to have sufficient S phase cells for analysis. For this reason, some portions of the present study required SV40-transformed XP-C cells that were actively growing and transfectable. However, because SV40 large T antigen accelerates cell cycle progression (144) and may subsequently increase replication stress, this raises a concern that SV40 transformation could affect ATR-mediated signaling. A prior study showed that SV40 large T antigen expression induces a low level of Chk1 phosphorylation (Ser317) even in the absence of DNA damage (145). However, in SV40-transformed XP-C cells that we used, Chk1 phosphorylation (Ser345) was not increased without damage but was robustly induced in response to UV (**Figure 3.1** and (141)). This suggests that damage-induced activation of the ATR-Chk1 pathway is not compromised or dysregulated in this transformed cell line.

In conclusion, we identified 6-4PP as the critical lesion that causes replication blockage and activation of the ATR-Chk1 pathway in S phase. The inability of CPD lesions to activate the ATR-Chk1 pathway is likely due to its efficient bypass in cells that have intact TLS polymerases.

Indeed, in cells that are unable to bypass CPD lesions (XP-Variant cells with defective DNA polymerase η), ATR pathway activation is markedly augmented and prolonged (141, 146). This suggests that when they cannot be bypassed, CPD lesions can activate the ATR pathway similarly to 6-4PP lesions which are typically difficult to bypass.

Activation of the ATR-Chk1 pathway by replication-blocking lesions promotes survival of DNA-damaged cells; however, it also likely increases mutation incorporation. Indeed, previous mouse studies showed that genetic or pharmacological inhibition of ATR suppresses UV carcinogenesis (62, 147). In parallel, multiple human epidemiological studies have shown that intake of caffeine (a nonspecific ATR inhibitor) is associated with decreased risk of developing UV-induced keratinocyte-derived skin cancers (65, 67). The cancer-preventive effect of ATR inhibition is likely due in part to increased UV-induced apoptosis (68), which eliminates damaged skin cells that are prone to incorporating DNA mutations and subsequent malignancy. In addition, ATR inhibition may directly prevent error-prone TLS that ultimately contributes to skin cancer development. This notion is supported by a prior study showing that caffeine abolishes TLS mediated by Rev3 (148), a catalytic subunit of DNA polymerase ζ that promotes error-prone bypass across 6-4PP. Because TLS across 6-4PP lesions is a highly mutagenic process, it will be relevant to determine whether ATR is required for this process. This study identifying the respective roles of the two major types of UV lesion provides a molecular basis for their distinct effects on DNA damage responses and insight into the mechanisms of UV carcinogenesis.

Author contributions

K.H., P.N. and M.K. designed the experiments.

K.H. and M.K. performed the experiments.

K.H. and M.K. analyzed the data.

J.M.S. helped with design and execution of replication track analysis.

K.H., P.N. and M.K. wrote the manuscript.

All authors discussed the results and interpretation and commented on the manuscript at all stages.

Acknowledgments

The authors thank Dr. Carlos F. M. Menck (University of São Paulo) for the gift of cDNAs of CPD-photolyase and 6-4PP-photolyase. This work was supported by the National Institutes of Health (R01-AR049832 and R01-AR067722 to P.N.; R21-ES019485 to J.M.S.), a Dermatology Foundation Career Development Award (to M.K.), University of Washington Royalty Research Fund (to J.M.S.), and the Michael Piepkorn Endowment for Dermatology Research at University of Washington. The authors declare no competing financial interests.

3.5 Methods

Cell lines and culture conditions

SV40-transformed, human XP-C fibroblast cell lines derived from two different patients (GM15983 (Line: XP4PA-SV-EB) (136, 149) and GM16093 (Line: XP14BRneo17) (139, 150)) were purchased from Coriell Cell Repositories (Camden, NJ) and were grown in Dulbecco's Modified Eagle Medium (DMEM; #11995-040, Life Technologies) supplemented with 10% Fetal Bovine Serum (FBS; #10438-026, Life Technologies) and 1% Penicillin-Streptomycin (#15140-122, Life Technologies). HCT116 $p53^{+/+}$ cell line was a kind gift from Dr. Bert Vogelstein (Johns Hopkins University) and was grown in McCoy's 5A Medium (#16600-082, Life Technologies) supplemented with 10% FBS and 1% Penicillin-Streptomycin. All cells were cultured at 37ºC in a humidified atmosphere of 5% CO_2. Cells were harvested by trypsinization using 0.05% Trypsin-EDTA (#25300, Life Technologies) for passage and for experiments.

Construction and transfection of lesion-specific photolyase plasmids

cDNAs of marsupial *Potorous tridactylus* CPD-photolyase (CPD-PL) (GenBank Accession No. D26020) and the plant *Arabidopsis thaliana* 6-4PP-photolyase (6-4PP-PL) (GenBank Accession No. NM_112432) were kind gifts from Dr. Carlos F. M. Menck (University of São Paulo) (18, 151). Photolyase cDNA was subcloned into pcDNA6/*myc*-His B mammalian expression vector with human cytomegalovirus promoter (V221-20, Life Technologies) to fuse with a polyhistidine tag (6x His) at the C-terminus of photolyase. Specifically, for constructing a plasmid encoding His-tagged CPD-PL, *Xho*I site at 5' and *Sac*II site at 3' were used to insert cDNA of CPD-PL into the expression vector. To construct a plasmid encoding His-tagged 6-4PP-PL, cDNA of 6-4PP-PL was first amplified by PCR using the following primers to add restriction sites: forward 5'-ACTCGAGACCATGCAACGATTCTGCGTCTG-3' (*Xho*I site); reverse 5'-ATATCCGCGGTTTGAGTTTTGGTCGTTGG-3' (*Sac*II site). The amplified product

was then subcloned into pcDNA6/*myc*-His B mammalian expression vector using *Xho*I site at 5' and *Sac*II site at 3'. pcDNA6/*myc*-His B mammalian expression vector without insert was used as a control vector.

Transfection experiments were performed using FuGENE HD Transfection Reagent (E231, Promega; F500, Switchgear Genomics) according to the manufacturer's instructions. For transfection of human XP-C fibroblast cell lines, 3 x 10^5 cells were plated on a 35-mm dish and allowed to grow at 37ºC in a humidified atmosphere of 5% CO_2 for 16 hr. Prior to transfection, cultured medium was removed, and fresh medium was then added to cells. Transfection mixture in final volume of 100 µl per 35-mm dish was prepared by diluting 2 µg plasmid DNA and 7 µl FuGENE HD in Opti-MEM I Reduced Serum Medium (#11058-021, Life Technologies) that was prewarmed to room temperature. For double transfection of CPD-PL and 6-4PP-PL, 1 µg plasmid DNA of each photolyase was mixed. The transfection mixture was incubated at room temperature for 15 min and then added to cells in a drop-wise manner. Cells were incubated at 37ºC in a humidified atmosphere of 5% CO_2 for 48 hr for subsequent experiments (UV irradiation followed by flow cytometry or replication track analysis).

UV irradiation and photorepair

Ultraviolet B (UVB) irradiation was performed using a panel of four UVB bulbs (RPR-3000, Southern New England Ultraviolet, Branford, CT) emitting radiation centered about 311 nm. UVB bulbs were covered by a Kodacel filter (K6808, Eastman Kodak, Rochester, NY) to eliminate any ultraviolet C (UVC) irradiation (<290 nm). UVB dose was monitored while irradiating cells using a Photolight IL400A radiometer equipped with a SEL240/UVB detector (International Light Technologies, Peabody, MA), and 30 mJ/cm^2 UVB irradiation typically required 40 sec. Prior to UVB irradiation, cells were rinsed once with warm Hank's Balanced Salt Solution without phenol red (HBSS; #14025-092, Life Technologies). Immediately after HBSS was removed, cells on a cell culture dish were placed under UVB bulbs without a dish lid

and were irradiated with UVB. Sham-irradiated cells were treated exactly the same way, except that cells were not exposed to UV irradiation. For experiments without photorepair, 2 ml of fresh medium was added to a 35-mm dish immediately after UV irradiation, and cells were incubated at 37ºC in the dark. For photorepair by visible light illumination, 2 ml of warm HBSS without phenol red was added to a 35-mm dish immediately following UV irradiation. The dish of cell culture was then illuminated by visible light from the bottom by placing a dish on a 3-mm thick glass surface sitting 6 mm above one fluorescent lamp (F13T5/WW, warm white, 766 lumens (mean), Sylvania) at room temperature for 2 hr for photorepair. For mock photorepair control ("Dark"), dishes were wrapped with aluminum foil and were placed on the glass above a fluorescent lamp same as visible light-illuminated samples ("Light").

Thymidine analog preparation

For stock solution, 5-bromo-2'-deoxyuridine (BrdU; B5002, Sigma; 15 mM), 5-iodo-2'-deoxyuridine (IdU; I7125, Sigma; 2 mM), and 5-ethynyl-2'-deoxyuridine (EdU; A10044, Life Technologies; 15 mM) were dissolved in Dulbecco's Phosphate-Buffered Saline (PBS; #14190-250, Life Technologies) at the indicated concentrations and stored at –20ºC. Stock solutions were diluted with cell culture medium to have final concentrations: 15 μM EdU and 20 μM BrdU for identifying replicating cells (flow cytometry analysis); 50 μM IdU and 10 μM EdU for labeling DNA (replication track analysis).

Flow cytometry analyses

For experiments determining the effect of each lesion type in activating the ATR-Chk1 pathway (**Figure 3.3**), XP-C cells (GM15983) were transfected with photolyase plasmids (or control vector) 48 hr prior to UV irradiation. Cell culture medium was replaced with 15 μM EdU-containing medium 1 hr prior to UV irradiation (47 hr after transfection), and cells were incubated at 37ºC for 1 hr. UVB irradiation (48 hr after transfection) and subsequent photorepair

were performed as described above. After 2 hr of visible light illumination for photorepair, HBSS was replaced with warm cell culture medium, and cells were incubated at 37ºC for 7 hr without light illumination. Cell culture medium was then replaced with 20 μM BrdU-containing medium for subsequent 1 hr incubation at 37ºC. After 1 hr incubation with BrdU (total 10 hr post-UV), cells on a 35-mm dish were harvested by trypsinization. Cell suspension was centrifuged at 200 x *g* for 5 min at 4ºC, and cells were resuspended in 1 ml of cold PBS. To fix cells in 2% formaldehyde, 143 μl of 16% paraformaldehyde (formaldehyde) aqueous solution (#15710, Electron Microscopy Sciences) was added into 1 ml of cell suspension, followed by incubation of cells in a 37ºC water bath for 10 min. Fixed cells were centrifuged at 700 x *g* for 5 min at 4ºC and were washed with 1 ml of cold PBS. Cells were pelleted by centrifugation at 700 x *g* for 10 min at 4ºC and then resuspended in ice-cold 90% methanol and incubated at –20ºC overnight for permeabilization. Next, cells were centrifuged at 700 x *g* for 5 min at 4ºC (this centrifugation speed and time was used hereafter), washed with 500 μl PBS, and then incubated with 125 μl of DNase reaction buffer containing 12.5 units of RQ1 RNase-free DNase (M6101, Promega) at 37ºC for 1 hr. DNase-treated cells were centrifuged and washed with 1 ml of 1% bovine serum albumin (BSA; A9647, Sigma) in PBS, and cells were incubated in 200 μl of 1% BSA in PBS at room temperature for 10 min for blocking. Each sample was split into three aliquots for different staining patterns: (i) Pacific Blue (PB) for EdU, Phycoerythrin (PE) for His tag, and Alexa Fluor 647 for CPD; (ii) PB for EdU, PE for His tag, and Alexa Fluor 647 for 6-4PP; and (iii) PB for EdU, PE for His tag, Alexa Fluor 647 for BrdU, and Alexa Fluor 488 for phosphorylation of Chk1 at Ser345. Each split sample (equivalent to half of the cells from a 35-mm dish) was stained with 100 μl of antibody dilution buffer (0.25% Tween-20-containing 1% BSA in PBS) containing the following primary antibodies at the indicated dilutions: anti-CPD mouse monoclonal $IgG_{2a\kappa}$ (1:1000, clone TDM-2, CAC-NM-DND-001, Cosmo Bio), anti-6-4PP mouse monoclonal $IgG_{2a\kappa}$ (1:1000, clone 64M-2, CAC-NM-DND-002, Cosmo Bio), anti-BrdU mouse monoclonal (1:25, clone MoBU-1, B35141, Life Technologies), or anti-phospho-Chk1 (Ser345) (133D3) rabbit

monoclonal (1:100, #2348, Cell Signaling Technology) antibodies. After overnight incubation with primary antibodies at 4ºC, cells were centrifuged and washed twice with 1 ml wash buffer (0.05% Tween-20-containing 1% BSA in PBS). For EdU detection, Pacific Blue azide was conjugated to EdU via $CuSO_4$-mediated Click chemistry reaction for 30 min at room temperature using Click-iT EdU Pacific Blue Flow Cytometry Assay Kit (C10418, Life Technologies; 250 µl reaction volume for one sample). After washing cells twice with 1 ml wash buffer, cells were resuspended in 100 µl of antibody dilution buffer containing the following secondary antibodies at the indicated dilutions and incubated for 30 min at room temperature in the dark: Alexa Fluor 647-conjugated donkey anti-mouse IgG (H+L) (1:800, A31571, Life Technologies) for staining patterns (i) and (ii); or Alexa Fluor 488-conjugated goat anti-rabbit IgG (H+L) (1:200, A11034, Life Technologies) and Alexa Fluor 647-conjugated donkey anti-mouse IgG (H+L) (1:200, A31571, Life Technologies) for staining pattern (iii). Cells were washed twice with 1 ml wash buffer, and the expression of His-tagged photolyase was detected by incubating cells in 100 µl of antibody dilution buffer containing anti-His-tag mouse monoclonal antibody (1:2000, clone OGHis, D291-3, $IgG_{2a\kappa}$, 1 µg/µl, MBL) that was conjugated with R-phycoerythrin (R-PE) using Zenon R-PE Mouse IgG_{2a} Labeling Kit (Z25155, Life Technologies) at a Fab:antibody molar ratio of 3:1. Following 1 hr incubation at room temperature in the dark, cells were washed twice and resuspended in 200 µl PBS. Cells were analyzed on a FACSCanto II Flow Cytometer (BD Biosciences), and the acquired data were analyzed using FlowJo version 9 (Tree Star). For DNA content analysis of cells that were labeled with EdU and BrdU (**Figure 3.3B**), EdU was conjugated to Pacific Blue azide, and BrdU was detected by mouse anti-BrdU antibody with Alexa Fluor 647 anti-mouse antibody. Cells were resuspended in 200 µl of PBS containing 2 µg propidium iodide (PI; P4170, Sigma) and 100 µg RNase A (#19101, Qiagen). A separate XP-C cell line (GM16093) was also tested (**Figure 3.S3**) using the same methods as used for the GM15983 cell line (**Figure 3.3**), except for the following three conditions: (i) 25% of the cells from a 60-mm dish were incubated with 15.6 µl of DNase reaction buffer containing 1.56 units of

RQ1 RNase-free DNase at 37ºC for 1 hr; (ii) Click chemistry reaction was performed with 62.5 µl reaction mixture for one sample; and (iii) cells were incubated with primary antibodies at room temperature for 1 hr.

For an experiment evaluating Chk1 phosphorylation as a function of cell cycle phases using thymidine analog incorporation (**Figures 3.1B–3.1E**), XP-C cells (GM15983) were incubated with 15 µM EdU-containing medium at 37ºC for 1 hr prior to UV irradiation. Cells were then UV-irradiated and incubated in fresh culture medium without EdU at 37ºC for 1 hr. Cells were harvested by trypsinization, fixed by 2% formaldehyde, permeabilized by 90% methanol, and blocked with 1% BSA in PBS, as described above. Each sample (equivalent to half of the cells from a 35-mm dish) was stained with 100 µl of antibody dilution buffer containing 1:100 dilution of anti-phospho-Chk1 (Ser345) (133D3) rabbit monoclonal antibody. After overnight incubation with primary antibody at 4ºC, cells were centrifuged and washed with 1 ml wash buffer. Pacific Blue azide was conjugated to EdU using 250 µl reaction mixture from Click-iT EdU Pacific Blue Flow Cytometry Assay Kit. Cells were then washed twice and resuspended in 100 µl of antibody dilution buffer containing 1:200 dilution of Alexa Fluor 488-conjugated goat anti-rabbit IgG (H+L) for incubation at room temperature for 30 min in the dark. Cells were washed twice with 1 ml wash buffer and resuspended in 200 µl of PBS containing 2 µg PI and 100 µg RNase A, followed by flow cytometry analysis.

For experiments determining the kinetics of phosphorylation of Chk1 following UV irradiation (**Figure 3.S1**) and an experiment evaluating Chk1 phosphorylation as a function of cell cycle phases (**Figure 3.1A**), HCT116 and XP-C (GM15983) cells were UV-irradiated and then incubated in culture medium at 37ºC in the dark until harvest. HCT116 cells were harvested by trypsinization immediately after sham or UV irradiation (0 hr), or 0.5, 1, 2, 4, 6, 8 hr after UV. XP-C cells were harvested by trypsinization immediately after sham or UV irradiation (0 hr), or 0.05, 0.5, 2, 4, 7, 10 hr after UV. Cells were then fixed in 2% formaldehyde, permeabilized by 90% methanol, and blocked with 1% BSA in PBS, as described above. Each

HCT116 sample (equivalent to 12.5% of the cells from a 35-mm dish) was stained with 100 µl of antibody dilution buffer containing 1:100 dilution of anti-phospho-Chk1 (Ser345) (133D3) rabbit monoclonal antibody at room temperature for 1 hr. Each XP-C sample (equivalent to 25% of the cells from a 60-mm dish) was stained with 100 µl of antibody dilution buffer containing 1:100 dilution of anti-phospho-Chk1 (Ser345) antibody at 4ºC overnight. Next, cells were washed twice and resuspended in 100 µl of antibody dilution buffer containing 1:200 dilution of Alexa Fluor 488-conjugated goat anti-rabbit IgG (H+L) for incubation at room temperature for 30 min in the dark. After washing twice, HCT116 cells were resuspended in 75 µl PBS containing 0.375 µg of FxCycle Violet Stain (F10347, Life Technologies), and XP-C cells were resuspended in 150 µl of PBS containing 1.5 µg PI and 75 µg RNase A, followed by flow cytometry analysis. For the kinetic analysis of phospho-Chk1 induction in S phase following UV irradiation (**Figure 3.S1**), fluorescence signals of phospho-Chk1 were measured in S phase cells that were defined as 2N < DNA content (FxCycle Violet or PI) < 4N.

For evaluating two different DNA treatments (HCl or DNase) for their abilities to simultaneously detect UV lesions and phosphoproteins (**Figure 3.S2**), XP-C (GM15983) cells were irradiated with 30 mJ/cm^2 UVB (or sham-irradiated) and were harvested immediately (0 hr) or 1 hr after irradiation. For DNase treatment, cells were fixed in 2% formaldehyde and permeabilized by overnight incubation in 90% methanol at –20ºC. Cells from a 35-mm dish were then treated with 31.25 µl of DNase reaction buffer containing 3.125 units of RQ1 RNase-free DNase (M6101, Promega) at 37ºC for 1 hr. For HCl treatment, harvested cells were directly incubated in 90% methanol at –20ºC overnight. Cells from a 35-mm dish were then resuspended in 100 µl of 2 N HCl diluted in water from 12 N HCl. After incubation of cells with HCl at room temperature for 10 min, cells were centrifuged and incubated in 100 µl of 0.1 M sodium tetraborate decahydrate (S248, Fisher Scientific) at room temperature for 5 min, and were resuspended in 500 µl PBS. DNase-treated or HCl-denatured cells were washed and blocked with 1% BSA in PBS. Each sample (equivalent to half of the cells from a 35-mm dish)

was stained with 100 µl of antibody dilution buffer containing 1:100 dilution of anti-phospho-Chk1 (Ser345) (133D3) rabbit monoclonal and 1:1000 dilution of anti-CPD mouse monoclonal antibodies at room temperature for 1 hr. Cells were washed twice and resuspended in 100 µl of antibody dilution buffer containing 1:200 dilution of Alexa Fluor 488-conjugated goat anti-rabbit IgG (H+L) and 1:800 dilution of Alexa Fluor 647-conjugated donkey anti-mouse IgG (H+L) for incubation at room temperature for 30 min in the dark. After washing twice, cells were resuspended in 150 µl PBS containing 0.75 µg of FxCycle Violet Stain (F10347, Life Technologies), followed by flow cytometry analysis.

For experiments validating lesion-specific photorepair of UV lesions in cells expressing polyhistidine (His)-tagged photolyase (**Figure 3.2**), 3 x 10^5 XP-C cells (GM15983) plated on a 35-mm dish were incubated at 37ºC for 16 hr and then transfected with His-tagged photolyase plasmid (or control vector). After 48 hr, cells were irradiated with 30 mJ/cm^2 UVB. For “0 hr” sample, cells were harvested immediately after UV (or sham) irradiation. For photorepair, 2 ml of HBSS was added to a 35-mm dish, and the dish of cell culture was illuminated at room temperature for 0.5, 1, 2, or 4 hr until harvest. After harvest, cells were fixed by 2% formaldehyde and permeabilized by 90% methanol incubation at –20ºC overnight. Next, cells were treated with 31.25 µl of DNase reaction buffer containing 3.125 units of RQ1 RNase-free DNase at 37ºC for 1 hr. After blocking, each sample (equivalent to half of the cells from a 35-mm dish) was stained with 100 µl of antibody dilution buffer containing 1:1000 dilution of anti-CPD or anti-6-4PP mouse monoclonal antibodies at room temperature for 1 hr. Cells were then washed twice and resuspended in 100 µl of antibody dilution buffer containing 1:800 dilution of Alexa Fluor 647-conjugated donkey anti-mouse IgG (H+L) for incubation at room temperature for 30 min in the dark. After washing twice, cells were resuspended and incubated at room temperature for 1 hr in 100 µl of antibody dilution buffer containing R-PE-conjugated anti-His-tag (clone OGHis) mouse monoclonal antibody (1:2000) that was conjugated with R-PE using Zenon R-PE Mouse IgG_{2a} Labeling Kit. Cells were washed twice and resuspended in 150 µl of

PBS containing 0.75 µg of FxCycle Violet Stain, followed by flow cytometry analysis.

For experiments detecting UV lesions that were surrounded by ssDNA (**Figures 3.5B and 3.5C**), 1 x 10^6 XP-C cells (GM15983) plated on a 60-mm dish were incubated at 37ºC for 17 hr. Cells were UV-irradiated and incubated in culture medium at 37ºC in the dark until harvest. Cells were harvested by trypsinization immediately (0 hr), 0.05, 0.5, 2, 4, 7, or 10 hr after UV irradiation, or immediately (0 hr) after sham irradiation. After harvest, cells were fixed in 2% formaldehyde and permeabilized by 90% methanol incubation at –20ºC overnight. Cells were split into two samples, which were subsequently treated with or without DNase. For DNase treatment, cells (equivalent to a half of 60-mm culture) were treated with 125 µl of DNase reaction buffer containing 12.5 units of RQ1 RNase-free DNase at 37ºC for 1 hr, followed by blocking in 1% BSA in PBS. For samples without DNase treatment, cells (equivalent to half of a 60-mm culture) were incubated in 1% BSA in PBS for blocking. Each sample (DNase-treated or untreated) was further split into two for subsequent immunostaining. Cells (equivalent to 25% of the cells from a 60-mm dish) were resuspended in 100 µl of antibody dilution buffer containing 1:1000 dilution of anti-CPD or anti-6-4PP mouse monoclonal antibodies at 4ºC overnight. Next, cells were washed twice and resuspended in 100 µl of antibody dilution buffer containing 1:800 dilution of Alexa Fluor 647-conjugated donkey anti-mouse IgG (H+L) for incubation at room temperature for 30 min in the dark. After washing twice, cells were resuspended in 200 µl of PBS containing 2 µg PI and 100 µg RNase A, followed by flow cytometry analysis. For the kinetics of lesion signals in S phase following UV irradiation (**Figure 3.5C**), fluorescence signals of CPD and 6-4PP were measured in S phase cells that were defined as 2N < DNA content (PI) < 4N.

Replication track analysis combined with flow sorting

For experiments quantitating DNA replication progression in cells before and after UV irradiation and photorepair (**Figure 3.4**), XP-C cells (GM15983) were transfected with

photolyase plasmids (or control vector) 48 hr prior to UV irradiation. Thirty-four hours after transfection, cell culture medium was replaced with fresh medium to increase viability of transfected cells. Cell culture medium was replaced with 50 μM IdU-containing medium 1.5 hr prior to UV irradiation (46.5 hr after transfection) and incubated at 37ºC for 1 hr. Cells were then rinsed with fresh medium twice and incubated in fresh medium without thymidine analogs for 30 min at 37ºC. UVB irradiation and subsequent photorepair were performed as mentioned above. Following 2 hr of visible light illumination, HBSS was replaced with 10 μM EdU-containing medium. After 1 hr incubation with EdU at 37ºC, cells were rinsed with fresh medium twice and incubated in fresh medium without thymidine analogs for 30 min at 37ºC. Cells were then harvested by trypsinization (3.5 hr after UV irradiation). In this experimental design, 30-minute incubation in fresh medium without thymidine analogs prior to sham or UV irradiation was critical to eliminate a potential discrepancy in lengths of labeled DNA between UV and sham samples in the 1st labeling, because incorporation of thymidine analogs that were already in cells may be inhibited immediately after UV irradiation but not after sham irradiation. In addition, to have a consistent labeling schedule between the 1st (pre-sham/UV) and 2nd (post-sham/UV) labeling periods, another 30-minute incubation without thymidine analogs was included immediately before harvest. After harvest, cells were fixed in 2% formaldehyde and permeabilized by overnight incubation in 90% methanol at –20ºC as described above. After blocking with 1% BSA in PBS at room temperature for 10 min, the expression of His-tagged protein was detected by incubating cells (from a 35-mm dish) in 200 μl of antibody dilution buffer containing anti-His-tag mouse monoclonal antibody (1:2000, clone OGHis, D291-3, $IgG_{2aκ}$, 1 μg/μl, MBL) that was conjugated with R-phycoerythrin (R-PE) using Zenon R-PE Mouse IgG_{2a} Labeling Kit (Z25155, Life Technologies) at a Fab:antibody molar ratio of 3:1. Following 1 hr incubation at room temperature in the dark, cells were washed and resuspended in 100 μl of 1% BSA in PBS and were sorted using a FACSAria Flow Sorter (BD Biosciences). Approximately 1 x 10^5 single cells that showed high signals of His tag (photolyase-expressing cells) were collected via flow sorting.

Cells transfected with control vector (no photolyase) were collected without flow sorting. Flow-sorted (photolyase-expressing) and unsorted (control vector-transfected) cells were centrifuged at 700 x *g* for 5 min and washed with 500 µl agarose insert buffer (10 mM Tris pH 7.5, 20 mM NaCl, 50 mM EDTA solution in water). Cells were centrifuged again and resuspended in 30 µl agarose insert buffer. To embed cells in agarose, an equal amount of melted 2% low-gelling-temperature (LGT) DNase-free agarose was added to the cell suspension, and the mixed solution was immediately transferred into an agarose insert mold and incubated at 4ºC for 1 hr. After solidification, the agarose gel insert was stored in agarose insert buffer in a 2-ml tube at 4ºC until use. To release genomic DNA from embedded cells, the agarose gel insert was incubated in 500 µl lysis buffer (100 mM EDTA pH 8.0, 0.2% sodium deoxycholate, 2% sodium lauryl sarcosine, 1 mg/ml proteinase K in water) at 55ºC overnight. After 55ºC incubation, agarose gel insert was kept at room temperature for 5 min to harden the gel. Agarose gel insert was washed four times at room temperature in 1 ml 1x TE buffer (10 mM Tris, 1 mM EDTA, pH 8.0) for 30 min each on a rocking platform. To release DNA from agarose gel insert, 300 µl 1x β-Agarase I Reaction Buffer (B0392S, New England Biolabs) was added to agarose gel insert, which was then melted by heating at 71ºC for 10 min. Melted agarose was digested by adding 3 µl of β-Agarase I (1000 units/ml, M0392L, New England Biolabs) and incubating at 42ºC for 20 hr. After digestion of agarose, 30 µl of 10x TE buffer (pH 8.0) was added to agarose-digested DNA solution to neutralize β-Agarase buffer (pH 6.5). Final volume of DNA solution was approximately 393 µl (30 µl agarose insert buffer, 30 µl 2% agarose, 300 µl 1x β-Agarase I Reaction Buffer, 3 µl β-Agarase I, 30 µl 10x TE buffer), and this DNA solution was used for microfluidic-assisted replication track analysis (maRTA) and immuno-slot blot. To align DNA fibers on glass coverslips using microfluidics, maRTA was performed as previously described (140), with modifications. Specifically, an oxygen plasma-treated PDMS (polydimethyl siloxane) patch with a series of microchannels (50–450 µm wide, 3–5 µm height) was laid on a silanized glass coverslip, and 1 µl of DNA solution was loaded at the edge of the PDMS patch. DNA

solution went through microchannels by capillary tension, and DNA fibers were aligned and bound to silanized coverslips. The PDMS patch was then separated from the coverslip. Coverslips onto which DNA was aligned and bound were air-dried overnight for subsequent immunostaining. Next, the coverslip was placed in a well of a 6-well plate and treated with 1.5 ml of 2.5 N HCl for 45 min on a rocking platform to denature DNA. HCl was removed and neutralized by rinsing with 2 ml of 0.1 M sodium borate (pH 8.5) and then 2 ml PBS, and coverslip was rinsed with 1 ml of 3% BSA in PBS. IdU and EdU signals were detected by the following sequential staining: (i) for 1st label (IdU, green signal): anti-IdU (mouse) and Alexa Fluor 488-conjugated anti-mouse antibodies; (ii) for 2nd label (EdU, red signal): biotin azide, Texas Red-NeutrAvidin, anti-avidin antibody (biotinylated), and Texas Red-NeutrAvidin. For EdU detection, 50 µl per coverslip of Click chemistry reaction mixture containing 20 µM biotin azide (B10184, Life Technologies), 11 mM sodium L-ascorbate (A4034, Sigma), and 2.2 mM $CuSO_4$ (C489, Fisher Scientific) was prepared in PBS immediately prior to use. EdU was conjugated with biotin azide via Click chemistry reaction for 30 min at room temperature. The coverslip was then rinsed twice with 1 ml of 3% BSA in PBS and was blocked in 1 ml blocking buffer (10% normal goat serum (ACL1200-100, Accurate Chemical), 5% BSA, 0.5% Tween-20 in PBS) at room temperature for 20 min. Biotin azide was then bound to NeutrAvidin through incubating the coverslip at room temperature for 1 hr with 20 µl of blocking buffer containing Texas Red-conjugated NeutrAvidin biotin-binding protein (1:15, A2665, Life Technologies). The coverslip was then washed three times with 1 ml of wash buffer (1% BSA, 0.1% Tween-20 in PBS) for 5 min each on a rocking platform. Next, DNA was stained with 20 µl of blocking buffer containing anti-BrdU/IdU mouse (clone B44) antibody (1:6, #347580, BD Biosciences) and biotinylated anti-avidin goat antibody (1:30, BA-0300, Vector Laboratories) at room temperature for 1 hr. After washing with 1 ml wash buffer for 5 min three times, DNA was stained with 20 µl of blocking buffer containing Alexa Fluor 488-conjugated goat anti-mouse IgG (H+L) (1:1000, A11001, Life Technologies) and Texas Red-NeutrAvidin (1:15, A2665, Life Technologies).

Following staining, the coverslip was washed with 1 ml wash buffer for 5 min three times, rinsed with 1 ml of water, and air-dried. The stained coverslip was mounted face down on a microscope slide and affixed with nail hardener at four corners of the coverslip, without the use of mounting medium.

Immunofluorescent images of labeled DNA were captured through GFP (green signal for IdU) and Texas Red (red signal for EdU) filter sets using a Zeiss Axiovert microscope with an oil-immersion 40x objective. The filter set corresponding to the 1st label (IdU; as the pre-sham/UV control) was used to select areas with adequate density of DNA fiber for image acquisition, and immunofluorescent images of two labels were acquired in each field (approximately 30–50 fields per coverslip). Track lengths of both labels (IdU, pre-sham/UV; EdU, post-sham/UV) in acquired immunofluorescent images were measured using the Zeiss AxioVision software. DNA fibers that were thick, faint, wavy, crossed, overlapped, truncated at the edge of an image, or shorter than 3 μm (indistinguishable from nonspecific dots) were excluded from measurement. A separate experiment using EdU as 1st label and IdU as 2nd label was performed to avoid detection bias against two different fluorescent signals, and this approach yielded a result highly analogous to the experiment using IdU as 1st label and EdU as 2nd label. To analyze track length data from two independent experiments, 250 track length values of each label were randomly selected from each experiment and were combined from two experiments (total 500 tracks of each label for each UV/transfection condition). Combined track length data were plotted as binned, cumulative distributions of track lengths (bins were in 4-μm increments). Statistical significance between track length distributions of 1st and 2nd labels was determined by Mann-Whitney test using Prism 5 (GraphPad Software).

Immuno-slot blot assay

For experiments validating the antibody specificity for UV lesions on ssDNA (**Figure 3.5A**), UV-irradiated DNA was prepared using two different methods. For “in cells” UV irradiation

samples, XP-C cells (GM15983) were irradiated with UVB 30 mJ/cm^2 as described above and then harvested by scraping immediately after irradiation. Genomic DNA was extracted from these UV-irradiated cells using QIAamp DNA Blood Mini Kit (#51104, Qiagen) and RNase A (#19101, Qiagen), and DNA concentrations were measured using NanoDrop 1000 UV-Vis spectrophotometer (Thermo Scientific). Next, DNA solutions were prepared in 100 µl of PBS per sample to have 120 ng (for ssDNA detection), 200 ng (for CPD detection), or 800 ng (for 6-4PP detection) of genomic DNA. For "*in vitro*" UV irradiation samples, genomic DNA was extracted from unirradiated XP-C cells (GM15983) using QIAamp DNA Blood Mini Kit and RNase A, and 100 µl of PBS containing the above-mentioned amount of extracted DNA was placed on a dish lid and was irradiated with UVB 30 mJ/cm^2. For heat denaturation, DNA solutions of "*in vitro*" and "in cells" UV irradiation samples in 1.5-ml tubes were boiled in 100ºC water for 10 min and rapidly chilled on ice for 15 min. Heat-denatured or non-denatured DNA solutions were spotted onto Hybond-N+ positively charged nylon membrane (RPN1210B, GE Healthcare) using Minifold II slot-blot system (SRC 072/0, Schleicher & Schuell, Inc.) under vacuum, and 100 µl of Milli-Q water was used to rinse each slot after loading DNA. Membranes were kept in the slot-blot system under vacuum for 10 min and then were baked at 80ºC using a gel dryer (Savant SGD4050) for 2 hr for DNA immobilization. After baking, membranes were incubated in blocking buffer (5% dry milk (#170-6404, Bio-Rad), 0.1% sodium azide (S2002, Sigma-Aldrich), 0.1% Tween-20 in PBS) on a shaker at room temperature for 30 min. Each membrane was then incubated in 3 ml of buffer (5% dry milk, 0.1% Tween-20 in PBS) containing mouse monoclonal antibodies against ssDNA (1:150, clone F7-26, IgM, MAB3299, Millipore), CPD (1:2000, TDM-2, $IgG_{2a\kappa}$, Cosmo Bio), or 6-4PP (1:500, 64M-2, $IgG_{2a\kappa}$, Cosmo Bio) on a shaker at 4ºC overnight. After three times of washing (1 min each) using wash buffer (0.1% Tween-20-containing PBS), membranes were incubated in 15 ml of buffer (1% dry milk, 0.1% Tween-20 in PBS) containing horseradish peroxidase (HRP)-linked goat anti-mouse IgM antibody (1:1500, sc-2973, Santa Cruz Biotechnology) or HRP-linked whole antibody against mouse IgG (from sheep) (1:2500,

NA931, GE Healthcare) at room temperature for 30 min. Membranes were washed three times (15 min each), and chemiluminescence was assessed using 2 ml of Amersham ECL Western Blotting Detection Reagent (RPN2209, GE Healthcare) or 1 ml of Luminata Forte Western HRP Substrate (WBLUF0100, Millipore). Membranes were then exposed to Kodak BioMax XAR Film (#165-1454, Carestream Health) for chemiluminescence detection. For total DNA (including dsDNA and ssDNA) detection as loading control, membranes were subsequently washed with wash buffer for 1 min three times, rinsed with PBS, and incubated with 1x SYBR Gold Nucleic Acid Gel Stain (S11494, Life Technologies) that was diluted in PBS on a shaker at room temperature for 10 min. Membranes were then washed with wash buffer for 1 min three times, and SYBR Gold signals were detected by FluorChem Q Imaging System (ProteinSimple) with 475 nm excitation channel and 537 nm emission filter.

For validation of lesion-specific photorepair in flow-sorted cells (**Figure 3.4B**), DNA prepared for maRTA was used for immuno-slot blot assay. DNA concentrations were determined by interpolating from logarithmic trendline of band intensities of standard DNA in agarose gel electrophoresis. DNA isolated from sorted cells was diluted in 100 µl of PBS to have 30 ng (for CPD detection) or 120 ng (for 6-4PP detection) of DNA. DNA solutions were boiled, rapidly chilled, and spotted onto Hybond-N+ positively charged nylon membrane. Subsequent steps of immuno-slot blot assay and SYBR Gold staining were performed as described above.

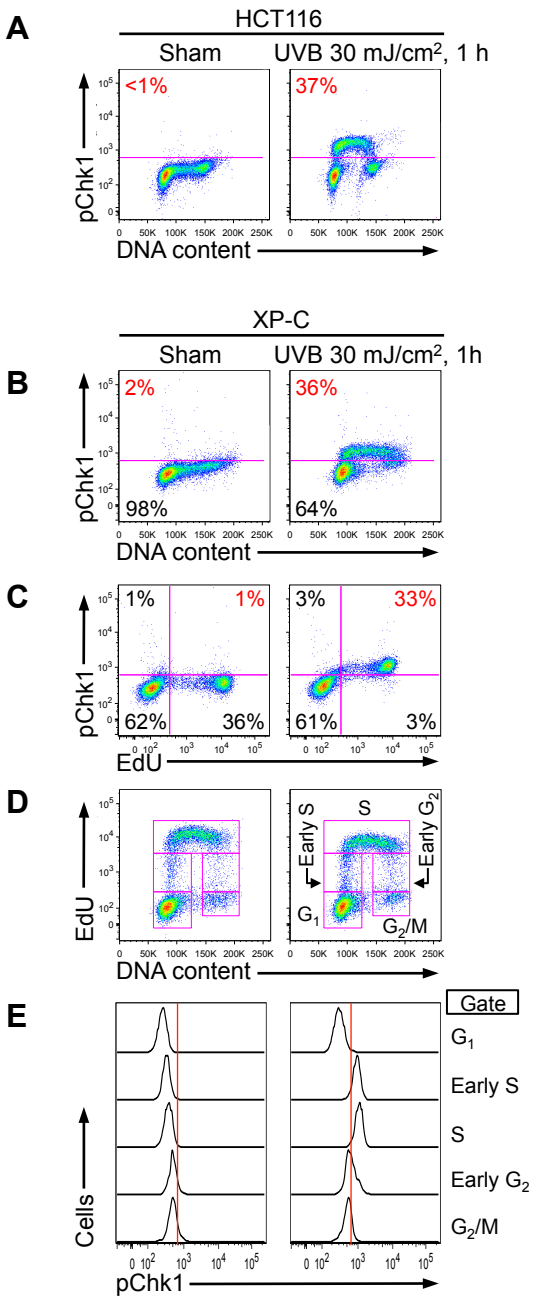

Figure 3.1 UV-induced phosphorylation of Chk1 is strictly limited to S phase as revealed by flow cytometry.

Cell cycle-specific induction of Chk1 phosphorylation in an unsynchronized population was assessed on a single cell basis by flow cytometry.

(**A**) HCT116 cells were sham- (left panel) or UVB- (right panel) irradiated and harvested after 1 h. Phosphorylation of Chk1 at Ser345 (pChk1) was evaluated as a function of DNA content to assess cell cycle-dependent pChk1 status. Percentage of pChk1(+) cells is shown in red.
(**B–E**) XP-C cells (GM15983) were pulse-labeled with EdU for 1 h, followed by sham (left panels) or UVB irradiation (right panels), and harvested 1 h after irradiation.
(**B**) Phosphorylation of Chk1 at Ser345 (pChk1) was evaluated as a function of DNA content. Percentage of pChk1(+) cells is shown in red.
(**C**) UV-induced pChk1 strongly correlates with EdU incorporation. Percentage of EdU(+) pChk1(+) cells is shown in red.
(**D**) EdU incorporation and DNA content were used to identify five cell cycle subpopulations (G_1, early S, S, early G_2, and G_2/M phases; pink boxes identify gates used).
(**E**) pChk1 was evaluated for the cell cycle subpopulations defined in panel D.

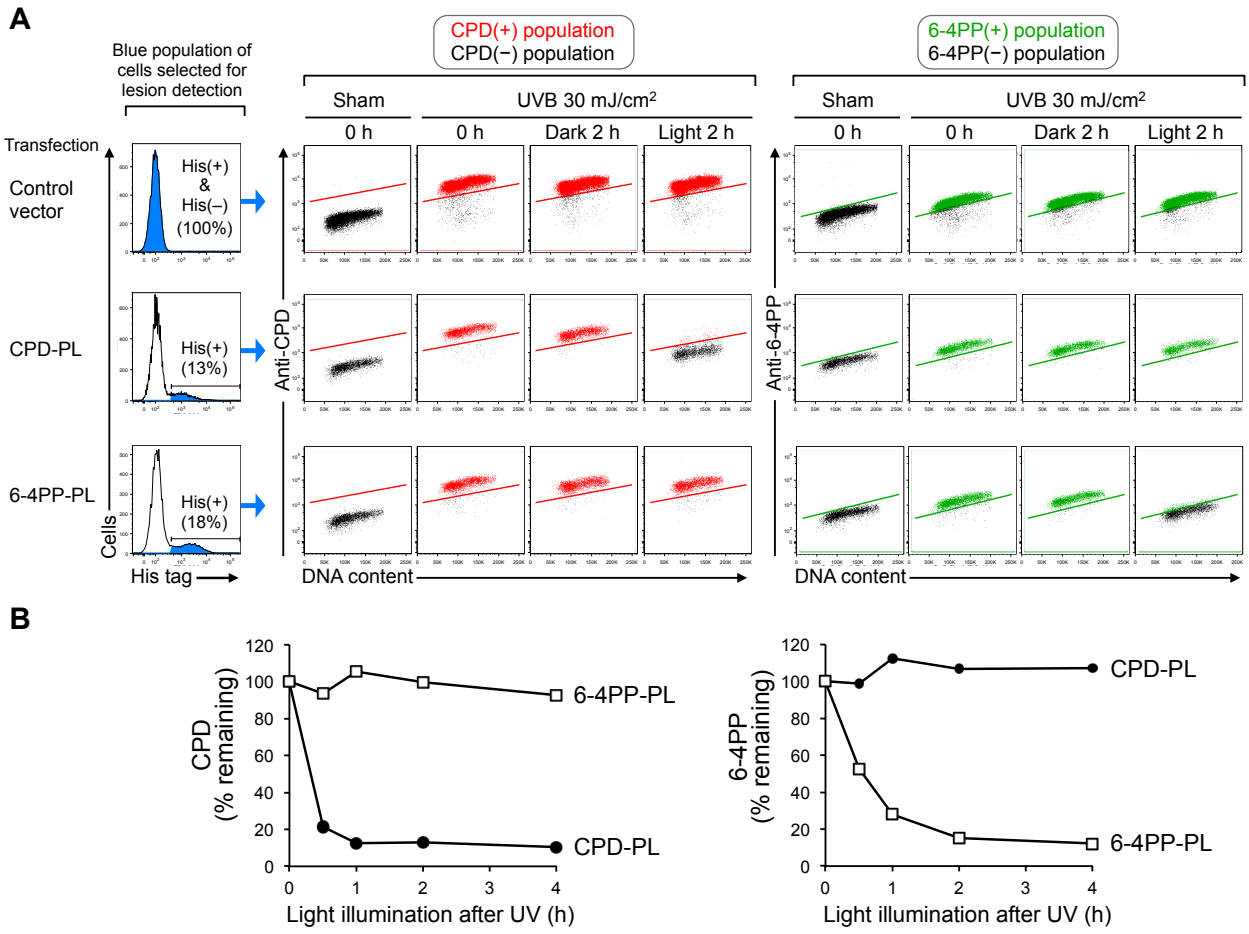

Figure 3.2 Selection of cells with a single type of UV lesion using photolyase and flow cytometry.

(**A**) Flow cytometry identifies photolyase-expressing cells that exhibit light-dependent, lesion-specific repair (photorepair) in all cell cycle phases. XP-C cells (GM15983) transfected with control vector, His-tagged CPD-photolyase (CPD-PL), or His-tagged 6-4PP-photolyase (6-4PP-PL) were sham- or UV-irradiated, and were harvested immediately (0 h) or after 2 h with (Light) or without (Dark) visible light illumination. Fixed cells were subjected to DNase treatment for lesion detection. Expression of photolyase was evaluated by level of His tag, and cell cycle phases were assessed by DNA content staining using FxCycle Violet dye. Left panels show histogram of His tag signal. Control vector-transfected cells (whole population including His(+) and His(–)) or photolyase-expressing cells (His(+)) were selected for lesion detection (as indicated in blue in histogram with percentage). Middle and right panels show the levels of CPD

or 6-4PP as a function of DNA content from these selected populations. CPD(+), 6-4PP(+), and lesion-negative populations are indicated in red, green, and black, respectively.
(**B**) Time course of CPD and 6-4PP photorepair by lesion-specific photolyase. XP-C cells were transfected with CPD-PL (closed circles) or 6-4PP-PL (open squares). Cells were sham- or UVB-irradiated (30 mJ/cm^2) and were subsequently illuminated with visible light until harvest at the indicated time points. Remaining lesions in photolyase-expressing cells (His tag-positive) were assessed by flow cytometry as in (A). Background signal (based on sham-treated cells) was subtracted, and lesion signal at 0 h (immediately after UV) was set to 100%.

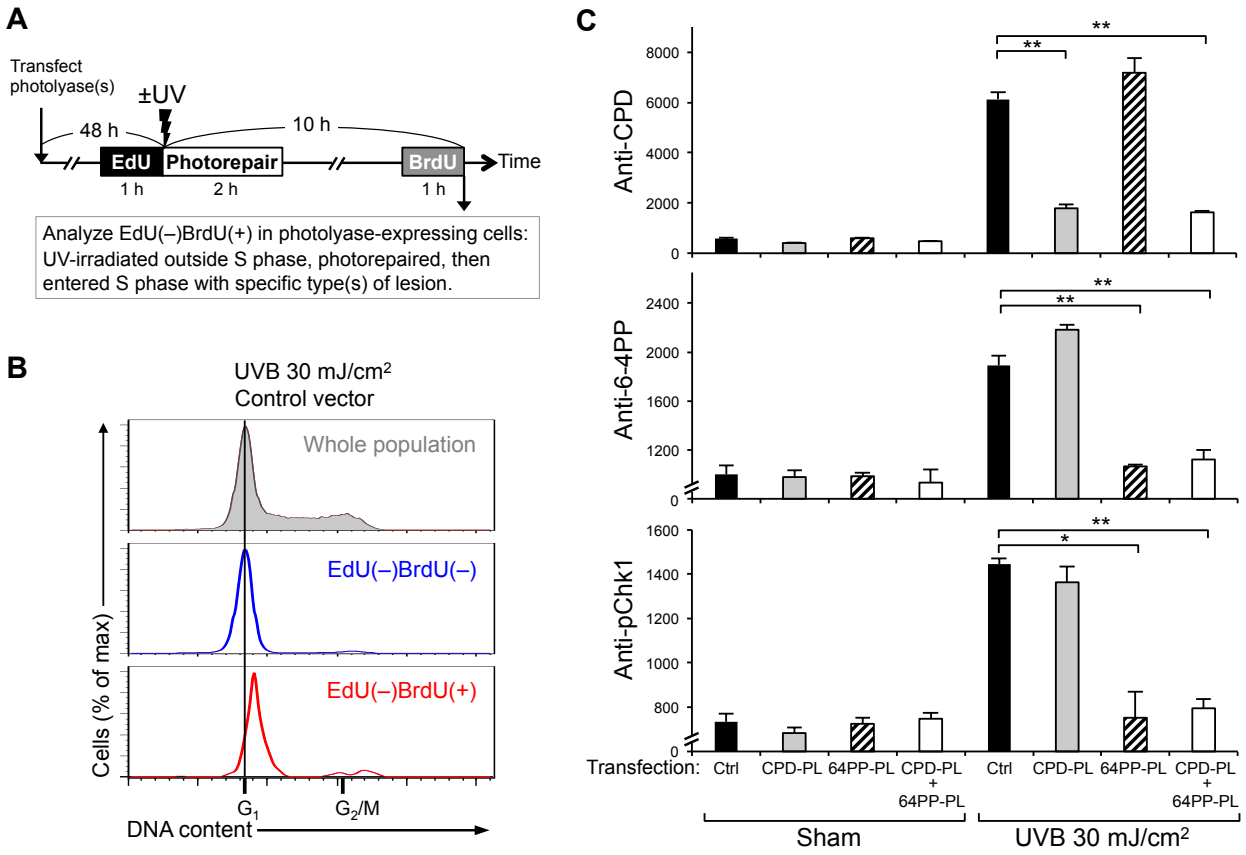

Figure 3.3 6-4PP, but not CPD, potently induces phosphorylation of Chk1.

(**A**) Experimental design for analyzing cells that enter S phase with a specific type of lesion. XP-C cells (GM15983) transfected with control vector (Ctrl), CPD-photolyase (CPD-PL), and/or 6-4PP-photolyase (64PP-PL) were labeled with EdU prior to UV. Following UVB 30 mJ/cm^2 irradiation, cells were illuminated with visible light for photorepair. Cells were labeled with BrdU prior to harvest. EdU(–)BrdU(+) population represents cells that were UV-irradiated outside S phase, photorepaired, and then entered S phase with specific type(s) of lesion. Photolyase-expressing cells (His tag-positive) were analyzed for levels of CPD, 6-4PP, and Chk1 phosphorylation at Ser345 (pChk1) in EdU(–)BrdU(+) population.

(**B**) EdU(–)BrdU(+) population of UV-irradiated cells is in early S phase. UV-irradiated, control vector-transfected cells were stained with propidium iodide for DNA content. Cell cycle profiles of whole population (gray) and its subpopulations of EdU(–)BrdU(–) (blue) and EdU(–)BrdU(+) (red) are shown.

(**C**) Phosphorylation of Chk1 is potently induced in cells with 6-4PP, but not in cells with CPD, upon S phase entry. The levels of CPD, 6-4PP, and pChk1 (Ser345) in cells that newly entered

S phase (EdU(–)BrdU(+) population) were evaluated using antibody-based flow cytometry assay. The mean ± SEM (four independent experiments) of fluorescence signals (arbitrary units) are shown. Statistical significance was determined by t-test. *, $P < 0.05$; **, $P < 0.01$.

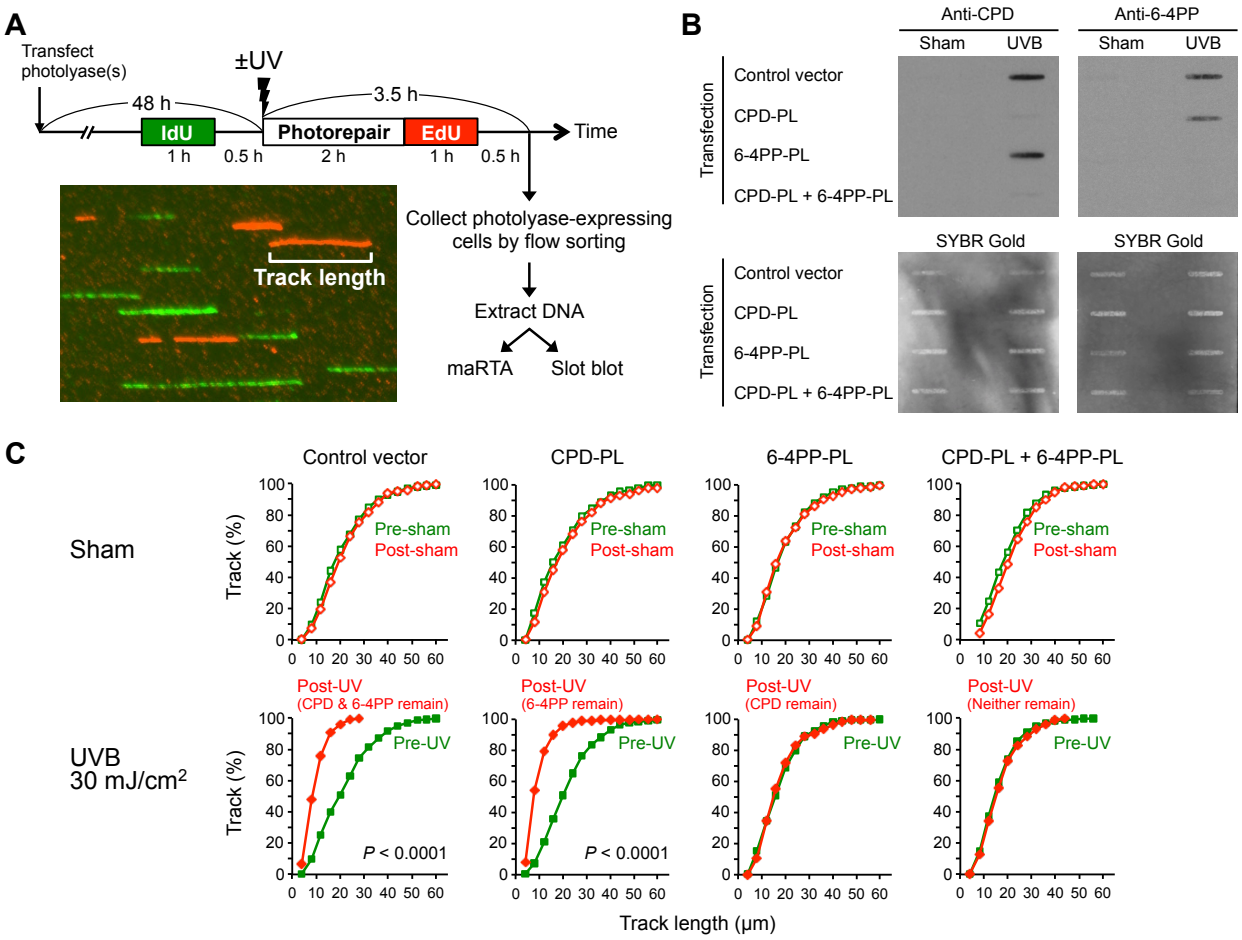

Figure 3.4 DNA replication is slowed by 6-4PP, but not CPD lesions.

(**A**) Experimental design to quantitate DNA replication progression in cells with specific type(s) of lesion(s). XP-C cells (GM15983) transfected with control vector, CPD-photolyase (PL), 6-4PP-PL, or both photolyases were labeled with IdU prior to sham or UVB 30 mJ/cm^2. Following sham or UV irradiation, cells were exposed to visible light for photorepair and were then labeled with EdU prior to harvest. Photolyase-expressing cells (His tag-positive population) were collected by flow sorting. Genomic DNA extracted from sorted (photolyase-expressing cells) or unsorted (for control vector) cells were subjected to immuno-slot blot or microfluidic-assisted replication track analysis (maRTA; a representative image of segments of labeled DNA ('tracks') is shown).

(**B**) Slot-blot validation of lesion-specific photorepair of DNA used for maRTA. Extracted genomic DNA was heat-denatured and then spotted onto membranes. Membranes were probed with anti-CPD or anti-6-4PP antibodies and were subsequently stained with SYBR Gold for total DNA detection.

(**C**) Replication is slowed on DNA with 6-4PP, but not on DNA with CPD. Genomic DNA was aligned through microchannels using microfluidics and stained for IdU and EdU (maRTA). Replication track lengths of 1st (IdU; pre-sham/UV) and 2nd (EdU; post-sham/UV) labels were measured in two independent experiments, and combined data are shown as cumulative distributions (n = 500 tracks for each label). The remaining lesion type(s) (as validated in (B)) are indicated in parentheses above each UV graph. Statistical significance was determined by Mann-Whitney test. Two conditions showed $P < 0.0001$ as indicated.

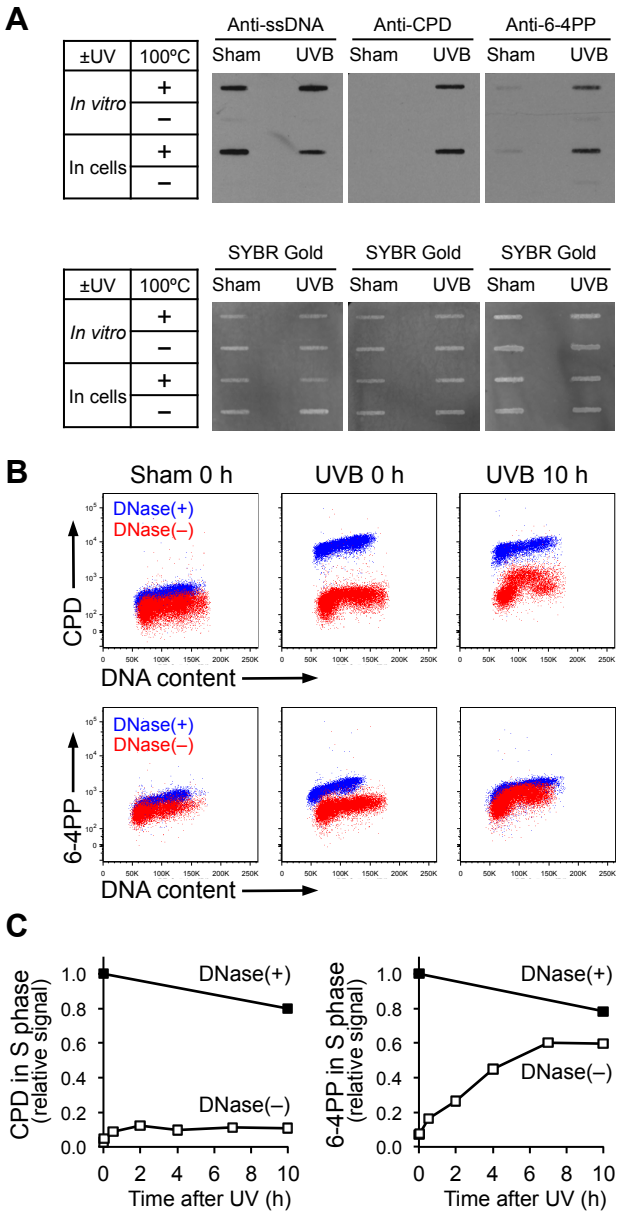

Figure 3.5 6-4PP lesions preferentially become surrounded by ssDNA.

(**A**) Lesion-specific antibodies recognize CPD or 6-4PP on ssDNA, but not on dsDNA. For "*in vitro*" UV irradiation samples, genomic DNA was extracted from unirradiated cells and subsequently irradiated with UVB 30 mJ/cm^2 *in vitro*. For "in cells" irradiation samples, genomic DNA was extracted from cells that were irradiated with UVB 30 mJ/cm^2. DNA was left untreated or heat-denatured at 100ºC for 10 min, and was spotted onto membranes for immuno-slot blot using antibodies specific for ssDNA, CPD, or 6-4PP. The same membranes were stained with SYBR Gold for total DNA detection.

(**B**) UV lesions on ssDNA under non-DNase condition become detectable in S phase long after UV, but not immediately after UV. XP-C cells (GM15983) were harvested immediately (0 h) or 10 h after sham or UVB 30 mJ/cm^2. Fixed cells were left untreated or treated with DNase. CPD and 6-4PP were detected using lesion-specific antibodies validated in panel A to only recognize the lesions when on ssDNA. DNA content was assessed using propidium iodide (PI). Flow cytometry data from two samples (DNase(+) and DNase(–)) were overlaid on each plot.
(**C**) In S phase cells, 6-4PP lesions are increasingly surrounded by ssDNA. Signal intensities of CPD and 6-4PP in S phase at various time points following UV were measured using the same flow cytometry assay as in panel B. Relative signal intensities of CPD or 6-4PP in S phase were calculated relative to 0 (sham irradiation at 0 h) and 1 (UVB 30 mJ/cm^2 at 0 h with DNase treatment).

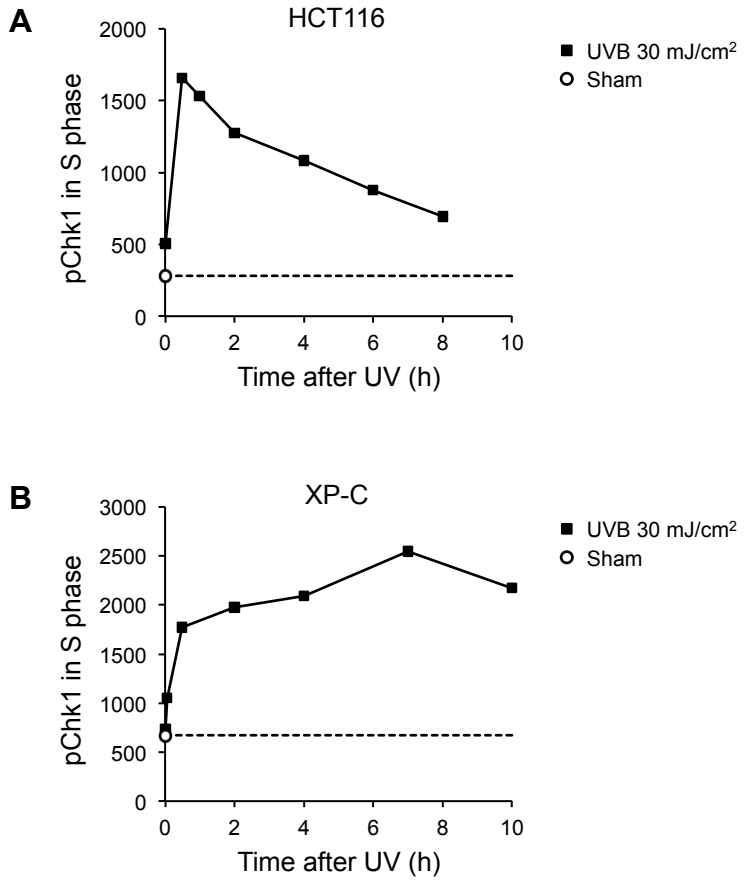

Figure 3.S1 Rapid induction and differential persistence of Chk1 phosphorylation following UV in NER-proficient and NER-deficient cells.

NER-proficient HCT116 (**A**) and NER-deficient XP-C (GM15983) (**B**) cells were irradiated with UVB 30 mJ/cm^2 and then harvested at various time points after UV. Sham samples were mock-irradiated (no UV) and harvested immediately (0 h). The level of Chk1 phosphorylation at Ser345 (pChk1) was measured in S phase cells using flow cytometry. Horizontal dotted line indicates the level of pChk1 that was detected in sham-treated cells harvested at 0 h.

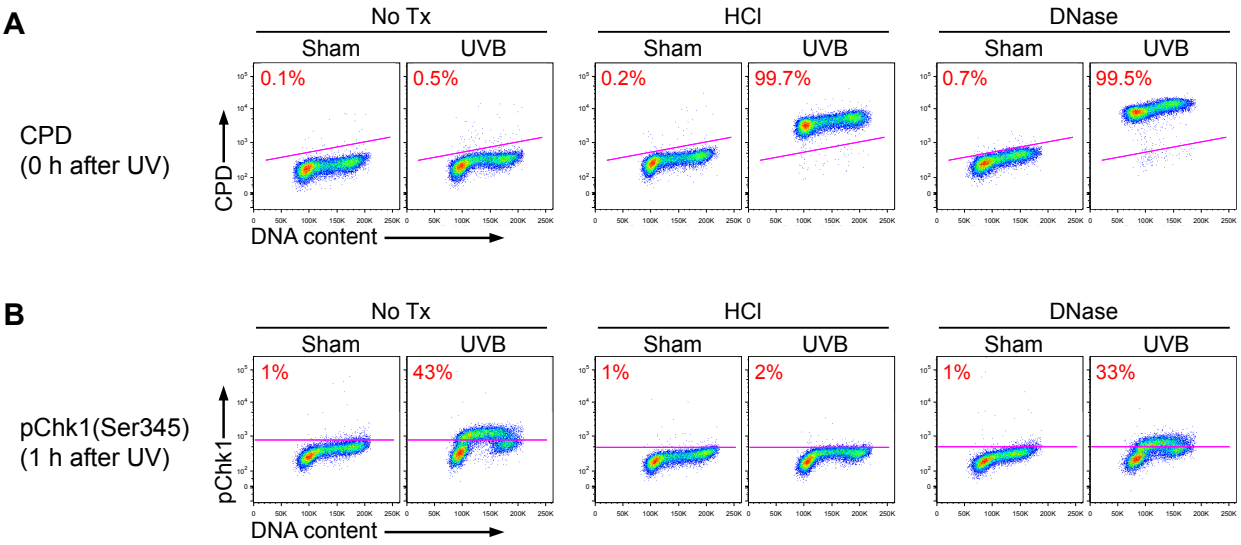

Figure 3.S2 Development of a flow cytometry assay allowing detection of UV lesions and phosphoproteins.

(**A and B**) DNase allows detection of both UV lesions and phosphoproteins. XP-C cells (GM15983) were harvested immediately (0 h) or 1 h after sham or UVB 30 mJ/cm^2 irradiation. After fixation, cells were treated with HCl or DNase, or left untreated (No Tx). Cells were stained with anti-CPD (**A**) or anti-phosphorylated Chk1 (Ser345) (**B**), in addition to staining of FxCycle Violet for DNA content. Percentage of CPD(+) cells and pChk1(+) cells are shown in panel A and B, respectively.

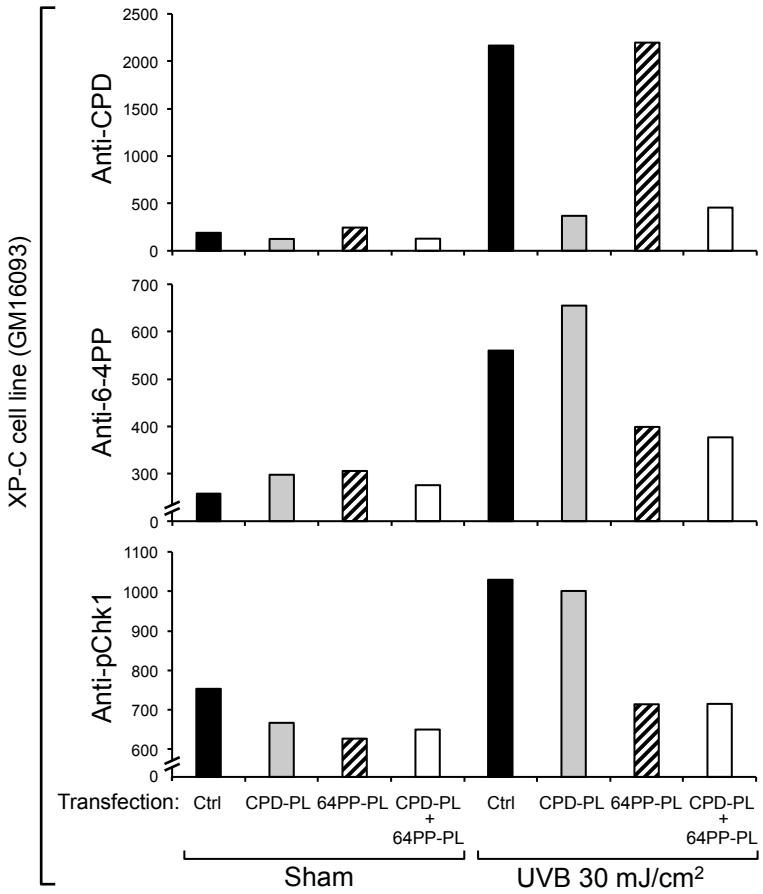

Figure 3.S3 Phosphorylation of Chk1 is potently induced by 6-4PP, but not CPD, in a separate XP-C cell line.

An XP-C cell line (GM16093) derived from a different patient was analyzed using the same experimental design as used for the GM15983 cell line in Figure 3.3A. The levels of CPD, 6-4PP, and phosphorylation of Chk1 at Ser345 (pChk1) in EdU(–)BrdU(+) cells (UV-irradiated outside S phase, underwent photorepair, and then entered S phase) were evaluated in control vector-transfected cells (Ctrl; black) and in cells expressing CPD-photolyase (CPD-PL; gray), 6-4PP-photolyase (64PP-PL; hatched), or both photolyases (white). Fluorescence signals detected by flow cytometry using the indicated antibodies are shown (arbitrary units; n = 1).

Chapter 4. Summary and future directions

4.1 Proposed model of lesion-specific ATR activation

UV irradiation generates two major types of DNA lesions (CPD and 6-4PP) that could eventually lead to development of skin cancer, the most prevalent cancer in humans. In response to UV, cells activate the ATR signaling pathway to survive DNA damage. We hypothesized that two structurally distinct types of UV-induced DNA lesions (CPD and 6-4PP) have different abilities to block DNA replication and activate the ATR-Chk1 pathway (Chapter 2). In the present study, by generating cells with a single type of UV lesions, we found that UV-induced replication blockage and ATR activation are mediated by 6-4PP, but not CPD (Chapter 3). Based on these findings, we propose a model for how 6-4PP lesions (but not CPD lesions) impede DNA replication, leading to ATR activation (**Figure 4.1**). In this model, stalled DNA replication promptly restarts downstream of CPD lesions, and the resulting ssDNA gaps are efficiently filled by TLS. As a result, ssDNA generated at CPD lesions may be short in length and transient in appearance and thus, not sufficient for ATR activation. In contrast, repriming downstream of 6-4PP lesions may be delayed or inhibited, and TLS across 6-4PP is profoundly blocked. Extensive and persistent ssDNA may therefore be preferentially generated at 6-4PP lesions, leading to potent ATR activation.

Although our data suggest that repriming could promptly occur at CPD lesions but tends to be delayed or blocked at 6-4PP lesions, it is unclear how repriming is differentially initiated at distinct types of lesions. One possibility is that efficient TLS may facilitate repriming so that TLS and repriming are both efficient at CPD, but not at 6-4PP lesions. This could be tested using XP-V cells with only CPD lesions: determine whether deficiency in Pol η impedes not only TLS

across CPD but also repriming downstream of CPD. TLS and repriming could be assessed by maRTA (as used for Figure 3.4) and lesion-specific antibodies that recognize lesions on ssDNA (as used for Figure 3.5). If inefficient TLS blocks repriming, delayed repriming downstream of 6-4PP lesions is likely a consequence of inefficient TLS across 6-4PP. Elucidating the interplay between TLS and repriming will provide insight into how cells tolerate DNA-distorting lesions during replication.

4.2 Significance: implications of our findings for mysteries in the field

While UV carcinogenesis has been extensively studied, the basis for some prior findings on mutagenic outcomes of UV-damaged cells remains elusive. Specifically, how the two major types of UV lesions differentially contribute to UV carcinogenesis remains unclear. Moreover, how UV exposure at varying wavelengths leads to differential mutagenicity is not well understood. It is possible that the status of ATR activation is critical in determining the contribution of UV lesions to induce mutations and cause cancers, due to the extensive involvement of ATR in replication progression, cell cycle transition, and DNA repair. Based on our findings of distinct roles of CPD and 6-4PP in ATR activation, we propose the following models that may explain differential mutagenic outcomes, depending on types of UV lesions and ATR activation status (**Figure 4.2**). In cells with both types of UV lesions, ATR is activated, leading to inhibition of new origin firing (**Figure 4.2A**). This decreases the likelihood of UV lesions being encountered by replicative polymerases and thus, reduces the need for TLS (a process that is inherently mutagenic). If ATR is inhibited in cells with both types of UV lesions, origin firing and mitotic entry would not be suppressed (**Figure 4.2B**). Under such circumstances, replicative polymerases more frequently encounter UV lesions. While cell cycle progression is not inhibited, 6-4PP lesions may prolong replication blockage, leading to premature mitotic entry without completion of DNA replication. In contrast, when CPD is the only major type of UV lesion present in cells, ATR is not activated, and DNA replication could be completed via TLS across CPD, a process that could increase a mutation burden (**Figure 4.2C**). These models may provide a plausible basis for two prior observations that remained mysteries in the field.

Why does 6-4PP photorepair in mice have no protective effect on UV tumorigenesis?

A prior study using photolyase transgenic mice demonstrated that while CPD

photorepair in skin decreased the incidence of skin tumor formation following chronic UV irradiation, photorepair of 6-4PP lesions had no effect on suppressing UV tumorigenesis (126). This is surprising because studies with UV-irradiated plasmids had shown that both CPD and 6-4PP lesions are mutagenic, with 6-4PP being even more mutagenic than CPD on a per-lesion basis (16, 133). The lack of an effect of 6-4PP photorepair on suppressing UV tumorigenesis in mice could be due to rapid NER of 6-4PP lesions. Because 6-4PP lesions are rapidly removed by NER (half-life of ~2 h), additional repair of 6-4PP via 6-4PP-photolyase would not be effective in suppressing UV tumorigenesis when NER is proficient. Notably, our findings may provide an alternative explanation for the observation that 6-4PP photorepair has no cancer-preventive effect. Because ATR activation is 6-4PP-dependent, photorepair of 6-4PP in UV-irradiated transgenic mice may significantly reduce ATR activation (**Figure 4.2C**). As a consequence, new replication origin firing, which is normally inhibited by ATR upon DNA damage, may occur. This facilitates DNA replication in the presence of CPD, an inherently error-prone process. Therefore, although 6-4PP photorepair may reduce 6-4PP-derived mutations, this effect may be offset by a greater increase in mutation incorporation resulted from TLS across the far more abundant CPD lesions, if ATR is not activated.

Why does UV mutagenesis peak at UVA-UVB border wavelengths?

Although the wavelength-dependent formation of UV-induced DNA lesions has been investigated (8, 9, 152), the relationship between UV wavelengths and mutagenicity is less well understood. While it has been known that more DNA lesions are generated at shorter wavelengths (9), mutagenicity does not consistently increase as wavelengths shorten. In fact, UV mutagenicity peaks at around 315 nm, the border between UVA and UVB (153). To date, it is not clear why these border wavelengths, rather than shorter wavelengths which generate more DNA lesions, show the highest mutagenicity. A noteworthy difference between UVA and UVB irradiation, which could be relevant to the highest mutagenicity at the border wavelengths,

is that 6-4PP can be generated by UVB, but not by UVA (9). Because our findings suggest that ATR activation is 6-4PP-dependent, it is likely that UVA does not activate ATR. Therefore, UVA-UVB border wavelengths would generate a substantial number of UV lesions (predominantly CPD lesions) without activating ATR. Consequently, new replication origin firing could occur even though a considerable number of CPD lesions are present. This increases TLS across CPD lesions, leading to high mutation frequency (**Figure 4.2C**). Further investigation is needed to test whether lack of ATR activation in cells with CPD lesions leads to high mutation frequency or not.

4.3 Future directions

Human epidemiological studies and mouse *in vivo* data demonstrate that intake of caffeine (a nonspecific ATR inhibitor) prevents UV-associated skin cancers. The cancer-preventive effect of caffeine is likely associated with ATR inhibition because genetic inhibition of ATR in mouse skin also prevents UV-induced carcinogenesis (69% fewer tumors), compared to littermate controls with normal ATR function (62). Enhanced apoptosis of UV-irradiated skin cells has been suggested as a mechanism by which caffeine protects skin from UV-induced cancer development (**Figure 4.2B**). Increased apoptosis by ATR inhibition could be due to prolonged replication blockage at 6-4PP lesions and would not occur in the absence of 6-4PP [following UVA irradiation (no 6-4PP generated) or after selective 6-4PP photorepair]. However, it remains unclear how ATR inhibition preferentially eliminates DNA-damaged cells that are particularly at risk of developing into cancers. Moreover, it has not been investigated whether there is a separate mechanism by which ATR inhibition could suppress UV carcinogenesis. Translationally, it would be important to determine the most effective timing (immediately or long after UV) for ATR inhibition to prevent skin carcinogenesis. These unanswered questions will broaden our understanding of UV-induced DNA damage responses, connecting checkpoint signaling with TLS, mutagenesis, and carcinogenesis.

Does ATR regulate TLS?

Translesion synthesis (TLS) is an important process for cells to cope with UV-induced replication blockage. TLS employs low-fidelity DNA polymerases to replicate across DNA lesions in a relatively error-prone manner. TLS needs to be tightly regulated because of its mutagenic potential. Regulation of TLS involves PCNA mono-ubiquitination, which in turn recruits TLS polymerases to the sites of DNA damage. Interestingly, growing evidence implies that ATR may also play a role in regulating TLS particularly for 6-4PP lesions. Indeed, a recent

study showed that caffeine (a nonspecific ATR inhibitor) abolishes TLS mediated by Rev3 (148), the catalytic subunit of polymerase ζ that has been implicated in 6-4PP bypass. Therefore, it is likely that caffeine could inhibit TLS across 6-4PP lesions. However, because caffeine targets multiple enzymes besides ATR, it is unclear whether ATR is indeed involved in highly mutagenic 6-4PP bypass. This could be tested by determining whether ATR inhibition preferentially increases the amount of 6-4PP lesions surrounded by ssDNA, using the experimental setting as described in **Figure 3.5**. An increase in ssDNA-surrounded 6-4PP lesions after ATR inhibition would suggest that ATR plays a role in TLS across 6-4PP. If ATR facilitates error-prone TLS, this could be another mechanism by which ATR inhibition suppresses UV carcinogenesis, in addition to sensitizing DNA-damaged cells to apoptosis.

Does ATR activation promote UV mutagenesis?

Upon replication stress, ATR regulates diverse cellular processes. The respective roles of ATR produce possibly conflicting effects on UV mutagenesis (**Figure 4.2A**). After UV irradiation, DNA-damaged cells in epidermis could be persistently arrested in S phase and are removed by outward transit from the basal layer of the epidermis and subsequent shedding from skin (154). In parallel, ATR inhibits new origin firing and arrests the cell cycle, allowing time for NER to remove UV lesions. Thus, ATR activation has been thought to have a protective effect on UV mutagenesis. However, a prior study that quantitated mutation frequency at the *HPRT* gene locus showed that depletion of ATR or Chk1 did not increase the UV-induced mutation frequency (155). These findings question the idea that UV-induced ATR activation protects cells from incorporating mutations. Instead, an intriguing hypothesis is that ATR activation promotes UV mutagenesis under some circumstances. This hypothesis is based on prior findings that ATR activation prevents breakage of stalled replication forks (57) and allows the recruitment of TLS polymerases to stalled replication forks (89). Thus, ATR may promote TLS across UV lesions and cell survival, but mutations may be incorporated during TLS. These surviving DNA-

damaged cells are at risk of developing into cancers. It would be relevant to investigate whether ATR activation is particularly important for cells to survive 6-4PP lesions, which are highly mutagenic, thereby increasing UV mutagenesis and subsequent malignant transformation.

When should ATR be inhibited to prevent UV carcinogenesis: immediately versus long after UV?

While ATR inhibition that sensitizes DNA-damaged cells to apoptosis has been considered as a promising strategy to prevent UV carcinogenesis, the optimal timing of ATR inhibition for cancer prevention has not been determined. Moreover, it is unknown whether ATR inhibition is effective for preventing either UVA- or UVB-induced carcinogenesis or both. The present study has implications for these translationally significant questions. Because we found that the ATR-Chk1 pathway is activated predominantly by 6-4PP lesions (half-life of ~2 h), the effective window for ATR inhibition to prevent UV carcinogenesis might be within the first several hours following UV exposure. Moreover, as we showed that CPD lesions have no effect on replication blockage and ATR activation, it is likely that ATR inhibition would not be effective in cells with only CPD lesions (such as exposure to UVA). To test these hypotheses, an *in vivo* study could be designed, comparing the cancer-protective effect of caffeine that is applied immediately or long after UVA or UVB irradiation.

In conclusion, our study dissecting the individual roles of two major UV-induced DNA lesions in ATR activation and replication blockage advances the current understanding of UV-associated DNA damage responses. However, it remains to be determined whether ATR is involved in error-prone translesion synthesis and whether ATR promotes mutation incorporation. Further investigation will enable us to better harness the ATR pathway for preventive as well as therapeutic strategies for UV-induced skin malignancies.

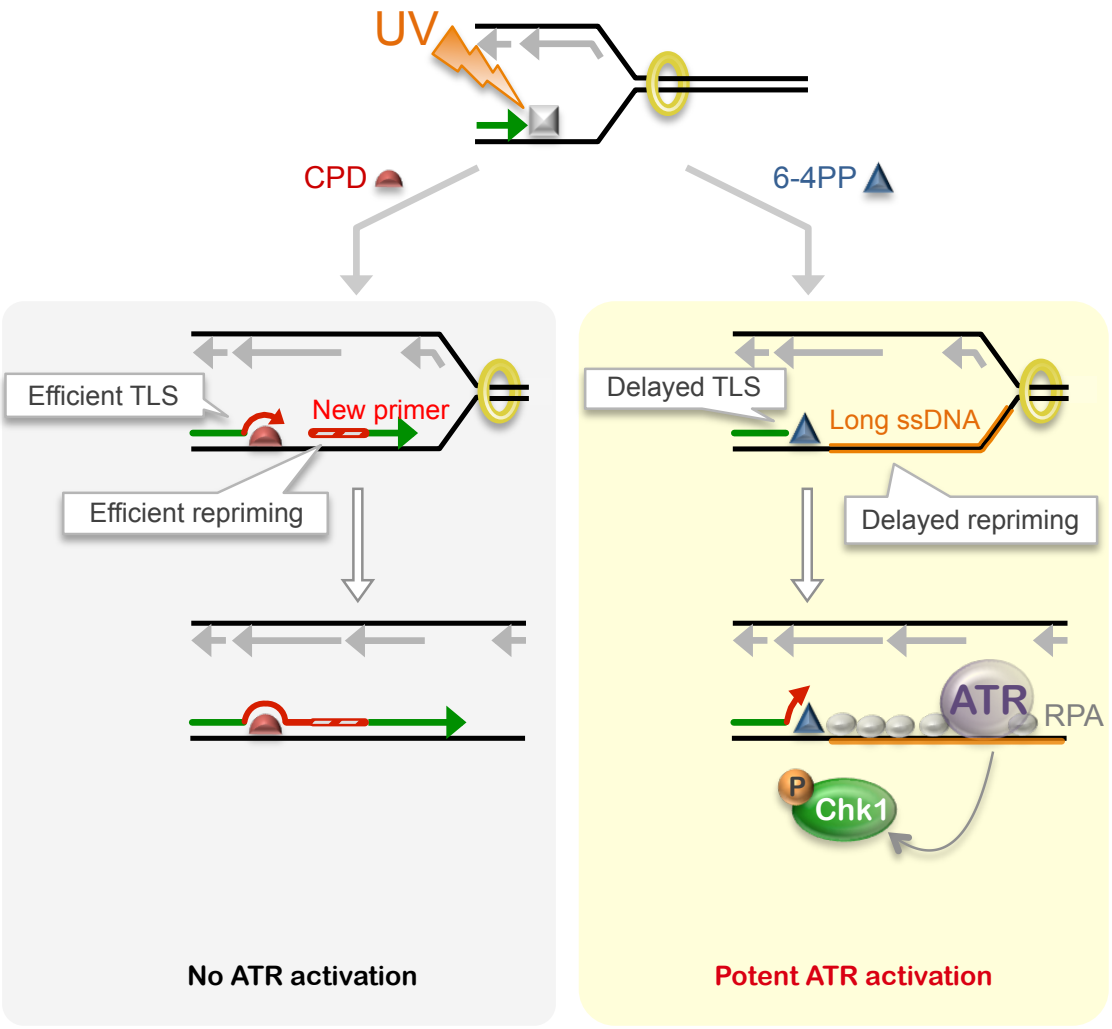

Figure 4.1 Proposed model depicting how 6-4PP lesions (but not CPD) impede DNA replication and activate the ATR-Chk1 pathway.

(**Left**) CPD lesions can be efficiently bypassed via translesion synthesis (TLS) and repriming. ATR is not activated due to lack of persistent single-stranded DNA (ssDNA).

(**Right**) TLS and repriming may be delayed or not occur at 6-4PP lesions, leading to generation of long ssDNA and activation of the ATR pathway.

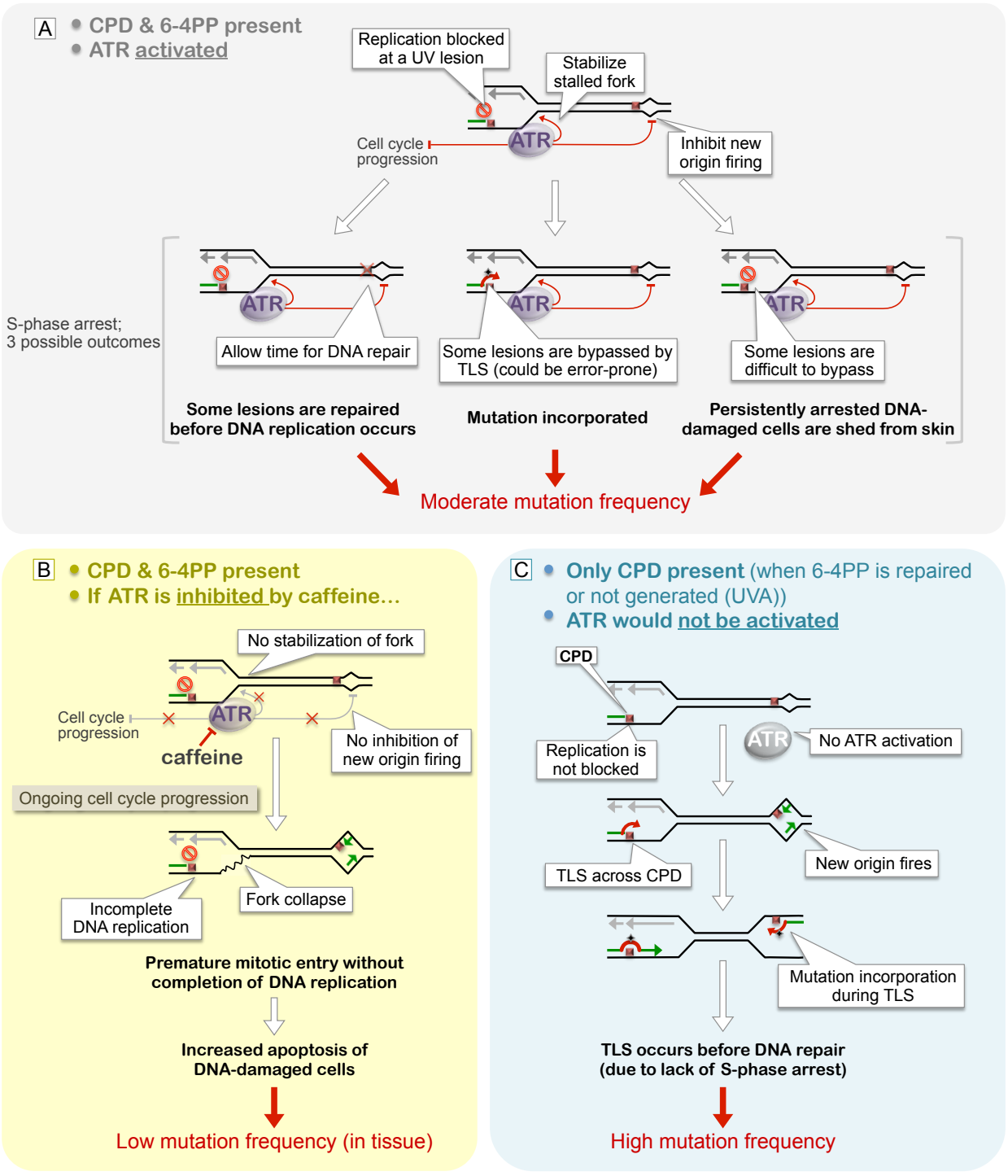

Figure 4.2 Proposed models for differential mutagenic outcomes, depending on types of UV lesions and ATR activation status.

(**A**) ATR activation in the presence of both CPD and 6-4PP lesions may moderately increase mutation frequency. ATR could reduce mutation incorporation by stabilizing stalled replication

forks for DNA repair, or by persistent S-phase arrest of DNA-damaged cells that are shed from skin. Conversely, ATR-mediated fork stabilization may enable inherently mutagenic translesion synthesis (TLS) to occur. Collectively, the net result of ATR activation in cells with both CPD and 6-4PP may be moderately increased mutation frequency.

(**B**) ATR inhibition in the presence of both CPD and 6-4PP lesions could reduce the mutation frequency. UV-irradiated cells in which ATR is inhibited (e.g., by caffeine) may be prone to replication fork collapse and premature mitotic entry, resulting in apoptosis of DNA-damaged cells and reduced mutation frequency.

(**C**) Cells with only CPD present may have high mutation frequency due to lack of ATR activation. New origin firing is not inhibited in UV-irradiated cells in which CPD is the only major type of lesions and ATR is thus not activated. Continued origin firing may facilitate DNA replication via TLS across CPD; however, the TLS process increases the mutation frequency.

References

1. Armstrong BK, Kricker A. The epidemiology of UV induced skin cancer. J Photochem Photobiol B. 2001;63(1-3):8-18. PMID: 11684447.

2. Rogers HW, Weinstock MA, Harris AR, Hinckley MR, Feldman SR, Fleischer AB, Coldiron BM. Incidence estimate of nonmelanoma skin cancer in the United States, 2006. Arch Dermatol. 2010;146(3):283-287. PMID: 20231499.

3. Siegel R, Ma J, Zou Z, Jemal A. Cancer statistics, 2014. CA Cancer J Clin. 2014;64(1):9-29. PMID: 24399786.

4. de Gruijl FR. Photocarcinogenesis: UVA vs UVB. Methods Enzymol. 2000;319:359-366. PMID: 10907526.

5. de Laat A, van der Leun JC, de Gruijl FR. Carcinogenesis induced by UVA (365-nm) radiation: the dose-time dependence of tumor formation in hairless mice. Carcinogenesis. 1997;18(5):1013-1020. PMID: 9163689.

6. de Gruijl FR, Sterenborg HJ, Forbes PD, Davies RE, Cole C, Kelfkens G, van Weelden H, Slaper H, van der Leun JC. Wavelength dependence of skin cancer induction by ultraviolet irradiation of albino hairless mice. Cancer Res. 1993;53(1):53-60. PMID: 8416751.

7. Runger TM. Role of UVA in the pathogenesis of melanoma and non-melanoma skin cancer. A short review. Photodermatol Photoimmunol Photomed. 1999;15(6):212-216. PMID: 10599968.

8. Perdiz D, Grof P, Mezzina M, Nikaido O, Moustacchi E, Sage E. Distribution and repair of bipyrimidine photoproducts in solar UV-irradiated mammalian cells. Possible role of Dewar photoproducts in solar mutagenesis. J Biol Chem. 2000;275(35):26732-26742. PMID: 10827179.

9. Besaratinia A, Yoon JI, Schroeder C, Bradforth SE, Cockburn M, Pfeifer GP. Wavelength dependence of ultraviolet radiation-induced DNA damage as determined by laser irradiation suggests that cyclobutane pyrimidine dimers are the principal DNA lesions produced by terrestrial sunlight. FASEB J. 2011;25(9):3079-3091. PMID: 21613571.

10. Douki T, Reynaud-Angelin A, Cadet J, Sage E. Bipyrimidine photoproducts rather than oxidative lesions are the main type of DNA damage involved in the genotoxic effect of solar UVA radiation. Biochemistry. 2003;42(30):9221-9226. PMID: 12885257.

11. Besaratinia A, Synold TW, Chen HH, Chang C, Xi B, Riggs AD, Pfeifer GP. DNA lesions induced by UV A1 and B radiation in human cells: comparative analyses in the overall genome and in the p53 tumor suppressor gene. Proc Natl Acad Sci U S A. 2005;102(29):10058-10063. PMID: 16009942.

12. Matsunaga T, Hatakeyama Y, Ohta M, Mori T, Nikaido O. Establishment and characterization of a monoclonal antibody recognizing the Dewar isomers of (6-4)photoproducts. Photochem Photobiol. 1993;57(6):934-940. PMID: 8367534.

13. Haiser K, Fingerhut BP, Heil K, Glas A, Herzog TT, Pilles BM, Schreier WJ, Zinth W, de Vivie-Riedle R, Carell T. Mechanism of UV-induced formation of Dewar lesions in DNA. Angew Chem Int Ed Engl. 2012;51(2):408-411. PMID: 22109845.

14. Rastogi RP, Richa, Kumar A, Tyagi MB, Sinha RP. Molecular mechanisms of ultraviolet radiation-induced DNA damage and repair. J Nucleic Acids. 2010;2010:592980. PMID: 21209706.

15. Kim JK, Patel D, Choi BS. Contrasting structural impacts induced by cis-syn cyclobutane dimer and (6-4) adduct in DNA duplex decamers: implication in mutagenesis and repair activity. Photochem Photobiol. 1995;62(1):44-50. PMID: 7638271.

16. Shachar S, Ziv O, Avkin S, Adar S, Wittschieben J, Reissner T, Chaney S, Friedberg EC, Wang Z, Carell T, Geacintov N, Livneh Z. Two-polymerase mechanisms dictate error-free and error-prone translesion DNA synthesis in mammals. EMBO J. 2009;28(4):383-393. PMID: 19153606.

17. Nikolaishvili-Feinberg N, Cordeiro-Stone M. Bypass replication in vitro of UV-induced photoproducts blocking leading or lagging strand synthesis. Biochemistry. 2001;40(50):15215-15223. PMID: 11735404.

18. de Lima-Bessa KM, Armelini MG, Chigancas V, Jacysyn JF, Amarante-Mendes GP, Sarasin A, Menck CF. CPDs and 6-4PPs play different roles in UV-induced cell death in normal and NER-deficient human cells. DNA Repair (Amst). 2008;7(2):303-312. PMID: 18096446.

19. Kamileri I, Karakasilioti I, Garinis GA. Nucleotide excision repair: new tricks with old bricks. Trends Genet. 2012;28(11):566-573. PMID: 22824526.

20. Sancar A, Lindsey-Boltz LA, Unsal-Kacmaz K, Linn S. Molecular mechanisms of mammalian DNA repair and the DNA damage checkpoints. Annu Rev Biochem. 2004;73:39-85. PMID: 15189136.

21. Marteijn JA, Lans H, Vermeulen W, Hoeijmakers JH. Understanding nucleotide excision repair and its roles in cancer and ageing. Nat Rev Mol Cell Biol. 2014;15(7):465-481. PMID: 24954209.

22. Moser J, Kool H, Giakzidis I, Caldecott K, Mullenders LH, Fousteri MI. Sealing of chromosomal DNA nicks during nucleotide excision repair requires XRCC1 and DNA ligase III alpha in a cell-cycle-specific manner. Mol Cell. 2007;27(2):311-323. PMID: 17643379.

23. Ogi T, Lehmann AR. The Y-family DNA polymerase kappa (pol kappa) functions in mammalian nucleotide-excision repair. Nat Cell Biol. 2006;8(6):640-642. PMID: 16738703.

24. Ogi T, Limsirichaikul S, Overmeer RM, Volker M, Takenaka K, Cloney R, Nakazawa Y, Niimi A, Miki Y, Jaspers NG, Mullenders LH, Yamashita S, Fousteri MI, Lehmann AR. Three DNA polymerases, recruited by different mechanisms, carry out NER repair synthesis in human cells. Mol Cell. 2010;37(5):714-727. PMID: 20227374.

25. Young AR, Chadwick CA, Harrison GI, Hawk JL, Nikaido O, Potten CS. The in situ repair kinetics of epidermal thymine dimers and 6-4 photoproducts in human skin types I and II. J Invest Dermatol. 1996;106(6):1307-1313. PMID: 8752675.

26. DiGiovanna JJ, Kraemer KH. Shining a light on xeroderma pigmentosum. J Invest Dermatol. 2012;132(3 Pt 2):785-796. PMID: 22217736.

27. Cleaver JE, Lam ET, Revet I. Disorders of nucleotide excision repair: the genetic and molecular basis of heterogeneity. Nat Rev Genet. 2009;10(11):756-768. PMID: 19809470.

28. Menck CF. Shining a light on photolyases. Nat Genet. 2002;32(3):338-339. PMID: 12410227.

29. Sancar A. Structure and function of DNA photolyase and cryptochrome blue-light photoreceptors. Chem Rev. 2003;103(6):2203-2237. PMID: 12797829.

30. Ciccia A, Elledge SJ. The DNA damage response: making it safe to play with knives. Mol Cell. 2010;40(2):179-204. PMID: 20965415.

31. Abraham RT. Cell cycle checkpoint signaling through the ATM and ATR kinases. Genes Dev. 2001;15(17):2177-2196. PMID: 11544175.

32. Kim ST, Lim DS, Canman CE, Kastan MB. Substrate specificities and identification of putative substrates of ATM kinase family members. J Biol Chem. 1999;274(53):37538-37543. PMID: 10608806.

33. Cimprich KA, Cortez D. ATR: an essential regulator of genome integrity. Nat Rev Mol Cell Biol. 2008;9(8):616-627. PMID: 18594563.

34. Ellison V, Stillman B. Biochemical characterization of DNA damage checkpoint complexes: clamp loader and clamp complexes with specificity for 5' recessed DNA. PLoS Biol. 2003;1(2):E33. PMID: 14624239.

35. Cotta-Ramusino C, McDonald ER, 3rd, Hurov K, Sowa ME, Harper JW, Elledge SJ. A DNA damage response screen identifies RHINO, a 9-1-1 and TopBP1 interacting protein required for ATR signaling. Science. 2011;332(6035):1313-1317. PMID: 21659603.

36. Delacroix S, Wagner JM, Kobayashi M, Yamamoto K, Karnitz LM. The Rad9-Hus1-Rad1 (9-1-1) clamp activates checkpoint signaling via TopBP1. Genes Dev. 2007;21(12):1472-1477. PMID: 17575048.

37. Lee J, Dunphy WG. Rad17 plays a central role in establishment of the interaction between TopBP1 and the Rad9-Hus1-Rad1 complex at stalled replication forks. Mol Biol Cell. 2010;21(6):926-935. PMID: 20110345.

38. Yan S, Michael WM. TopBP1 and DNA polymerase-alpha directly recruit the 9-1-1 complex to stalled DNA replication forks. J Cell Biol. 2009;184(6):793-804. PMID: 19289795.

39. Kumagai A, Lee J, Yoo HY, Dunphy WG. TopBP1 activates the ATR-ATRIP complex. Cell. 2006;124(5):943-955. PMID: 16530042.

40. Mordes DA, Glick GG, Zhao R, Cortez D. TopBP1 activates ATR through ATRIP and a PIKK regulatory domain. Genes Dev. 2008;22(11):1478-1489. PMID: 18519640.

41. Burrows AE, Elledge SJ. How ATR turns on: TopBP1 goes on ATRIP with ATR. Genes Dev. 2008;22(11):1416-1421. PMID: 18519633.

42. Liu S, Shiotani B, Lahiri M, Marechal A, Tse A, Leung CC, Glover JN, Yang XH, Zou L. ATR autophosphorylation as a molecular switch for checkpoint activation. Mol Cell. 2011;43(2):192-202. PMID: 21777809.

43. Stokes MP, Rush J, Macneill J, Ren JM, Sprott K, Nardone J, Yang V, Beausoleil SA, Gygi SP, Livingstone M, Zhang H, Polakiewicz RD, Comb MJ. Profiling of UV-induced ATM/ATR signaling pathways. Proc Natl Acad Sci U S A. 2007;104(50):19855-19860. PMID: 18077418.

44. Tibbetts RS, Brumbaugh KM, Williams JM, Sarkaria JN, Cliby WA, Shieh SY, Taya Y, Prives C, Abraham RT. A role for ATR in the DNA damage-induced phosphorylation of p53. Genes Dev. 1999;13(2):152-157. PMID: 9925639.

45. Speroni J, Federico MB, Mansilla SF, Soria G, Gottifredi V. Kinase-independent function of checkpoint kinase 1 (Chk1) in the replication of damaged DNA. Proc Natl Acad Sci U S A. 2012;109(19):7344-7349. PMID: 22529391.

46. Smits VA. Spreading the signal: dissociation of Chk1 from chromatin. Cell Cycle. 2006;5(10):1039-1043. PMID: 16721053.

47. Smits VA, Reaper PM, Jackson SP. Rapid PIKK-dependent release of Chk1 from chromatin promotes the DNA-damage checkpoint response. Curr Biol. 2006;16(2):150-159. PMID: 16360315.

48. Liu Q, Guntuku S, Cui XS, Matsuoka S, Cortez D, Tamai K, Luo G, Carattini-Rivera S, DeMayo F, Bradley A, Donehower LA, Elledge SJ. Chk1 is an essential kinase that is regulated by Atr and required for the G(2)/M DNA damage checkpoint. Genes Dev. 2000;14(12):1448-1459. PMID: 10859164.

49. Helt CE, Cliby WA, Keng PC, Bambara RA, O'Reilly MA. Ataxia telangiectasia mutated (ATM) and ATM and Rad3-related protein exhibit selective target specificities in response to different forms of DNA damage. J Biol Chem. 2005;280(2):1186-1192. PMID: 15533933.

50. Zhao H, Piwnica-Worms H. ATR-mediated checkpoint pathways regulate phosphorylation and activation of human Chk1. Mol Cell Biol. 2001;21(13):4129-4139. PMID: 11390642.

51. Boutros R, Dozier C, Ducommun B. The when and wheres of CDC25 phosphatases. Curr Opin Cell Biol. 2006;18(2):185-191. PMID: 16488126.

52. Furnari B, Rhind N, Russell P. Cdc25 mitotic inducer targeted by chk1 DNA damage checkpoint kinase. Science. 1997;277(5331):1495-1497. PMID: 9278510.

53. Peng CY, Graves PR, Thoma RS, Wu Z, Shaw AS, Piwnica-Worms H. Mitotic and G2 checkpoint control: regulation of 14-3-3 protein binding by phosphorylation of Cdc25C on serine-216. Science. 1997;277(5331):1501-1505. PMID: 9278512.

54. Sanchez Y, Wong C, Thoma RS, Richman R, Wu Z, Piwnica-Worms H, Elledge SJ. Conservation of the Chk1 checkpoint pathway in mammals: linkage of DNA damage to Cdk regulation through Cdc25. Science. 1997;277(5331):1497-1501. PMID: 9278511.

55. Lopez-Girona A, Tanaka K, Chen XB, Baber BA, McGowan CH, Russell P. Serine-345 is required for Rad3-dependent phosphorylation and function of checkpoint kinase Chk1 in fission yeast. Proc Natl Acad Sci U S A. 2001;98(20):11289-11294. PMID: 11553781.

56. Santocanale C, Diffley JF. A Mec1- and Rad53-dependent checkpoint controls late-firing origins of DNA replication. Nature. 1998;395(6702):615-618. PMID: 9783589.

57. Toledo LI, Altmeyer M, Rask MB, Lukas C, Larsen DH, Povlsen LK, Bekker-Jensen S, Mailand N, Bartek J, Lukas J. ATR prohibits replication catastrophe by preventing global exhaustion of RPA. Cell. 2013;155(5):1088-1103. PMID: 24267891.

58. Friedel AM, Pike BL, Gasser SM. ATR/Mec1: coordinating fork stability and repair. Curr Opin Cell Biol. 2009;21(2):237-244. PMID: 19230642.

59. Nghiem P, Park PK, Kim Y, Vaziri C, Schreiber SL. ATR inhibition selectively sensitizes G1 checkpoint-deficient cells to lethal premature chromatin condensation. Proc Natl Acad Sci U S A. 2001;98(16):9092-9097. PMID: 11481475.

60. Huang MT, Xie JG, Wang ZY, Ho CT, Lou YR, Wang CX, Hard GC, Conney AH. Effects of tea, decaffeinated tea, and caffeine on UVB light-induced complete carcinogenesis in SKH-1 mice: demonstration of caffeine as a biologically important constituent of tea. Cancer Res. 1997;57(13):2623-2629. PMID: 9205068.

61. Lu YP, Lou YR, Xie JG, Peng QY, Liao J, Yang CS, Huang MT, Conney AH. Topical applications of caffeine or (-)-epigallocatechin gallate (EGCG) inhibit carcinogenesis and selectively increase apoptosis in UVB-induced skin tumors in mice. Proc Natl Acad Sci U S A. 2002;99(19):12455-12460. PMID: 12205293.

62. Kawasumi M, Lemos B, Bradner JE, Thibodeau R, Kim YS, Schmidt M, Higgins E, Koo SW, Angle-Zahn A, Chen A, Levine D, Nguyen L, Heffernan TP, Longo I, Mandinova A, Lu YP, Conney AH, Nghiem P. Protection from UV-induced skin carcinogenesis by genetic inhibition of the ataxia telangiectasia and Rad3-related (ATR) kinase. Proc Natl Acad Sci U S A. 2011;108(33):13716-13721. PMID: 21844338.

63. Jacobsen BK, Bjelke E, Kvale G, Heuch I. Coffee drinking, mortality, and cancer incidence: results from a Norwegian prospective study. J Natl Cancer Inst. 1986;76(5):823-831. PMID: 3457969.

64. Hakim IA, Harris RB, Weisgerber UM. Tea intake and squamous cell carcinoma of the skin: influence of type of tea beverages. Cancer Epidemiol Biomarkers Prev. 2000;9(7):727-731. PMID: 10919744.

65. Abel EL, Hendrix SO, McNeeley SG, Johnson KC, Rosenberg CA, Mossavar-Rahmani Y, Vitolins M, Kruger M. Daily coffee consumption and prevalence of nonmelanoma skin cancer in Caucasian women. Eur J Cancer Prev. 2007;16(5):446-452. PMID: 17923816.

66. Rees JR, Stukel TA, Perry AE, Zens MS, Spencer SK, Karagas MR. Tea consumption and basal cell and squamous cell skin cancer: results of a case-control study. J Am Acad Dermatol. 2007;56(5):781-785. PMID: 17261341.

67. Song F, Qureshi AA, Han J. Increased caffeine intake is associated with reduced risk of basal cell carcinoma of the skin. Cancer Res. 2012;72(13):3282-3289. PMID: 22752299.

68. Heffernan TP, Kawasumi M, Blasina A, Anderes K, Conney AH, Nghiem P. ATR-Chk1 pathway inhibition promotes apoptosis after UV treatment in primary human keratinocytes: potential basis for the UV protective effects of caffeine. J Invest Dermatol. 2009;129(7):1805-1815. PMID: 19242509.

69. Koo SW, Hirakawa S, Fujii S, Kawasumi M, Nghiem P. Protection from photodamage by topical application of caffeine after ultraviolet irradiation. Br J Dermatol. 2007;156(5):957-964. PMID: 17388926.

70. Lu YP, Lou YR, Li XH, Xie JG, Lin Y, Shih WJ, Conney AH. Stimulatory effect of topical application of caffeine on UVB-induced apoptosis in mouse skin. Oncol Res. 2002;13(2):61-70. PMID: 12392153.

71. Loeb LA, Monnat RJ, Jr. DNA polymerases and human disease. Nat Rev Genet. 2008;9(8):594-604. PMID: 18626473.

72. Yang W. Damage repair DNA polymerases Y. Curr Opin Struct Biol. 2003;13(1):23-30. PMID: 12581656.

73. Friedberg EC, Fischhaber PL, Kisker C. Error-prone DNA polymerases: novel structures and the benefits of infidelity. Cell. 2001;107(1):9-12. PMID: 11595180.

74. Friedberg EC. Suffering in silence: the tolerance of DNA damage. Nat Rev Mol Cell Biol. 2005;6(12):943-953. PMID: 16341080.

75. Prakash S, Johnson RE, Prakash L. Eukaryotic translesion synthesis DNA polymerases: specificity of structure and function. Annu Rev Biochem. 2005;74:317-353. PMID: 15952890.

76. McCulloch SD, Kunkel TA. The fidelity of DNA synthesis by eukaryotic replicative and translesion synthesis polymerases. Cell Res. 2008;18(1):148-161. PMID: 18166979.

77. Kunkel TA. DNA replication fidelity. J Biol Chem. 2004;279(17):16895-16898. PMID: 14988392.

78. Goodman MF. Error-prone repair DNA polymerases in prokaryotes and eukaryotes. Annu Rev Biochem. 2002;71:17-50. PMID: 12045089.

79. Johnson RE, Prakash S, Prakash L. Efficient bypass of a thymine-thymine dimer by yeast DNA polymerase, Poleta. Science. 1999;283(5404):1001-1004. PMID: 9974380.

80. Johnson RE, Kondratick CM, Prakash S, Prakash L. hRAD30 mutations in the variant form of xeroderma pigmentosum. Science. 1999;285(5425):263-265. PMID: 10398605.

81. Masutani C, Kusumoto R, Yamada A, Dohmae N, Yokoi M, Yuasa M, Araki M, Iwai S, Takio K, Hanaoka F. The XPV (xeroderma pigmentosum variant) gene encodes human DNA polymerase eta. Nature. 1999;399(6737):700-704. PMID: 10385124.

82. Cleaver JE. Xeroderma pigmentosum: variants with normal DNA repair and normal sensitivity to ultraviolet light. J Invest Dermatol. 1972;58(3):124-128. PMID: 5013606.

83. Friedberg EC, Lehmann AR, Fuchs RP. Trading places: how do DNA polymerases switch during translesion DNA synthesis? Mol Cell. 2005;18(5):499-505. PMID: 15916957.

84. Waters LS, Minesinger BK, Wiltrout ME, D'Souza S, Woodruff RV, Walker GC. Eukaryotic translesion polymerases and their roles and regulation in DNA damage tolerance. Microbiol Mol Biol Rev. 2009;73(1):134-154. PMID: 19258535.

85. Johnson RE, Haracska L, Prakash S, Prakash L. Role of DNA polymerase eta in the bypass of a (6-4) TT photoproduct. Mol Cell Biol. 2001;21(10):3558-3563. PMID: 11313481.

86. Fujii S, Fuchs RP. Defining the position of the switches between replicative and bypass DNA polymerases. EMBO J. 2004;23(21):4342-4352. PMID: 15470496.

87. Garg P, Burgers PM. Ubiquitinated proliferating cell nuclear antigen activates translesion DNA polymerases eta and REV1. Proc Natl Acad Sci U S A. 2005;102(51):18361-18366. PMID: 16344468.

88. Bienko M, Green CM, Crosetto N, Rudolf F, Zapart G, Coull B, Kannouche P, Wider G, Peter M, Lehmann AR, Hofmann K, Dikic I. Ubiquitin-binding domains in Y-family polymerases regulate translesion synthesis. Science. 2005;310(5755):1821-1824. PMID: 16357261.

89. Chen YW, Cleaver JE, Hatahet Z, Honkanen RE, Chang JY, Yen Y, Chou KM. Human DNA polymerase eta activity and translocation is regulated by phosphorylation. Proc Natl Acad Sci U S A. 2008;105(43):16578-16583. PMID: 18946034.

90. Gohler T, Sabbioneda S, Green CM, Lehmann AR. ATR-mediated phosphorylation of DNA polymerase eta is needed for efficient recovery from UV damage. J Cell Biol. 2011;192(2):219-227. PMID: 21242293.

91. Hirano Y, Sugimoto K. ATR homolog Mec1 controls association of DNA polymerase zeta-Rev1 complex with regions near a double-strand break. Curr Biol. 2006;16(6):586-590. PMID: 16546083.

92. Elvers I, Johansson F, Groth P, Erixon K, Helleday T. UV stalled replication forks restart by re-priming in human fibroblasts. Nucleic Acids Res. 2011;39(16):7049-7057. PMID: 21646340.

93. Lopes M, Foiani M, Sogo JM. Multiple mechanisms control chromosome integrity after replication fork uncoupling and restart at irreparable UV lesions. Mol Cell. 2006;21(1):15-27. PMID: 16387650.

94. Foiani M, Lucchini G, Plevani P. The DNA polymerase alpha-primase complex couples DNA replication, cell-cycle progression and DNA-damage response. Trends Biochem Sci. 1997;22(11):424-427. PMID: 9397683.

95. Bianchi J, Rudd SG, Jozwiakowski SK, Bailey LJ, Soura V, Taylor E, Stevanovic I, Green AJ, Stracker TH, Lindsay HD, Doherty AJ. PrimPol bypasses UV photoproducts during eukaryotic chromosomal DNA replication. Mol Cell. 2013;52(4):566-573. PMID: 24267451.

96. Mouron S, Rodriguez-Acebes S, Martinez-Jimenez MI, Garcia-Gomez S, Chocron S, Blanco L, Mendez J. Repriming of DNA synthesis at stalled replication forks by human PrimPol. Nat Struct Mol Biol. 2013;20(12):1383-1389. PMID: 24240614.

97. Garcia-Gomez S, Reyes A, Martinez-Jimenez MI, Chocron ES, Mouron S, Terrados G, Powell C, Salido E, Mendez J, Holt IJ, Blanco L. PrimPol, an archaic primase/polymerase operating in human cells. Mol Cell. 2013;52(4):541-553. PMID: 24207056.

98. Quinet A, Vessoni AT, Rocha CR, Gottifredi V, Biard D, Sarasin A, Menck CF, Stary A. Gap-filling and bypass at the replication fork are both active mechanisms for tolerance of low-dose ultraviolet-induced DNA damage in the human genome. DNA Repair (Amst). 2014;14:27-38. PMID: 24380689.

99. Karras GI, Jentsch S. The RAD6 DNA damage tolerance pathway operates uncoupled from the replication fork and is functional beyond S phase. Cell. 2010;141(2):255-267. PMID: 20403322.

100. Ziegler A, Leffell DJ, Kunala S, Sharma HW, Gailani M, Simon JA, Halperin AJ, Baden HP, Shapiro PE, Bale AE, et al. Mutation hotspots due to sunlight in the p53 gene of nonmelanoma skin cancers. Proc Natl Acad Sci U S A. 1993;90(9):4216-4220. PMID: 8483937.

101. Brash DE, Rudolph JA, Simon JA, Lin A, McKenna GJ, Baden HP, Halperin AJ, Ponten J. A role for sunlight in skin cancer: UV-induced p53 mutations in squamous cell carcinoma. Proc Natl Acad Sci U S A. 1991;88(22):10124-10128. PMID: 1946433.

102. Ziegler A, Jonason AS, Leffell DJ, Simon JA, Sharma HW, Kimmelman J, Remington L, Jacks T, Brash DE. Sunburn and p53 in the onset of skin cancer. Nature. 1994;372(6508):773-776. PMID: 7997263.

103. Jonason AS, Kunala S, Price GJ, Restifo RJ, Spinelli HM, Persing JA, Leffell DJ, Tarone RE, Brash DE. Frequent clones of p53-mutated keratinocytes in normal human skin. Proc Natl Acad Sci U S A. 1996;93(24):14025-14029. PMID: 8943054.

104. Zhang W, Remenyik E, Zelterman D, Brash DE, Wikonkal NM. Escaping the stem cell compartment: sustained UVB exposure allows p53-mutant keratinocytes to colonize adjacent epidermal proliferating units without incurring additional mutations. Proc Natl Acad Sci U S A. 2001;98(24):13948-13953. PMID: 11707578.

105. Chao DL, Eck JT, Brash DE, Maley CC, Luebeck EG. Preneoplastic lesion growth driven by the death of adjacent normal stem cells. Proc Natl Acad Sci U S A. 2008;105(39):15034-15039. PMID: 18815380.

106. Rosso S, Zanetti R, Martinez C, Tormo MJ, Schraub S, Sancho-Garnier H, Franceschi S, Gafa L, Perea E, Navarro C, Laurent R, Schrameck C, Talamini R, Tumino R, Wechsler J. The multicentre south European study 'Helios'. II: Different sun exposure patterns in the aetiology of basal cell and squamous cell carcinomas of the skin. Br J Cancer. 1996;73(11):1447-1454. PMID: 8645596.

107. Choi JH, Pfeifer GP. The role of DNA polymerase eta in UV mutational spectra. DNA Repair (Amst). 2005;4(2):211-220. PMID: 15590329.

108. Yoon JH, Prakash L, Prakash S. Highly error-free role of DNA polymerase eta in the replicative bypass of UV-induced pyrimidine dimers in mouse and human cells. Proc Natl Acad Sci U S A. 2009;106(43):18219-18224. PMID: 19822754.

109. Barak Y, Cohen-Fix O, Livneh Z. Deamination of cytosine-containing pyrimidine photodimers in UV-irradiated DNA. Significance for UV light mutagenesis. J Biol Chem. 1995;270(41):24174-24179. PMID: 7592621.

110. Peng W, Shaw BR. Accelerated deamination of cytosine residues in UV-induced cyclobutane pyrimidine dimers leads to CC-->TT transitions. Biochemistry. 1996;35(31):10172-10181. PMID: 8756482.

111. Tu Y, Dammann R, Pfeifer GP. Sequence and time-dependent deamination of cytosine bases in UVB-induced cyclobutane pyrimidine dimers in vivo. J Mol Biol. 1998;284(2):297-311. PMID: 9813119.

112. Burger A, Fix D, Liu H, Hays J, Bockrath R. In vivo deamination of cytosine-containing cyclobutane pyrimidine dimers in E. coli: a feasible part of UV-mutagenesis. Mutat Res. 2003;522(1-2):145-156. PMID: 12517420.

113. Vu B, Cannistraro VJ, Sun L, Taylor JS. DNA synthesis past a 5-methylC-containing cis-syn-cyclobutane pyrimidine dimer by yeast pol eta is highly nonmutagenic. Biochemistry. 2006;45(30):9327-9335. PMID: 16866379.

114. Jiang N, Taylor JS. In vivo evidence that UV-induced C-->T mutations at dipyrimidine sites could result from the replicative bypass of cis-syn cyclobutane dimers or their deamination products. Biochemistry. 1993;32(2):472-481. PMID: 8422356.

115. Tissier A, Frank EG, McDonald JP, Iwai S, Hanaoka F, Woodgate R. Misinsertion and bypass of thymine-thymine dimers by human DNA polymerase iota. EMBO J. 2000;19(19):5259-5266. PMID: 11013228.

116. McCoy H, Kenney MA. Magnesium and immune function: recent findings. Magnes Res. 1992;5(4):281-293. PMID: 1296765.

117. Prakash S, Prakash L. Translesion DNA synthesis in eukaryotes: a one- or two-polymerase affair. Genes Dev. 2002;16(15):1872-1883. PMID: 12154119.

118. Masutani C, Kusumoto R, Iwai S, Hanaoka F. Mechanisms of accurate translesion synthesis by human DNA polymerase eta. EMBO J. 2000;19(12):3100-3109. PMID: 10856253.

119. Narita T, Tsurimoto T, Yamamoto J, Nishihara K, Ogawa K, Ohashi E, Evans T, Iwai S, Takeda S, Hirota K. Human replicative DNA polymerase delta can bypass T-T (6-4) ultraviolet photoproducts on template strands. Genes Cells. 2010;15(12):1228-1239. PMID: 21070511.

120. Yoon JH, Prakash L, Prakash S. Error-free replicative bypass of (6-4) photoproducts by DNA polymerase zeta in mouse and human cells. Genes Dev. 2010;24(2):123-128. PMID: 20080950.

121. Zou L, Elledge SJ. Sensing DNA damage through ATRIP recognition of RPA-ssDNA complexes. Science. 2003;300(5625):1542-1548. PMID: 12791985.

122. Vidal-Eychenie S, Decaillet C, Basbous J, Constantinou A. DNA structure-specific priming of ATR activation by DNA-PKcs. J Cell Biol. 2013;202(3):421-429. PMID: 23897887.

123. MacDougall CA, Byun TS, Van C, Yee MC, Cimprich KA. The structural determinants of checkpoint activation. Genes Dev. 2007;21(8):898-903. PMID: 17437996.

124. McCulloch SD, Kokoska RJ, Masutani C, Iwai S, Hanaoka F, Kunkel TA. Preferential cis-syn thymine dimer bypass by DNA polymerase eta occurs with biased fidelity. Nature. 2004;428(6978):97-100. PMID: 14999287.

125. Mouret S, Baudouin C, Charveron M, Favier A, Cadet J, Douki T. Cyclobutane pyrimidine dimers are predominant DNA lesions in whole human skin exposed to UVA radiation. Proc Natl Acad Sci U S A. 2006;103(37):13765-13770. PMID: 16954188.

126. Jans J, Schul W, Sert YG, Rijksen Y, Rebel H, Eker AP, Nakajima S, van Steeg H, de Gruijl FR, Yasui A, Hoeijmakers JH, van der Horst GT. Powerful skin cancer protection by a CPD-photolyase transgene. Curr Biol. 2005;15(2):105-115. PMID: 15668165.

127. Sancar A. DNA excision repair. Annu Rev Biochem. 1996;65:43-81. PMID: 8811174.

128. Rudolph CJ, Upton AL, Lloyd RG. Replication fork stalling and cell cycle arrest in UV-irradiated Escherichia coli. Genes Dev. 2007;21(6):668-681. PMID: 17369400.

129. Byun TS, Pacek M, Yee MC, Walter JC, Cimprich KA. Functional uncoupling of MCM helicase and DNA polymerase activities activates the ATR-dependent checkpoint. Genes Dev. 2005;19(9):1040-1052. PMID: 15833913.

130. Wold MS. Replication protein A: a heterotrimeric, single-stranded DNA-binding protein required for eukaryotic DNA metabolism. Annu Rev Biochem. 1997;66:61-92. PMID: 9242902.

131. Dart DA, Adams KE, Akerman I, Lakin ND. Recruitment of the cell cycle checkpoint kinase ATR to chromatin during S-phase. J Biol Chem. 2004;279(16):16433-16440. PMID: 14871897.

132. Kemp MG, Akan Z, Yilmaz S, Grillo M, Smith-Roe SL, Kang TH, Cordeiro-Stone M, Kaufmann WK, Abraham RT, Sancar A, Unsal-Kacmaz K. Tipin-replication protein A interaction mediates Chk1 phosphorylation by ATR in response to genotoxic stress. J Biol Chem. 2010;285(22):16562-16571. PMID: 20233725.

133. Jansen JG, Tsaalbi-Shtylik A, Hendriks G, Gali H, Hendel A, Johansson F, Erixon K, Livneh Z, Mullenders LH, Haracska L, de Wind N. Separate domains of Rev1 mediate two modes of DNA damage bypass in mammalian cells. Mol Cell Biol. 2009;29(11):3113-3123. PMID: 19332561.

134. Adimoolam S, Lin CX, Ford JM. The p53-regulated cyclin-dependent kinase inhibitor, p21 (cip1, waf1, sdi1), is not required for global genomic and transcription-coupled nucleotide excision repair of UV-induced DNA photoproducts. J Biol Chem. 2001;276(28):25813-25822. PMID: 11331289.

135. Rouget R, Auclair Y, Loignon M, Affar el B, Drobetsky EA. A sensitive flow cytometry-based nucleotide excision repair assay unexpectedly reveals that mitogen-activated protein kinase signaling does not regulate the removal of UV-induced DNA damage in human cells. J Biol Chem. 2008;283(9):5533-5541. PMID: 18093981.

136. Emmert S, Kobayashi N, Khan SG, Kraemer KH. The xeroderma pigmentosum group C gene leads to selective repair of cyclobutane pyrimidine dimers rather than 6-4 photoproducts. Proc Natl Acad Sci U S A. 2000;97(5):2151-2156. PMID: 10681431.

137. Mori T, Nakane M, Hattori T, Matsunaga T, Ihara M, Nikaido O. Simultaneous establishment of monoclonal antibodies specific for either cyclobutane pyrimidine dimer or (6-4)photoproduct from the same mouse immunized with ultraviolet-irradiated DNA. Photochem Photobiol. 1991;54(2):225-232. PMID: 1780359.

138. Takagi S, McFadden ML, Humphreys RE, Woda BA, Sairenji T. Detection of 5-bromo-2-deoxyuridine (BrdUrd) incorporation with monoclonal anti-BrdUrd antibody after deoxyribonuclease treatment. Cytometry. 1993;14(6):640-648. PMID: 8404370.

139. Arlett CF, Plowman PN, Rogers PB, Parris CN, Abbaszadeh F, Green MH, McMillan TJ, Bush C, Foray N, Lehmann AR. Clinical and cellular ionizing radiation sensitivity in a patient with xeroderma pigmentosum. Br J Radiol. 2006;79(942):510-517. PMID: 16714754.

140. Sidorova JM, Li N, Schwartz DC, Folch A, Monnat RJ, Jr. Microfluidic-assisted analysis of replicating DNA molecules. Nat Protoc. 2009;4(6):849-861. PMID: 19444242.

141. Bomgarden RD, Lupardus PJ, Soni DV, Yee MC, Ford JM, Cimprich KA. Opposing effects of the UV lesion repair protein XPA and UV bypass polymerase eta on ATR checkpoint signaling. EMBO J. 2006;25(11):2605-2614. PMID: 16675950.

142. Boyle J, Ueda T, Oh KS, Imoto K, Tamura D, Jagdeo J, Khan SG, Nadem C, Digiovanna JJ, Kraemer KH. Persistence of repair proteins at unrepaired DNA damage distinguishes diseases with ERCC2 (XPD) mutations: cancer-prone xeroderma pigmentosum vs. non-cancer-prone trichothiodystrophy. Hum Mutat. 2008;29(10):1194-1208. PMID: 18470933.

143. Oh KS, Imoto K, Emmert S, Tamura D, DiGiovanna JJ, Kraemer KH. Nucleotide excision repair proteins rapidly accumulate but fail to persist in human XP-E (DDB2 mutant) cells. Photochem Photobiol. 2011;87(3):729-733. PMID: 21388382.

144. Dickmanns A, Zeitvogel A, Simmersbach F, Weber R, Arthur AK, Dehde S, Wildeman AG, Fanning E. The kinetics of simian virus 40-induced progression of quiescent cells into S phase depend on four independent functions of large T antigen. J Virol. 1994;68(9):5496-5508. PMID: 8057432.

145. Hein J, Boichuk S, Wu J, Cheng Y, Freire R, Jat PS, Roberts TM, Gjoerup OV. Simian virus 40 large T antigen disrupts genome integrity and activates a DNA damage response via Bub1 binding. J Virol. 2009;83(1):117-127. PMID: 18922873.

146. Despras E, Daboussi F, Hyrien O, Marheineke K, Kannouche PL. ATR/Chk1 pathway is essential for resumption of DNA synthesis and cell survival in UV-irradiated XP variant cells. Hum Mol Genet. 2010;19(9):1690-1701. PMID: 20123862.

147. Conney AH, Lu YP, Lou YR, Kawasumi M, Nghiem P. Mechanisms of Caffeine-Induced Inhibition of UVB Carcinogenesis. Front Oncol. 2013;3:144. PMID: 23785666.

148. Takezawa J, Aiba N, Kajiwara K, Yamada K. Caffeine abolishes the ultraviolet-induced REV3 translesion replication pathway in mouse cells. Int J Mol Sci. 2011;12(12):8513-8529. PMID: 22272088.

149. Legerski R, Peterson C. Expression cloning of a human DNA repair gene involved in xeroderma pigmentosum group C. Nature. 1992;359(6390):70-73. PMID: 1522891.

150. Abbaszadeh F, Clingen PH, Arlett CF, Plowman PN, Bourton EC, Themis M, Makarov EM, Newbold RF, Green MH, Parris CN. A novel splice variant of the DNA-PKcs gene is associated with clinical and cellular radiosensitivity in a patient with xeroderma pigmentosum. J Med Genet. 2010;47(3):176-181. PMID: 19797196.

151. Chigancas V, Sarasin A, Menck CF. CPD-photolyase adenovirus-mediated gene transfer in normal and DNA-repair-deficient human cells. J Cell Sci. 2004;117(Pt 16):3579-3592. PMID: 15252127.

152. Freeman SE, Hacham H, Gange RW, Maytum DJ, Sutherland JC, Sutherland BM. Wavelength dependence of pyrimidine dimer formation in DNA of human skin irradiated in situ with ultraviolet light. Proc Natl Acad Sci U S A. 1989;86(14):5605-5609. PMID: 2748607.

153. Ikehata H, Higashi S, Nakamura S, Daigaku Y, Furusawa Y, Kamei Y, Watanabe M, Yamamoto K, Hieda K, Munakata N, Ono T. Action spectrum analysis of UVR genotoxicity for skin: the border wavelengths between UVA and UVB can bring serious mutation loads to skin. J Invest Dermatol. 2013;133(7):1850-1856. PMID: 23407394.

154. Stout GJ, Westdijk D, Calkhoven DM, Pijper O, Backendorf CM, Willemze R, Mullenders LH, de Gruijl FR. Epidermal transit of replication-arrested, undifferentiated keratinocytes in UV-exposed XPC mice: an alternative to in situ apoptosis. Proc Natl Acad Sci U S A. 2005;102(52):18980-18985. PMID: 16365302.

155. Sproul CD, Rao S, Ibrahim JG, Kaufmann WK, Cordeiro-Stone M. Is activation of the intra-S checkpoint in human fibroblasts an important factor in protection against UV-induced mutagenesis? Cell Cycle. 2013;12(22):3555-3563. PMID: 24091629.

Curriculum Vitae

Kai-Feng Hung, D.D.S., Ph.D.

EDUCATION

2015 **Ph.D.**, **Oral Biology**
University of Washington, School of Dentistry, Seattle, WA

2004 **M.S.**, **Oral and Maxillofacial Surgery**
National Yang-Ming University, School of Dentistry, Taipei, Taiwan

2000 **D.D.S.**, **Dentistry**
Taipei Medical University, School of Dentistry, Taipei, Taiwan

---

RESEARCH TRAINING

2010–2015 Graduate Research Assistant, Dr. Paul Nghiem's Laboratory, Division of Dermatology, University of Washington, Seattle, WA

2009–2015 Ph.D. Student, Graduate Program in Oral Biology, School of Dentistry, University of Washington, Seattle, WA
Advisor: Paul Nghiem, M.D., Ph.D., Professor and Head, Division of Dermatology, University of Washington
Doctoral Dissertation: Distinct effects of the two major types of UV-induced DNA lesions on DNA damage responses

2006–2008 Ph.D. Student, Graduate Program in Oral Biology, School of Dentistry, National Yang-Ming University, Taiwan
Advisor: Jeng-Fan Lo, Ph.D., Associate Professor, Institute of Oral Biology, School of Dentistry, National Yang-Ming University

2000–2002 Master's Student, Graduate Program in Oral and Maxillofacial Surgery, School of Dentistry, National Yang-Ming University, Taiwan
Research Advisor: Kuo-Wei Chang, D.D.S., Ph.D., Professor, Department of Dentistry, National Yang-Ming University
Clinical Advisor: Shou-Yen Kao, D.D.S., D.M.Sc., Associate Professor, Oral and Maxillofacial Surgery, Taipei Veterans General Hospital, Taiwan
Master's Thesis: Differential expression of caveolin-1 and E-cadherin in oral carcinogenesis

---

CLINICAL TRAINING

2004–2005 Clinical Fellow, Division of Oral and Maxillofacial Surgery, Department of Dentistry, Taipei Veterans General Hospital, Taiwan

2003–2004 Chief Resident, Division of Oral and Maxillofacial Surgery, Department of Dentistry, Taipei Veterans General Hospital, Taiwan

2000–2004 Resident, Division of Oral and Maxillofacial Surgery, Department of Dentistry, Taipei Veterans General Hospital, Taiwan

---

FACULTY POSITIONS HELD

2004–2009 Lecturer, Oral and Maxillofacial Surgery, Department of Dentistry, National Yang-Ming University, Taiwan

---

HOSPITAL POSITIONS HELD

2006–2009 Attending Physician, Division of Oral and Maxillofacial Surgery, Tzu Chi General Hospital, Taipei, Taiwan

2005–2006 Attending Physician, Division of Oral and Maxillofacial Surgery, Department of Dentistry, Taipei Veterans General Hospital, Taiwan

---

HONORS

2014 Albert M. Kligman Travel Fellowship Award, Society for Investigative Dermatology Annual Meeting, Albuquerque, NM

2013 Graduate School Fund for Excellence and Innovation (GSFEI) Graduate Student Travel Award, School of Dentistry, University of Washington

2011 1st Place Poster Award, 6th Annual South Lake Union Group (SLUG) Research Symposium, Seattle, WA

2009 Graduate School Fund for Excellence and Innovation (GSFEI) Top Scholar Award, School of Dentistry, University of Washington

2004 Oral Presentation Award, 4th Taiwan Congress on Oral and Maxillofacial Surgery Annual Meeting, Tainan, Taiwan

2003 Oral Presentation Award, 3th Taiwan Congress on Oral and Maxillofacial Surgery Annual Meeting, Changhua, Taiwan

2002 Best Graduate of Year Award, National Yang-Ming University, Taipei, Taiwan

---

BOARD CERTIFICATION

2004 Diplomate, National Board of Oral and Maxillofacial Surgery, Taiwan

---

LICENSE TO PRACTICE

2000–present Dental License, Taiwan

PROFESSIONAL ORGANIZATIONS

2010–present Member, Taiwan Head and Neck Tumor Society

2005–2009 Member, Academic Affairs Committee and International Affairs Committee, Association of Oral and Maxillofacial Surgeons, Taiwan

2000–present Member, Taiwan Dental Association

PUBLICATIONS

Original Articles:

1. **Hung KF**, Lai KC, Liu TY, Liu CJ, Lee TC, Lo JF. Asb6 upregulation by Areca nut extracts is associated with betel quid-induced oral carcinogenesis. *Oral Oncol*. 45(6):543-8, 2009.
2. Fong Y, Chou SJ, **Hung KF**, Wu HT, Kao SY. An investigation of the differential expression of Her2/neu gene expression in normal oral mucosa, epithelial dysplasia, and oral squamous cell carcinoma in Taiwan. *J Chin Med Assoc*. 71(3):123-7, 2008.
3. **Hung KF**, Chang CS, Liu CJ, Lui MT, Cheng CY, Kao SY. Differential expression of E-cadherin in metastatic lesions comparing to primary oral squamous cell carcinoma. *J Oral Pathol Med*. 35(10):589-94, 2006.
4. **Hung KF**, Lin SC, Liu CJ, Chang CS, Chang KW, Kao SY. The biphasic differential expression of the cellular membrane protein, caveolin-1, in oral carcinogenesis. *J Oral Pathol Med*. 32(8):461-7, 2003.

Case Reports:

1. Liaw YC, Kuang SH, Chen YW, **Hung KF**, Tsai HC, Kao SY, Fong JH. Multimodality treatment for rehabilitation of adult orthodontic patient with complicated dental condition and jaw relation. *J Chin Med Assoc*. 71(11):594-600, 2008.
2. Kao SY, Lui MT, Fong J, Wu DC, Wu CH, Tu HF, **Hung KF**, Yeung TC. A method using vestibulo-sulcoplasty combining a split-thickness skin graft and a palatal keratinized mucosa graft for peri-implant tissue secondary to oral cancer surgery. *J Oral Implantol*. 31(4):186-91, 2005.
3. Kao SY, Yeung TC, **Hung KF**, Chou IC, Wu CH, Chang RC. Transpositioned flap vestibuloplasty combined with implant surgery in the severely resorbed atrophic edentulous ridge. *J Oral Implantol*. 28(4):194-9, 2002.

Manuscript Submitted:

1. **Hung KF**, Sidorova JM, Nghiem P, Kawasumi M. UV-induced replication blockage and ATR activation are mediated by 6-4 photoproducts.

PRESENTATIONS

2014 Society for Investigative Dermatology Annual Meeting, Albuquerque, NM; "UV-induced activation of the ATR-Chk1 pathway is mediated by 6-4PPs (not CPDs) via replication blockade", oral and poster presentations

2013 American Association of Oral and Maxillofacial Surgeons Annual Meeting, Orlando, FL; "Comparison of complication rates between lateral versus inferior fixation of reconstruction plate for free fibular flap reconstruction of mandible", poster presentation

2013 Seattle Genetic Instability and Cancer Symposium, Seattle, WA; "Which sunlight-induced pyrimidine dimer best activates the UV-DNA damage response?" poster presentation

2013 University of Washington Oral Health Sciences Student/Trainee Symposium, Seattle, WA; "Differential effect of distinct types of DNA damage on the ATR-Chk1 pathway", oral presentation

2013 Keystone Symposia: Genomic Instability and DNA Repair, Banff, Canada; "Which sunlight-induced pyrimidine dimer best activates the UV-DNA damage response?" poster presentation

2012 7th South Lake Union Group (SLUG) Research Symposium, Seattle, WA; "Which sunlight-induced pyrimidine dimer best activates the UV-DNA damage response?" poster presentation

2011 6th South Lake Union Group (SLUG) Research Symposium, Seattle, WA; "How does sunlight activates skin SOS signals?" poster presentation

2009 9th Taiwan Congress on Oral and Maxillofacial Surgery Annual Meeting, Taipei, Taiwan; "Comparison of the complications between conventional and modified mandibular reconstruction after mandibulectomy", oral presentation

2006 7th Asian Congress on Oral and Maxillofacial Surgery, Hong Kong, China; "Asb6 upregulation by Areca nut extracts is associated with betel quid-induced oral carcinogenesis", poster presentation

2005 5th Taiwan Congress on Oral and Maxillofacial Surgery Annual Meeting, Taipei, Taiwan; "Profiling the DNA repair genes in oral cancer patients", oral presentation

2004 6th Asian Congress on Oral and Maxillofacial Surgery, Tokyo, Japan; "Differential expression of E-cadherin in metastatic lesions comparing to primary oral squamous cell carcinoma", poster presentation

2004 4th Taiwan Congress on Oral and Maxillofacial Surgery Annual Meeting, Tainan, Taiwan; "Multimodality treatment for rehabilitation of adult orthodontic patient", oral presentation

2003 3th Taiwan Congress on Oral and Maxillofacial Surgery Annual Meeting, Changhua, Taiwan; "The biphasic expression of cellular membrane protein, caveolin-1, in oral carcinogenesis", oral presentation